Sonora Elf Owl Model fitting of JWST Archival Y Dwarfs

Joshua Miller

A senior thesis submitted to the faculty of
Brigham Young University
in partial fulfillment of the requirements for the degree of

Bachelor of Science

Denise Stephens, Advisor

Department of Physics and Astronomy

Brigham Young University

ABSTRACT

Sonora Elf Owl Model fitting of JWST Archival Y Dwarfs

Joshua Miller
Department of Physics and Astronomy, BYU
Bachelor of Science

With increasing capabilities to see cooler objects, we are now capable of observing cooler Y type brown dwarfs. New spectral images necessitate the need for accurate models to descirbe the features of these objects in order to understand their properties. In this project I run forward modeling algorithms using the Sonora Elf Owl models against spectra taken by JWST. I compare these models made for earlier type brown dwarfs with the observed spectra to determine how useful these high resolution models are in determining Y dwarf atmospheric properties. I find that there are hidden factors in these atmospheres that become significant amongst the Y dwarfs causing the model spectra to diverge at specific wavelength regimes.

Keywords: Brown Dwarfs, Y Dwarfs, Atmospheric Modeling, Infrared Spectroscopy, JWST, Forward Modeling, Carbon to Oxygen Ratio

ACKNOWLEDGMENTS

This work was made possible by the funding and resources provided by the Department of Physics and Astronomy at Brigham Young University. The observations used in this project largely came from the #2124, #2302, and #12970 programs provided by NASA and Mikulski Archive for Space Telescopes at the Space Telescope Science Institute. Calculations, modeling, and figures were made through python 3 and various associated packages. ChatGPT through OpenAI was used in editing portions of this work.

Contents

List of Figures

List of Tables

Chapter 1

Introduction

Brown dwarfs exist in the range of objects that form in the universe between the largest exoplanets and the smallest stars that sustain fusion reactions. They are interesting to study because they are bright enough to observe directly but cool enough to form complex chemistry in their atmospheres. Additionally, unlike exoplanets, they are often found away from brighter sources, allowing us to extract well-defined spectra.

With new space-based telescopes and high-resolution imaging in the near-infrared spectrum, brown dwarfs are excellent targets for understanding extrasolar atmospheric evolution. In this section, I first discuss the basic characteristics of brown dwarfs, their classifications, and the general physics behind them. I then discuss the motivation for this research in the context of the broader research landscape. Afterwards, I introduce the method used in this work—modeling. Finally, I detail the project itself and its research question.

1.1 Spectral Type and Characteristics

The primary distinction used to define a brown dwarf is its mass. Brown dwarfs are typically defined as having masses between 13 and 80 Jupiter masses (Dupuy et al. 2015). The upper end of this

range corresponds to the threshold required for an object to sustain hydrogen fusion and maintain thermal equilibrium. Objects below 80 Jupiter masses cannot perform hydrogen fusion and are instead supported by electron degeneracy pressure. While some brown dwarfs at the higher end of this mass range can fuse lithium following their initial collapse, this process is short-lived, allowing them to cool over time (Morley et al. 2024).

The spectra of brown dwarfs generally follow a blackbody curve, particularly for the hotter objects, and peak in the infrared portion of the spectrum. According to Wien's law, brighter brown dwarfs are hotter. Because brown dwarfs do not undergo fusion, their heat originates from their initial gravitational collapse from the interstellar medium (Marley & Robinson 2015). As a result, they cool over time as they radiate away their internal energy.

Depending on spectral type, brown dwarfs exhibit many absorption features that depend on the molecular composition above their photosphere. Water and carbon dioxide are commonly present, along with silicates and other complex compounds. Kirkpatrick et al. first defined the L spectral type for the brightest and hottest brown dwarfs, formally distinguishing them from M dwarfs. L-type brown dwarfs exist in the temperature range of approximately 1400 K to 2700 K. They typically have few to no clouds, contain many neutral metals in their atmospheres, and show strong signatures of metal hydrides such as CrH and FeH, as well as simple molecules like TiO and VO.

The next classification is the T spectral type, which spans temperatures from roughly 600 K to 1400 K. These objects tend to have more clouds, causing their spectra to vary over time. Metal hydride features diminish as these species settle below the photosphere (Ackerman & Marley 2001). In their place, more prominent water absorption bands and methane features appear (Burgasser et al. 2003).

Finally, the Y dwarf spectral type, which is the focus of this research, represents the coolest class of brown dwarfs. Y dwarfs exist at temperatures below 600 K, placing them in the same temperature range as several objects in our solar system. At these temperatures, many heavier compounds have

condensed out of the atmosphere. However, their spectra remain intricate and complex due to the wide range of molecules that can form under low-temperature conditions (Kirkpatrick et al. 2012). Because Y-type brown dwarfs are both cool and intrinsically faint, they require sophisticated near- and mid-infrared space-based telescopes to obtain high-resolution data.

1.2 Motivation

Our solar system contains only eight planets, with only about half of them possessing substantial atmospheres. This represents a very limited sample size for studying the atmospheres of substellar objects. Even among the gas giants, atmospheric composition varies significantly.

Exoplanet research is a rapidly growing field in astronomy and has produced many exciting discoveries over the past few decades. However, current observational capabilities make it difficult to directly image and characterize exoplanet atmospheres, as they are generally too faint relative to their host stars.

Brown dwarfs provide an excellent opportunity for studying extrasolar atmospheres because they are bright enough to be observed with current telescopes while still being cool enough to host many of the molecular species expected in exoplanet atmospheres. While brighter L-type brown dwarfs are easier to observe, they tend to contain fewer molecular species. Cooler Y-type brown dwarfs, on the other hand, exhibit richer chemistry but are much fainter and more challenging to observe. Nevertheless, they are not beyond the reach of modern instrumentation. This places Y dwarfs at the frontier of observational capability and scientific discovery.

1.3 Modeling

Neutral elements, such as those commonly observed in bright stars, produce clean and well-defined spectral lines, many of which appear in the optical regime. These features are well understood, easily

identifiable, and have predictable broadening behavior. However, this research does not deal with the clean spectra of A-type stars. Y-type brown dwarfs emit very little flux in the optical, requiring observations in the infrared. Furthermore, molecular species do not produce simple spectral lines; instead, they generate complex absorption bands that broaden and overlap with one another.

Due to the complexity of brown dwarf spectra, atmospheric models are essential for interpreting observations. These models simulate brown dwarf atmospheres using a set of physical parameters. Based on established principles of fluid dynamics, heat transfer, and chemical equilibrium, the models generate synthetic spectra by varying these parameters. The resulting spectra are then statistically compared to observational data to determine the most probable atmospheric conditions.

This project primarily uses the Sonora Elf Owl models developed by (Beiler et al. 2023). The Sonora Elf Owl models incorporate five key parameters: effective temperature, surface gravity, vertical mixing (Kzz), metallicity, and the carbon-to-oxygen ratio (C/O). Each of these parameters is discussed in greater detail later in this thesis.

An additional important topic in brown dwarf research is their thermal evolution over time. While this concept is only tangentially related to the present work, it is worth mentioning briefly. Because brown dwarfs do not generate energy through fusion, they gradually radiate away the heat from their initial collapse, causing them to cool over time. As they cool, they also contract due to the reduced thermal pressure supporting them, leading to an increase in surface gravity. As a result, it is often difficult to determine whether a cool brown dwarf is cool due to advanced age or low mass (Marley & Robinson 2015). If the mass can be constrained, it may be possible to estimate age, which has important implications for studies of galactic archaeology and the initial mass function.

1.4 Project

L-type brown dwarfs began to be studied in the late 1990s, with T-type brown dwarfs following in the early 2010s. Since then, advances in telescope technology and atmospheric modeling have significantly improved our ability to study these objects. We are now capable of observing even the faintest brown dwarfs. The James Webb Space Telescope (JWST) provides high-resolution spectral data in the near- and mid-infrared, making it possible to study Y-type brown dwarfs in unprecedented detail. Modeling of L- and T-type brown dwarfs is relatively mature, though some complexities remain, particularly at the L/T transition.

In this work, I apply the statistical modeling techniques developed for warmer brown dwarfs to cooler Y dwarfs using high-resolution Sonora Elf Owl models and JWST spectral data. I analyze seven Y-type brown dwarfs, comparing model spectra to observations spanning wavelengths from 0.9 μm to 14 μm. I examine the statistical significance of the model fits and identify discrepancies between the models and observed data. Finally, I explore where current models fail to reproduce observations, particularly in comparison to warmer brown dwarfs, and discuss the implications for our understanding of Y-type brown dwarf atmospheres.

This is a new area of brown dwarf research. Y type brown dwarfs have unique challenges associated with their spectroscopy which could unlock understanding as to how brown dwarfs form and what the atmospheric dynamics and compositions are. This research will help us understand the effectiveness of brown dwarf forward modeling, the constraints, and it will help us explore the possibilities of future academic work in understanding cool worlds which have insights into both exoplanets and dwarf stars.

Chapter 2

Methods

2.1 Targets

Seven objects are used for this study were obtained from JWST archival data from program 2124 (PI: Jacqueline Faherty) (Faherty et al. 2021). The object names and basic information are provided in Table 2.1. The objects were selected based on their physical properties, specifically their low temperatures (cooler than 700 K) and brightness (between 12.3 and 15.5 mag). They were also chosen to help create a standard spectral library for Y dwarfs, as these are among the first Y dwarfs to receive high-resolution spectra.

Four of the objects in Table 2.1 have limited spectral coverage with no supplemental data sources, making it difficult to perform meaningful analysis on them. I use 2220 later in this paper to compare and demonstrate why the lack of data makes these objects unsuitable for detailed study at the present time. One of the objects, 0415, is not a Y dwarf but a late-type T dwarf. It was included in the observations as a comparison object. This source has been observed by several telescopes, resulting in a well-defined spectrum. Because 0415 is a late-type T dwarf with extensive

Object	Short	Spectral Type	J Mag	Reference	Data Range
2MASSI J0415195-093506	0415	T8	15.320+-0.030	(Knapp et al. 2004)	0.83-15 μm
WISE J053516.80-750024.9	0535	Y1	22.132+-0.071	(Leggett et al. 2015)	0.60-14 μm
WISE J014656.66+423410.0	0146	T9.5	20.690+0.070	(Dupuy et al. 2015)	0.83-5.14 μm
WISE J222055.31-362817.4	2220	Y0	20.640+-0.050	(Leggett et al. 2015)	0.90-5.14 μm
WISEA J082507.37+280548.2	0825	Y0.5	22.401+-0.050	(Schneider et al. 2015)	0.60-14 μm
WISE J140518.39+553421.3	1405	Y0.5	21.060+-0.060	(Leggett et al. 2013)	0.60-14 μm
WISE J154151.65-225024.9	1541	Y1	21.120+-0.060	(Leggett et al. 2013)	0.60-14 μm

Table 2.1 Data ranges of spectra compiled and used for target objects. Data from the 1-5 μm range comes from the JWST NIRSPEC instrument from program 2124. Data ranging from 4-14 μm comes from the JWST MIRI instrument by program 2302. Additionally, HST data using the WFC3 camera provides data in the 0.9-1.7 μm range. 0415 additionally receives data from Keck (Kirkpatrick et al. 2008)(0.6-2.5) and Spitzer (Suárez & Metchev 2022)(5.2-14.5). Spectral type and the magnitude given in the J filter are given. 0415 is well studied and its spectral type is well established. However, the other spectral types are debated and need more consensus. What is provided is the earliest possible spectral type of each object.

observational coverage, it provides a useful comparison between well-studied brown dwarf spectra and the more novel Y dwarf spectra.

To supplement the data from program 2124, I also use data from JWST program 2302 (PI: Michael Cushing) (Cushing et al. 2021). To supplement and compare newer data to older data, I have Hubble Space Telescope data for some objects. This comes from program 12970 (PI: Michael Cushing) using the WFC3 instrument and F125W filter. For 0415, to fill beyond the 5 μm range, I have Spitzer Space Telescope data (Kirkpatrick et al. 2008) and to overlap and fill the 1 μm range I have spectra from Keck (Suárez & Metchev 2022).

2.2 Measurements

The spectra from program 2124 were obtained using the JWST NIRSpec instrument with the G395H grism. Observations were taken using the S200A1 slit with three dithers. The resulting spectra cover a wavelength range of approximately 2.8–5.3 μm. The data were processed and reduced using the standard JWST reduction pipeline.

For objects 0535, 0825, 1405, and 1541 I use data from program 2302 obtained with the JWST MIRI MRS instrument. Observations were taken using the S200A1 slit with four dithers. These spectra cover a wavelength range of approximately 5.0–16 μm. However, due to known issues with the detector, data beyond 14 μm are unreliable, and data beyond 12 μm have large error bars. As a result, my analysis consistently cuts off at 12 μm. These data were also processed and reduced using the standard JWST reduction pipeline. All flux units have been converted to janskys to ensure consistency between the models and the observed spectra.

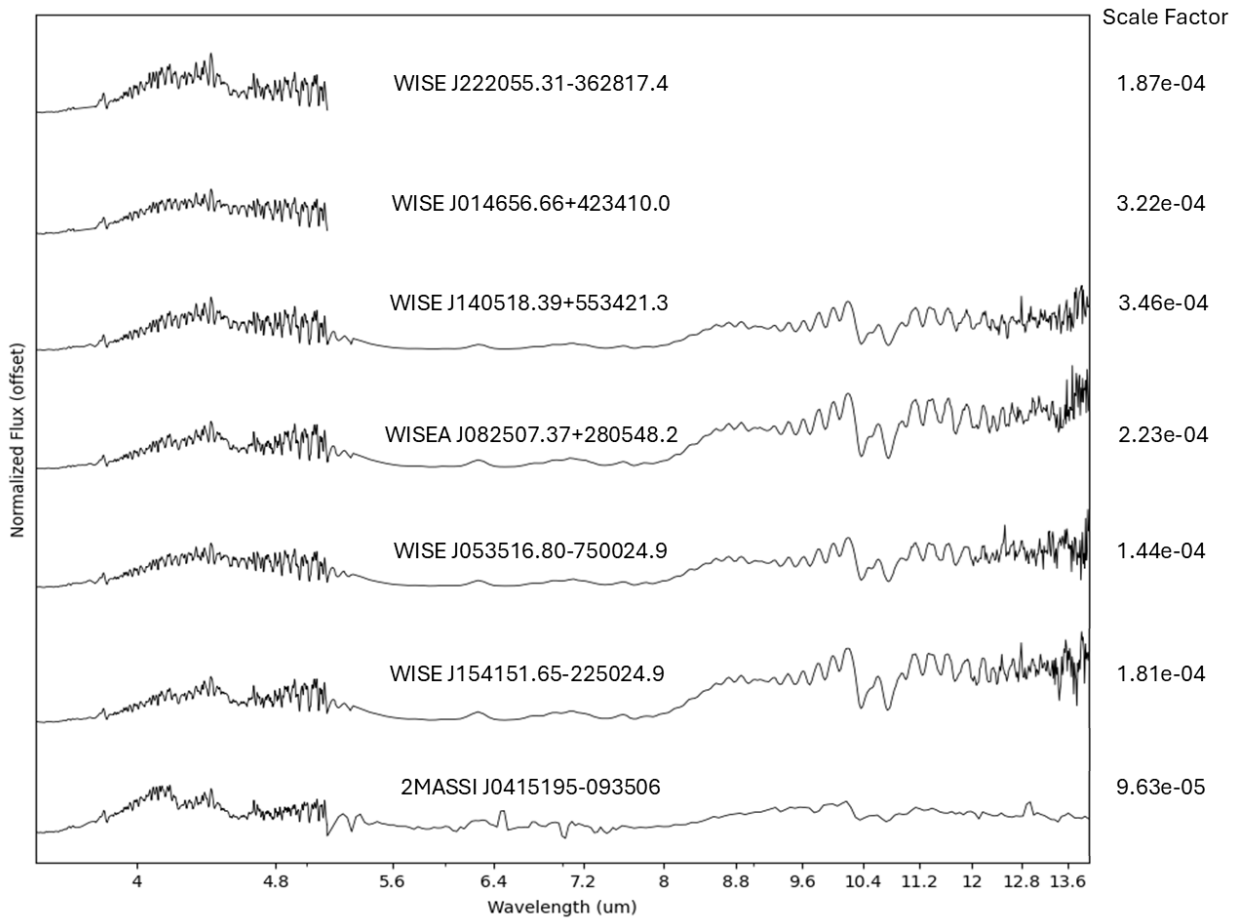

Figure 2.1 Normalized spectra from 3.5 μm to 14 μm for all objects within this study on a log plot. The full SIMBAD name for each is given along with the scale factor used to normalize each spectra to one at its peak then added to an offset so they stack vertically. The spectra is in energy per unit surface area, per unit time, per unit frequency. Originally in janskys.

2.3 Fitting Code

In astronomy, spectra are typically used to determine the elemental composition of astronomical objects. Neutral elements often produce well-defined absorption lines, which allow for relatively straightforward determination of elemental abundances and compositions. These spectral lines can be affected by factors such as redshift and line broadening. Brown dwarfs, however, are cool enough to form more complex molecules, which produce broad and complicated absorption bands rather than discrete spectral lines. In addition, brown dwarfs are fully convective, leading to atmospheric inhomogeneities such as regions of varying molecular abundances.

Because of the complexity involved in understanding the atmospheric composition and dynamics of brown dwarfs, atmospheric models are required to interpret their spectra. These models simulate brown dwarf atmospheres using known physics of heat transfer and molecule formation processes to predict what a spectrum with a given set of parameters would look like when observed.

2.3.1 Sonora Elf Owl

In this work, I use the Sonora Elf Owl models. As described by the authors,

> "The Sonora Elf Owl Models is a successor to the Sonora Bobcat and Sonora Cholla models. The Sonora Elf Owl model grid includes cloud-free radiative-convective equilibrium model atmospheres with vertical mixing induced disequilibrium chemistry with sub-solar to super-solar atmospheric metallicities and Carbon-to-Oxygen ratio. The atmospheric models have been computed using the open-source radiative-convective equilibrium model PICASO. The parameters included within this grid are effective temperature (Teff), gravity (log(g)), vertical eddy diffusion coefficient (log(Kzz)), atmospheric metallicity ([M/H]), and Carbon-to-Oxygen ratio (C/O)" (Mukherjee et al. 2024).

I use the Sonora Elf Owl Models as opposed to other model sets because the models are in high resolution. Many previous studies including work done by other students in my group have lower resolution spectra from other telescope sources. JWST is a unique and sophisticated instrument that gives us high resolution data with small errors. The model resolution must be greater than the observed data so that interpolating the data does not create false statistics.

It is important to be selective when choosing which parameters to model. Including too many free parameters is both computationally expensive and can lead to overfitting the models to the observed spectra. The goal of this work is to understand the most important physical processes governing brown dwarf atmospheres. By comparing the Sonora Elf Owl models to the observed spectra of my objects, I am able to constrain their atmospheric properties using the parameters described above.

2.3.2 Forward Modeling

For this project, I adapted code developed by a graduate student in my research group that determines how similar each model is to a given observed spectrum and returns a total X^2 value for each model (Turner et al. 2025). The inherited code required modifications to its data structure. It was originally designed for low-resolution models that required minimal memory. In contrast, I worked with high-resolution models that could not be stored entirely in RAM, making it necessary to refactor the code.

I then processed each spectrum, restricting the model grid to effective temperatures between 200 K and 600 K. An exception was made for object 0415, which is a hotter brown dwarf used for comparison. In this case, I used effective temperatures within 100 K of the generally accepted value in the literature, approximately 800 K (Sanghi et al. 2023).

There is also the possibility that some brown dwarfs form in binary systems. Such systems would produce spectra that are not well represented by any single model but instead by a linear

combination of two models. To account for this, I analyzed each object using a binary model fitting code. This code operates similarly to the single-model fitting code but evaluates a two-dimensional grid of model combinations. Each model is combined with every other model, and a X^2 analysis is performed on the resulting composite spectra. To reduce computational time, I constrain the models used in the binary fitting to those corresponding to the best fitting results from the single-model analysis. Both model fitting codes are provided in the appendix of this paper.

Chapter 3

Results

In this chapter I do an analysis of each of the objects in this sample. I will comment on the effectiveness of the best fit models and what this may imply about the atmospheric composition and dynamics of these objects. I will start with the late type T-dwarf, 0415, as our model object to compare against the other objects. I treat each object individually as a case to showcase the effectiveness of using the Elf Owls to forward model.

For each object, with the exception of 0146 and 2220, I provide two figures. The first figure will show the spectra of the object and the best fit model for that spectra when weighting only the NIRSPEC components of that data. The second figure will have the best fit model when weighting only the MIRI portion of the data. I perform this separate X^2 analysis for each target because the two wavelength regions behave differently. This allows for comparing the effectivness of the models across the brown dwarfs spectrum. Many other researchers may only use data from one source which, as will hopefully become apparent, may result in inaccurate conclusions about the objects atmospheric properties. For each object I also provide a table which lists the best three fits for the NIRSPEC and MIRI regions for comparison.

In the discussion section I switch to using the best fit models of the entire spectra for each object. To do this I appropriately weight different sections of the spectra depending on the resolution of

each section of data. This allows me to do an overall discussion of the forward models concerning this sample of Y dwarfs.

3.1 Objects

3.1.1 2MASSI J0415195-093506

Starting with our standard star, 0415 is typical of what is found in the literature for a T dwarf spectrum. The J, H, and K bands around 1 μm are prominent, with good signal before a pronounced valley of low flux, followed by the largest peak at around 4 μm. Up to this point, most of the absorption is due to water or methane. In fact, water in Earth's atmosphere would also wash out any flux in these same bands, which is why the J, H, and K filters are commonly used. Moving beyond 4 μm, the flux does not return to near zero at any point, but there are regions of weaker flux. This is where the chemistry becomes particularly interesting. Carbon monoxide and carbon dioxide likely play a significant role in the absorption in this region, and we shall see that the carbon-to-oxygen ratio greatly affects the fits in this portion of the spectrum.

Looking at Figure 3.1, we see the best fit model when weighting only the NIRSPEC data and ignoring the other parts of the spectrum. Figure 3.3 shows the best fit model when weighting only the MIRI data. Neither best fit model is very good at describing the whole spectra. The NIRSPEC fitted model predicts too much flux at around 4.3 μm and significantly underpredicts all the flux past 7 μm. The MIRI fit provides a decent fit from 7-12 μm and does well at 4.3 μm though it makes a sacrifice underfitting the features before and after 4.3 μm. Particularly, it overestimates the flux absorption by carbon monoxide. The best fit parameters are shown in Table 3.1.

We find that both model fits have similar surface temperatures. They both predict a high carbon to oxygen ratio of 2.5. Both show that the 0415 is metal poor compared to the Sun. The models diverge when predicting surface gravity and vertical mixing. The NIRSPEC best fits predict high

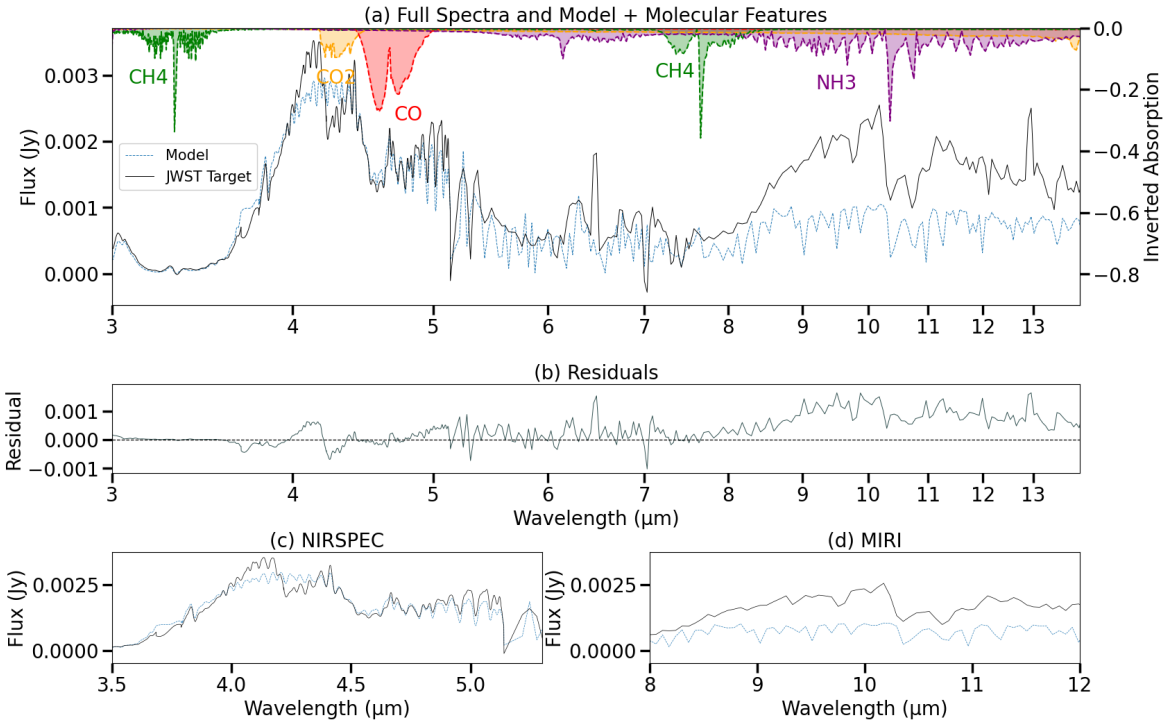

Figure 3.1 This plot shows the best fit weighted to the NIRSPEC data for 0415. Plot (a) show the spectra from 3.5 μm to 14 μm displaying the best fit model over the observed data. Molecular absorption is shown for refrence on the inverted axes. Plot (b) shows the residuals of the model fit to the data. Plots (c) and (d) zoom in on the 3.5-5.3 μm and 5-12 μm region for better resolution, respectively.

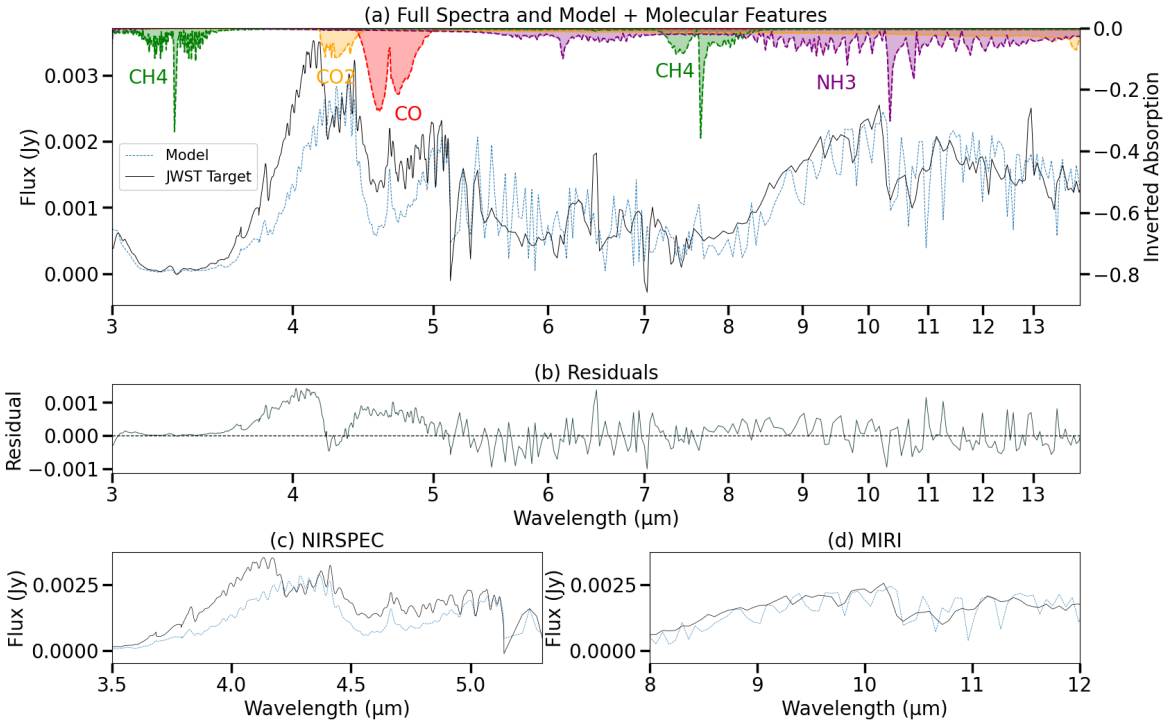

Figure 3.2 This plot shows the best fit weighted to the MIRI data for 0415. Plot (a) show the spectra from 3.5 μm to 14 μm displaying the best fit model over the observed data. Molecular absorption is shown for refrence on the inverted axes. Plot (b) shows the residuals of the model fit to the data. Plots (c) and (d) zoom in on the 3.5-5.3 μm and 5-12 μm region for better resolution, respectively.

surface gravity and high rates of vertical mixing. We will see consistently throught the analysis that surface gravity is poorly constrained and is discussed more later. Vertical mixing is important for dredging up material from below the photosphere into the atmosphere of the brown dwarf. The NIRSPEC best fits predict that there should be more carbon monoxide present then carbon dioxide. However, this object is cool enough that these molecules should have fallen below the photosphere necessitating a process for circulating them up into the atmosphere. The NIRSPEC best fits predict a high vertical mixing value of 10e8 m/s² to allow for the absorption to be seen.

Weighting	teff	grav	kzz	mh	co	Reduced X²
NIRSPEC 1	700	1780	8	-1	2.5	112.042
NIRSPEC 2	650	3160	9	-1	2.5	112.637
NIRSPEC 3	700	3160	8	-1	2.5	113.268
MIRI 1	750	17	4	-0.5	2.5	35.509
MIRI 2	800	17	4	-0.5	2.5	32.618
MIRI 3	850	17	2	-0.5	2.5	32.659
Binary	750	1780	7	-1	2.5	
	700	1780	7	0.5	2.5	165.572

Table 3.1 The best three forward model fitting parameters are given with the reduced X² value for 0415 when considering only the NIRSPEC (3-5 μm) region of spectra. Below that is the best three forward model fitting parameters with the reduced X² value when considering only the MIRI (5-12 μm). Finally, a single binary forward model shows the best fitted parameters.

There is a possibility any of my objects could be a binary object. This would affect the observed spectra. I use a foward modeling code to find binary best fits similar to my single fit analyses. Figure 3.3 shows the best binary fit based on a weighting proportional to the resolution of the NIRSPEC and MIRI data. We see that the binary model fits better than any single-component model. At both higher and lower energies, the model converges more closely on the observations. This improvement

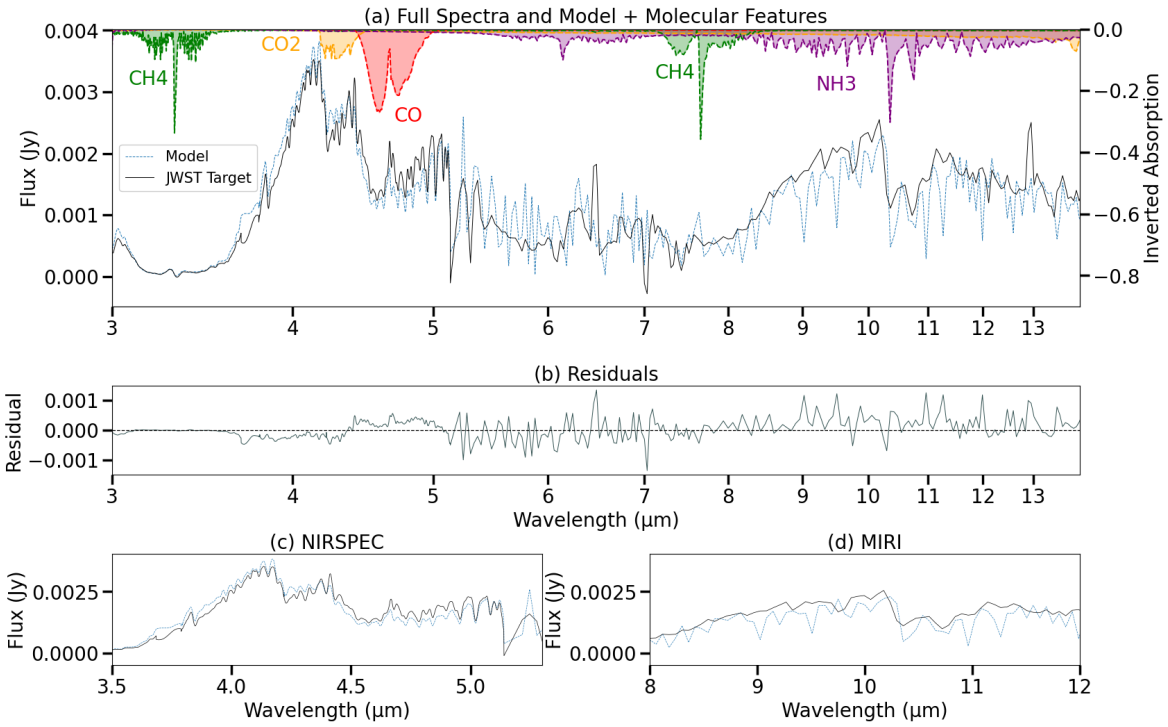

Figure 3.3 Graph showing the spectra of 0415 from 0.9-14 μm using the binary fit modeling. Two models were added together and scaled then forward modeled to create a best fit. Plot (a) show the spectra from 3.5 μm to 14 μm displaying the best fit models over the observed data and scaled. Molecular absorption is shown for refrence on the inverted axes. Plot (b) shows the residuals of the models fit to the data. Plots (c) and (d) zoom in on the 3.5-5.3 μm and 5-12 μm region for better resolution, respectively.

is expected when additional parameters are introduced. However, we must be careful not to overfit and should accept binary models only when they significantly outperform the single-component fits.

In the case of 0415, the binary fit is only marginally better than the single best fit models. Moreover, the issues present in the single-component models persist in the binary fit. At 4.3 μm the model still overpredicts the flux and it underpredicts past 7 μm, and I am unable to explain these discrepencies.

3.1.2 WISE J053516.80-750024.9

This object, is our first case compared to the T8 dwarf 0415. It has many typical features of a low-brightness brown dwarf. There is nearly no flux in the J, H, and K bands. Another prominent feature is that the hump around 4 μm is approximately the same magnitude as the flux beyond 8 μm, indicating that the blackbody emission is redder than that of 0415. The models predict this cooler effective surface temperature.

Weighting	teff	grav	kzz	mh	co	Reduced X^2
NIRSPEC 1	400	562	8	-1	2.5	79.732
NIRSPEC 2	425	562	7	-1	2.5	80.191
NIRSPEC 3	425	562	8	-1	2.5	80.270
MIRI 1	525	3160	7	0.7	0.5	1492.020
MIRI 2	525	3160	4	0.7	0.5	1507.002
MIRI 3	550	3160	7	0.7	0.5	1508.647

Table 3.2 The best three forward model fitting parameters are given with the reduced X^2 value for 0535 when considering only the NIRSPEC (3-5 μm) region of spectra. Below that is the best three forward model fitting parameters with the reduced X^2 value when considering only the MIRI (5-12 μm).

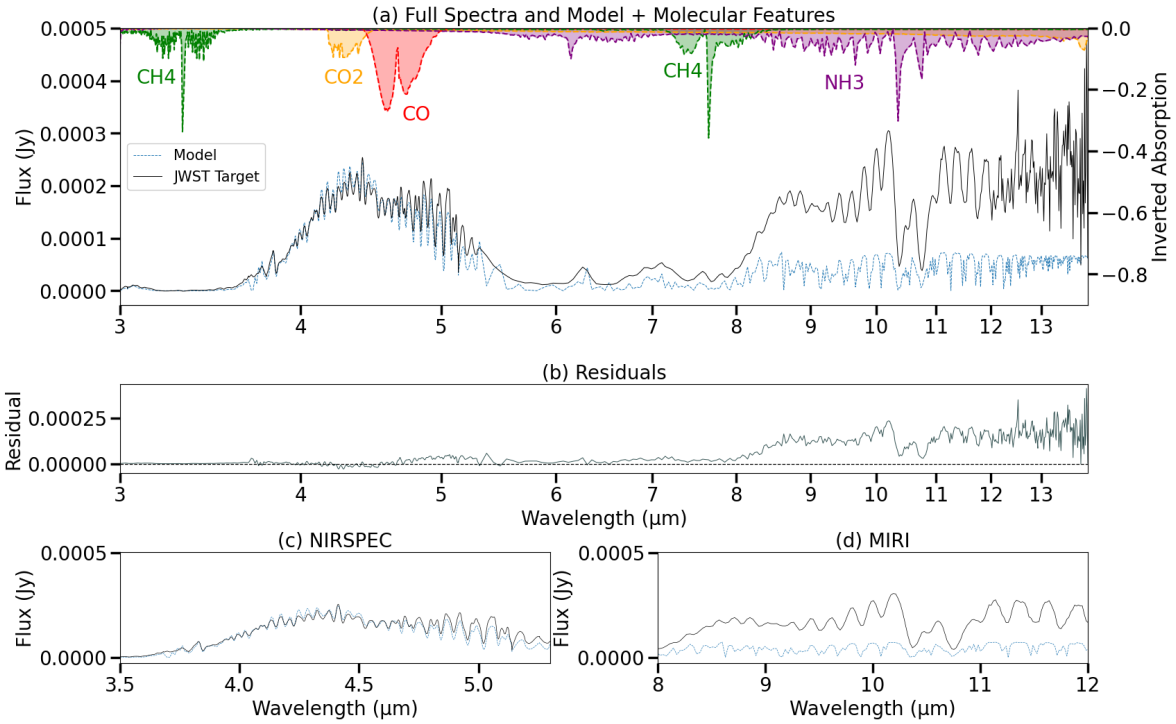

Figure 3.4 This plot shows the best fit weighted to the NIRSPEC data for 0535. Plot (a) show the spectra from 3.5 μm to 14 μm displaying the best fit model over the observed data. Molecular absorption is shown for refrence on the inverted axes. Plot (b) shows the residuals of the model fit to the data. Plots (c) and (d) zoom in on the 3.5-5.3 μm and 5-12 μm region for better resolution, respectively.

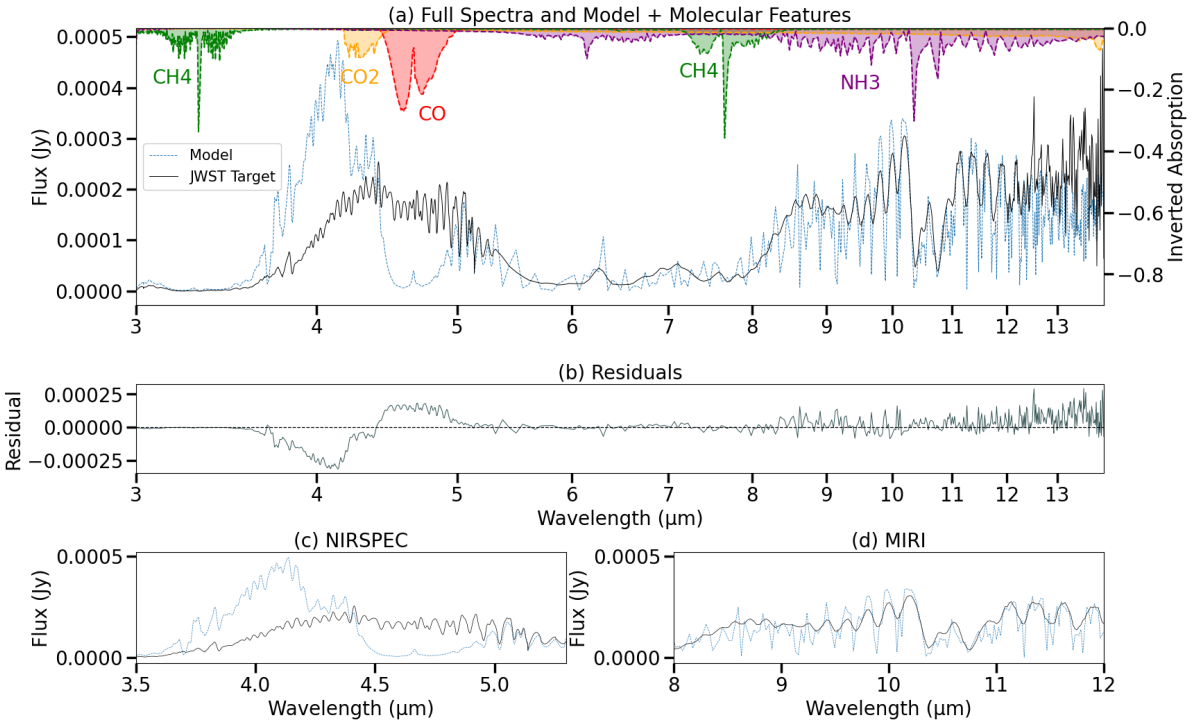

Figure 3.5 This plot shows the best fit weighted to the MIRI data for 0535. Plot (a) show the spectra from 3.5 μm to 14 μm displaying the best fit model over the observed data. Molecular absorption is shown for refrence on the inverted axes. Plot (b) shows the residuals of the model fit to the data. Plots (c) and (d) zoom in on the 3.5-5.3 μm and 5-12 μm region for better resolution, respectively.

Figure 3.4 shows a convincing fit in the 3–5 μm range when weighted to the NIRSPEC data. However, beyond 7 μm the model underpredicts the flux strength. The best fit model has a similar overall shape to the observed spectrum but is an order of magnitude fainter than the observations. It also misses the strong ammonia feature at 10.5 μm. In Figure 3.5, we see that it is possible to fit the spectrum beyond 7 μm more accurately, but doing so causes the model to significantly overestimate the flux at 4 μm and overestimate the carbon monoxide absorption. The MIRI weighted data predicts a hotter and denser object with a very different metallicity and a lower carbon-to-oxygen ratio than the NIRSPEC weighted data.

3.1.3 WISE J014656.66+423410.0

This object illustrates that more complete data is necessary to meaningfully constrain or correct the models. We can nearly perfectly fit the 3–5 μm region using the available models, even though we know from the other targets with more complete spectral coverage that the full spectrum out to 12 μm is never well fit. This demonstrates that limited data can lead to inaccurate conclusions regarding the validity of the models and the assumptions we make about these objects properties.

Weighting	teff	grav	kzz	mh	co	Reduced X^2
NIRSPEC 1	600	3160	4	-0.5	2.5	20.791
NIRSPEC 2	575	3160	4	-0.5	2.5	20.963
NIRSPEC 3	550	3160	4	-0.5	2.5	21.613

Table 3.3 The best three forward model fitting parameters are given with the reduced X^2 value for 0146

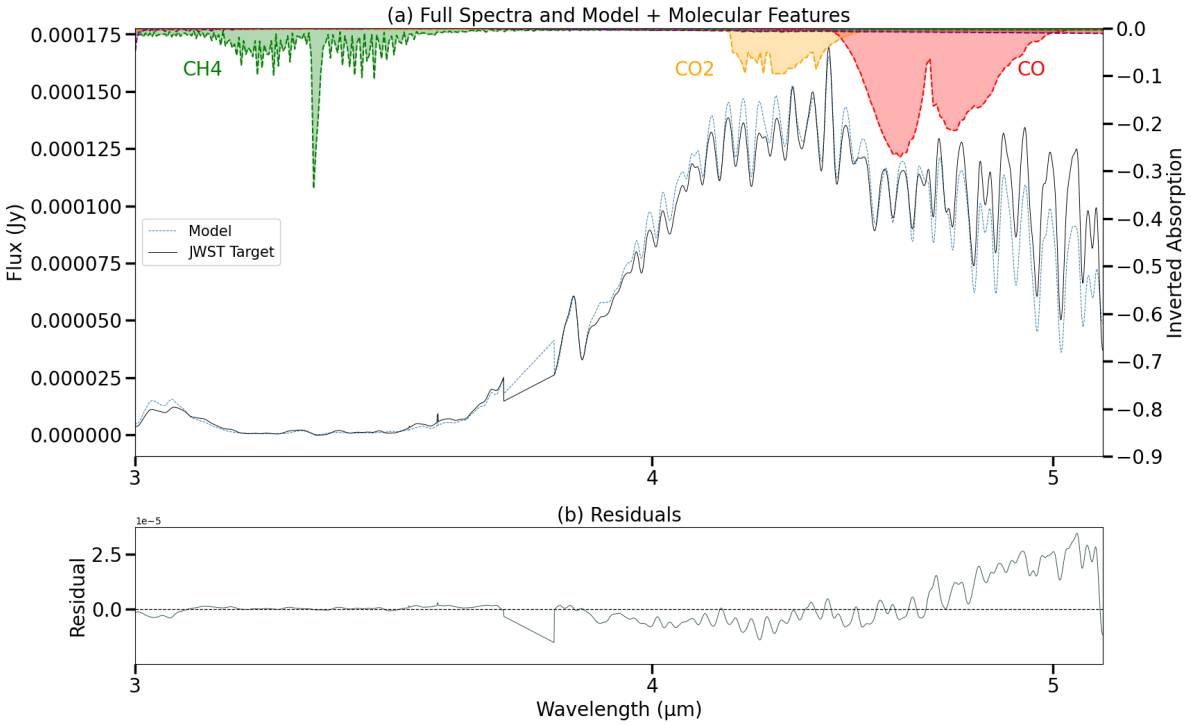

Figure 3.6 Plot (a) shows the spectra from 3.5 μm to 14 μm displaying the best fit model over the observed data for 0146. Molecular absorption is shown for refrence on the inverted axes. Plot (b) shows the residuals of the model fit to the data.

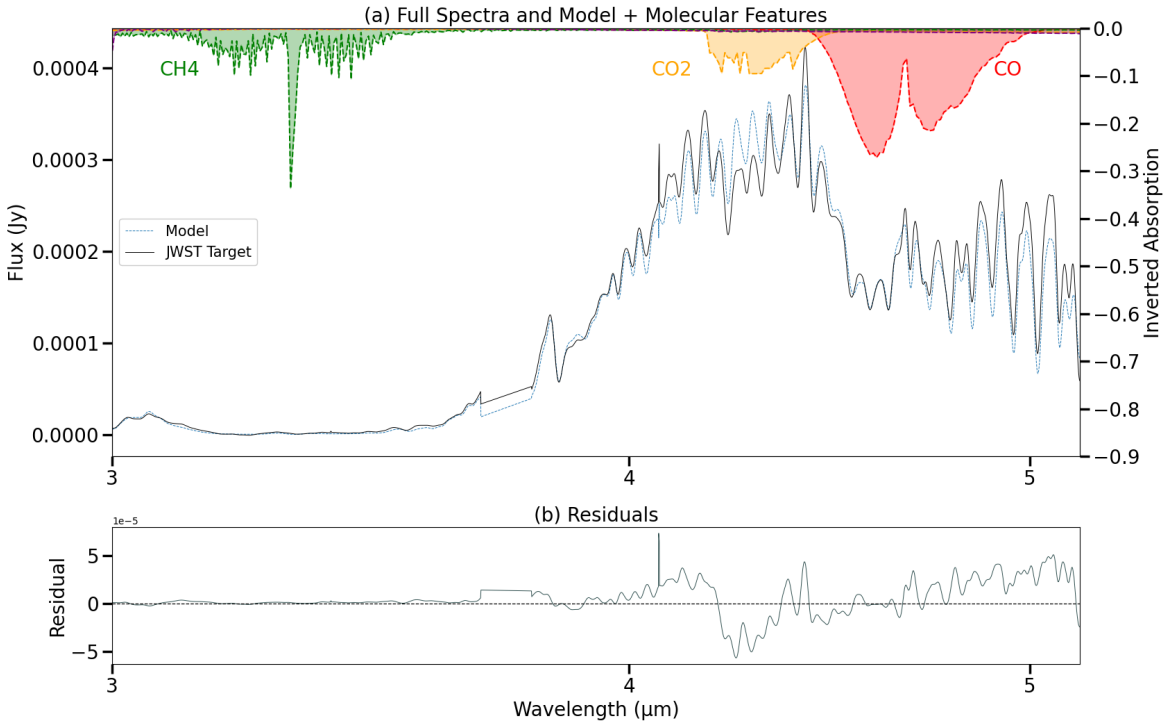

Figure 3.7 Plot (a) shows the spectra from 3.5 μm to 14 μm displaying the best fit model over the observed data for 2220. Molecular absorption is shown for refrence on the inverted axes. Plot (b) shows the residuals of the model fit to the data.

3.1.4 WISE J222055.31-362817.4

The results for object 2220 reiterate those found for 0146. From the limited data we do have of both 0146 and 2220 we do see that the models favor a high carbon to oxygen ratio, a low metallicity, and higher values for vertical mixing. This would suggest that these objects are much older than the Sun. They would have formed a long time ago and significantly cooled to the present day. The presence of high levels of carbon require strong mixing in order to dredge up the atmosphere.

Weighting	teff	grav	kzz	mh	co	Reduced X^2
NIRSPEC 1	500	3160	7	-0.5	2.5	87.454
NIRSPEC 2	525	3160	7	-0.5	2.5	89.339
NIRSPEC 3	475	3160	8	-0.5	2.5	89.499

Table 3.4 The best three forward model fitting parameters are given with the reduced X^2 value for 2220.

3.1.5 WISEA J082507.37+280548.2

Returning to more insightful spectra, we encounter a strongly misbehaving example in 0825. Figure 3.8 shows a close fit to the NIRSPEC data when weighted accordingly, but the model completely fails to produce the appropriate strenght in flux beyond 7 μm. Conversely, when weighted to the MIRI data, as shown in Figure 3.10, the model significantly overpredicts the flux below 4.4 μm and underpredicts it above this wavelength. Neither model provides an adequate description of the atmosphere of 0825.

Object 0825 exhibits drastic changes in fitted parameters between the two forward models. Every value changes substantially between fits. Most suprising is the change from being metal poor to metal rich and moving from the high extreme of carbon to oxygen to the low extreme. The lower carbon-to-oxygen ratio in the MIRI-weighted fit increases the flux around 4.2 μm, while

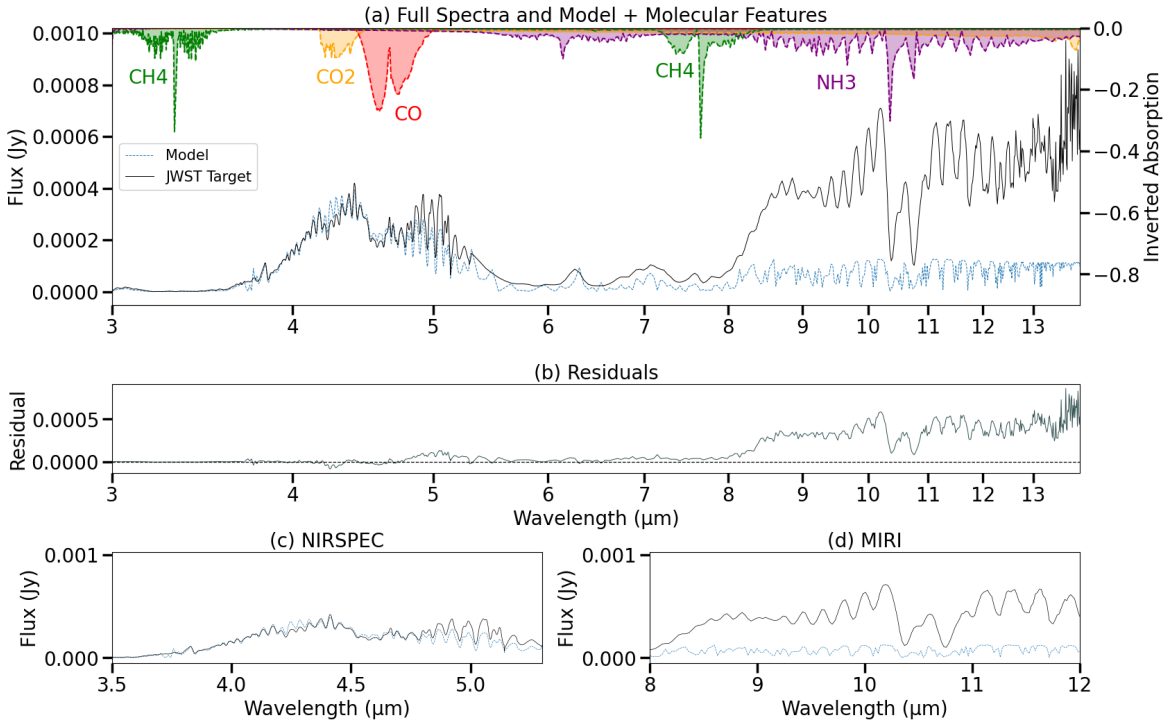

Figure 3.8 This plot shows the best fit weighted to the NIRSPEC data for 0825. Plot (a) show the spectra from 3.5 μm to 14 μm displaying the best fit model over the observed data. Molecular absorption is shown for refrence on the inverted axes. Plot (b) shows the residuals of the model fit to the data. Plots (c) and (d) zoom in on the 3.5-5.3 μm and 5-12 μm region for better resolution, respectively.

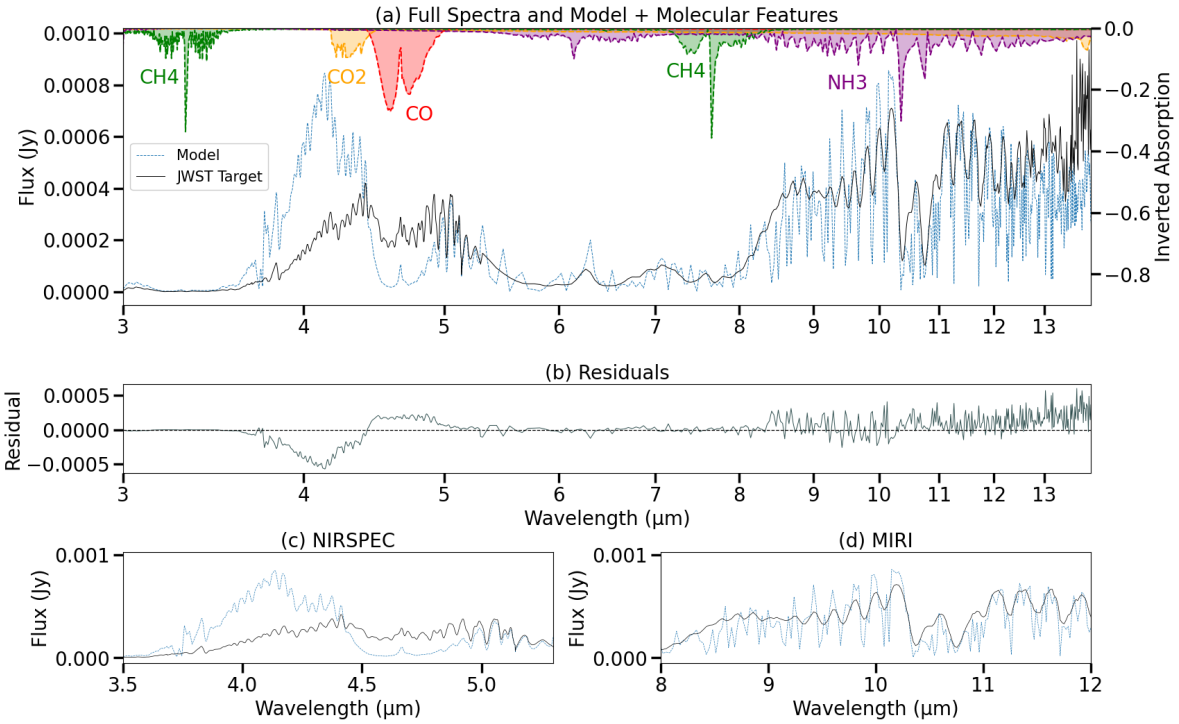

Figure 3.9 This plot shows the best fit weighted to the MIRI data for 0825. Plot (a) show the spectra from 3.5 μm to 14 μm displaying the best fit model over the observed data. Molecular absorption is shown for refrence on the inverted axes. Plot (b) shows the residuals of the model fit to the data. Plots (c) and (d) zoom in on the 3.5-5.3 μm and 5-12 μm region for better resolution, respectively.

enhanced vertical mixing amplifies the discrepancy at the inversion point where the model begins to underpredict the flux.

Weighting	teff	grav	kzz	mh	co	Reduced X^2
NIRSPEC 1	400	316	8	-1	2.5	145.351
NIRSPEC 2	400	316	9	-1	2.5	145.638
NIRSPEC 3	425	562	9	-1	2.5	146.951
MIRI 1	525	3160	4	1	0.5	2602.245
MIRI 2	550	3160	4	1	0.5	2614.245
MIRI 3	525	3160	7	1	0.5	2619.542
Binary	450	1000	2	0.5	2.5	
	450	316	7	1	0.5	3696.862

Table 3.5 The best three forward model fitting parameters are given with the reduced X^2 value for 0825 when considering only the NIRSPEC (3-5 μm) region of spectra. Below that is the best three forward model fitting parameters with the reduced X^2 value when considering only the MIRI (5-12 μm). Finally, a single binary forward model shows the best fitted parameters.

Because of the great discrepency in best fit models for 0825, I thought this could be an indicator that this is a binary system. The binary fit, as shown in Figure 3.10, unfortunately, does not perform better than the NIRSPEC or MIRI best fits, and clearly still makes compromises. Based my other analyses, we will need to better constrain our understanding of the atmospheric interactions of single Y dwarfs and demonstrate effective forward modeling before making assumptions of the binary structure.

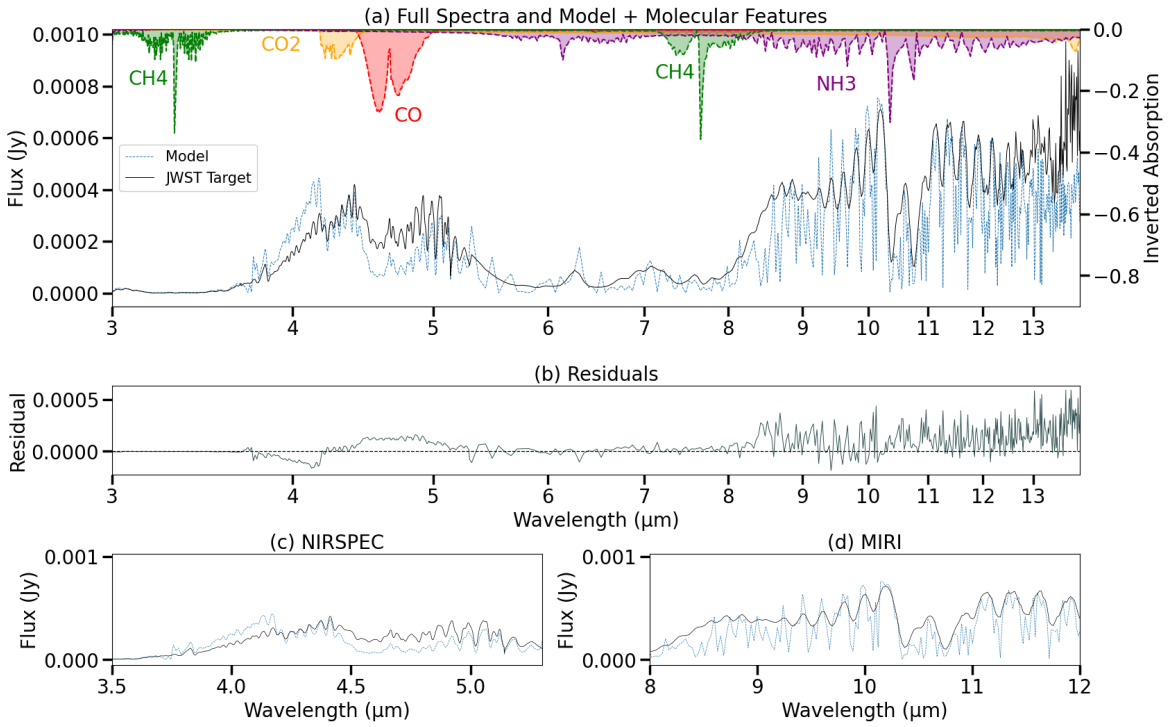

Figure 3.10 Graph showing the spectra of 0825 from 0.9-14 μm using the binary fit modeling. Two models were added together and scaled then forward modeled to create a best fit. Plot (a) show the spectra from 3.5 μm to 14 μm displaying the best fit models over the observed data and scaled. Molecular absorption is shown for refrence on the inverted axes. Plot (b) shows the residuals of the models fit to the data. Plots (c) and (d) zoom in on the 3.5-5.3 μm and 5-12 μm region for better resolution, respectively.

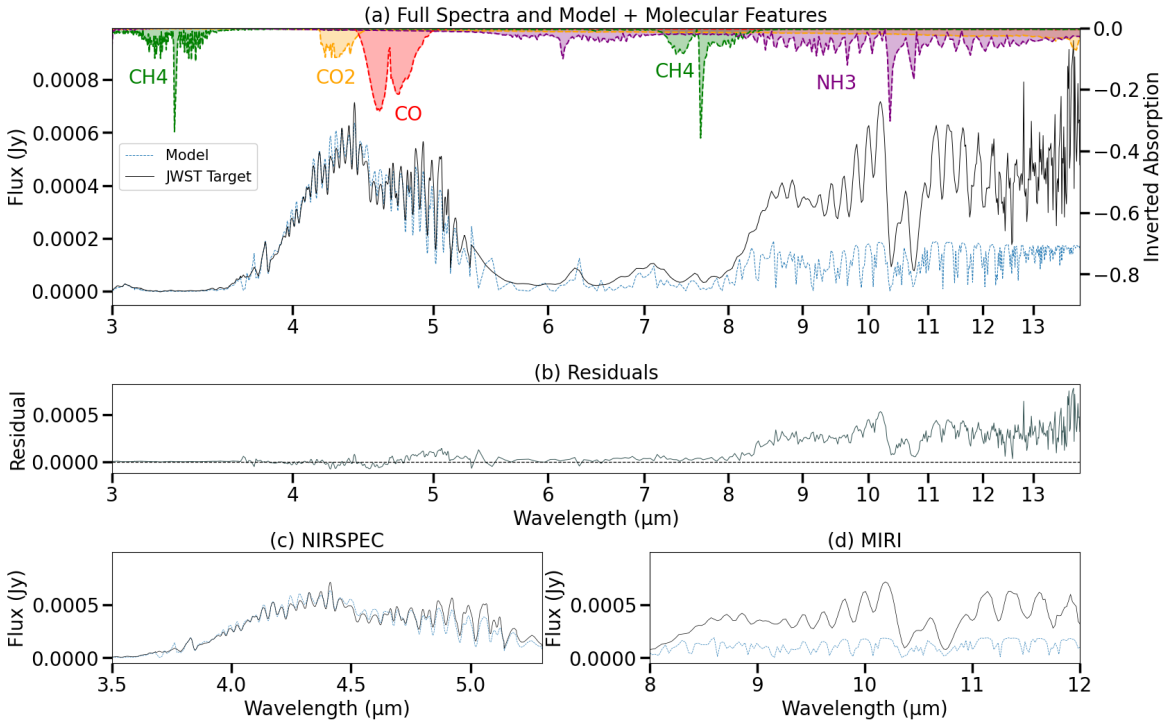

Figure 3.11 This plot shows the best fit weighted to the NIRSPEC data for 1405. Plot (a) show the spectra from 3.5 μm to 14 μm displaying the best fit model over the observed data. Molecular absorption is shown for refrence on the inverted axes. Plot (b) shows the residuals of the model fit to the data. Plots (c) and (d) zoom in on the 3.5-5.3 μm and 5-12 μm region for better resolution, respectively.

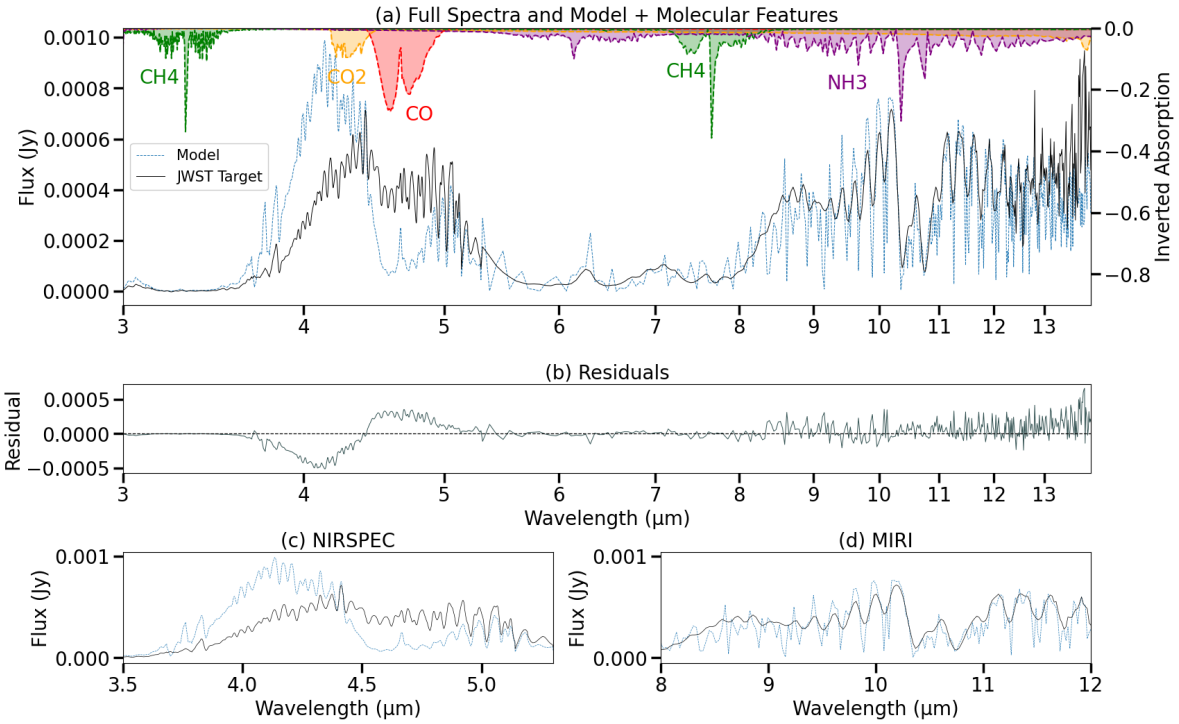

Figure 3.12 This plot shows the best fit weighted to the MIRI data for 1405. Plot (a) show the spectra from 3.5 μm to 14 μm displaying the best fit model over the observed data. Molecular absorption is shown for refrence on the inverted axes. Plot (b) shows the residuals of the model fit to the data. Plots (c) and (d) zoom in on the 3.5-5.3 μm and 5-12 μm region for better resolution, respectively.

3.1.6 WISE J140518.39+553421.3

A similar pattern is exhibited for object 1405. The NIRSPEC data can be fit reasonably well when considered in isolation, but the model fails to reproduce the magnitude of the flux beyond 7 μm. When weighted to the MIRI data, the fit across the NIRSPEC wavelength range inaccurately describes the shape of the spectra. Most significantly, the absorption features that affect the spectra are the carbon monoxide and ammonia features, the shape of which is correctly accounted for given I weight the wavelength regime each respectively inhabits.

Weighting	teff	grav	kzz	mh	co	Reduced X^2
NIRSPEC 1	400	562	8	-1	2.5	70.053
NIRSPEC 2	375	562	9	-1	2.5	70.265
NIRSPEC 3	425	562	8	-1	2.5	71.276
MIRI 1	525	3160	4	0.7	0.5	1461.242
MIRI 2	550	3160	4	1	0.5	1481.361
MIRI 3	525	3160	4	1	0.5	1491.368

Table 3.6 The best three forward model fitting parameters are given with the reduced X^2 value for 1405 when considering only the NIRSPEC (3-5 μm) region of spectra. Below that is the best three forward model fitting parameters with the reduced X^2 value when considering only the MIRI (5-12 μm).

3.1.7 WISE J154151.62-225024.9

The spectrum of 1541 provides a detailed and representative example of a Y-type brown dwarf. It exhibits a first peak in flux around 4 μm followed by a drop beyond 5 μm, and the brightest emission beginning around 8 μm and extending through 12 μm with a strong ammonia absorption feature. As with the other brown dwarfs, we observe similar spectral patterns and similar failures in the model fits. We see there is a disparity between effective surface temperatures and between surface gravities.

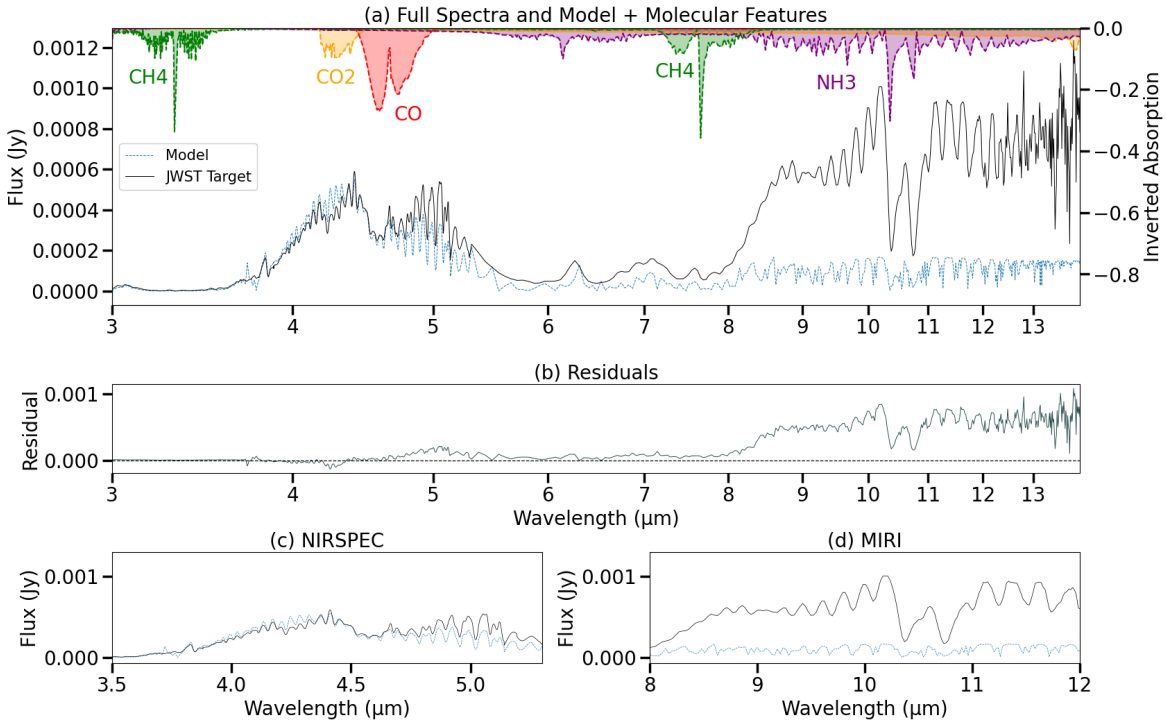

Figure 3.13 This plot shows the best fit weighted to the NIRSPEC data for 1541. Plot (a) show the spectra from 3.5 μm to 14 μm displaying the best fit model over the observed data. Molecular absorption is shown for refrence on the inverted axes. Plot (b) shows the residuals of the model fit to the data. Plots (c) and (d) zoom in on the 3.5-5.3 μm and 5-12 μm region for better resolution, respectively.

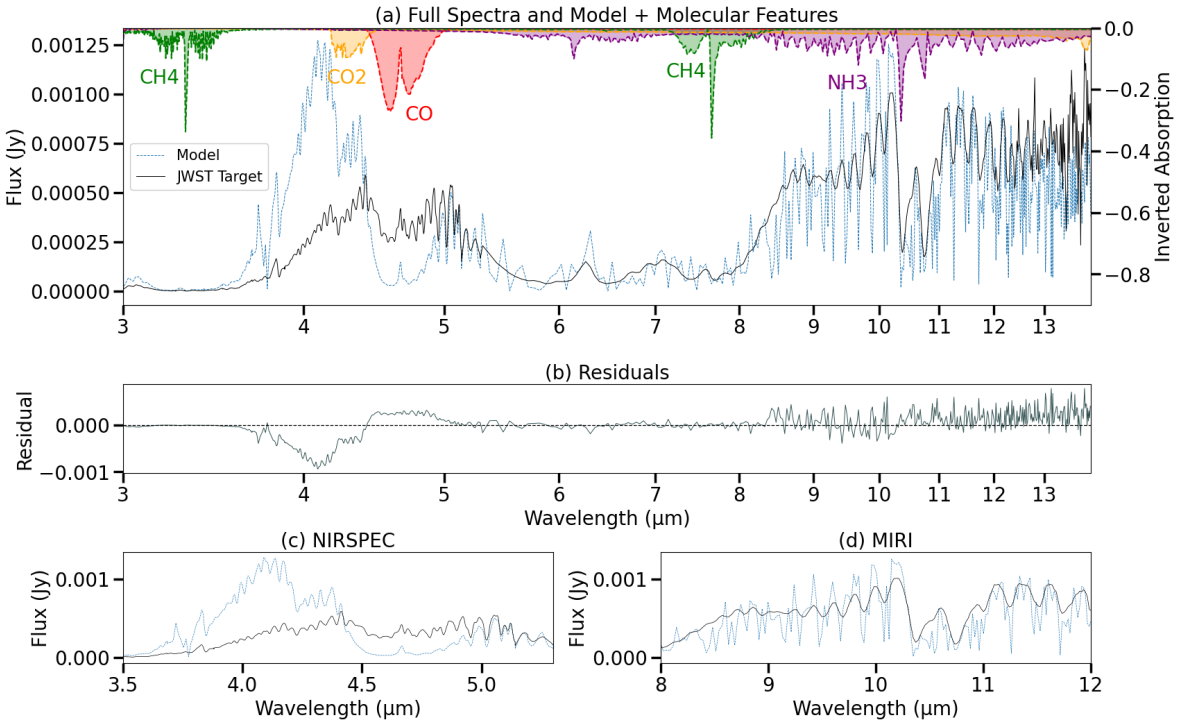

Figure 3.14 This plot shows the best fit weighted to the MIRI data for 1541. Plot (a) show the spectra from 3.5 μm to 14 μm displaying the best fit model over the observed data. Molecular absorption is shown for refrence on the inverted axes. Plot (b) shows the residuals of the model fit to the data. Plots (c) and (d) zoom in on the 3.5-5.3 μm and 5-12 μm region for better resolution, respectively.

We also see the NIRSPEC favors higher vertical mixing, lower metallicities, and higher carbon to oxygen ratio. The greater strenght in carbon dioxide is apparent in the MIRI best fit model.

Weighting	teff	grav	kzz	mh	co	Reduced X^2
NIRSPEC 1	425	562	9	-1	2.5	154.778
NIRSPEC 2	450	562	8	-1	2.5	456.160
NIRSPEC 3	425	562	8	-1	2.5	156.653
MIRI 1	550	3160	4	1	0.5	2571.732
MIRI 2	575	3160	4	1	0.5	2604.176
MIRI 3	525	3160	4	1	0.5	2617.600

Table 3.7 The best three forward model fitting parameters are given with the reduced X^2 value for 1541 when considering only the NIRSPEC (3-5 μm) region of spectra. Below that is the best three forward model fitting parameters with the reduced X^2 value when considering only the MIRI (5-12 μm).

3.2 Discussion

Now that we have gone over extreme best fits for each of the objects, I will share the general trends for each of the parameters and an analysis of what needs to be improved to make forward modeling useful for Y type brown dwarfs. The previous subsection showed best fits separating the NIRSPEC and MIRI data ranges, but in this section the analysis will be done using the overall best fits which appropriately consider resolution differences between the NIRSPEC and MIRI parts of the spectra. These best fits for each object are shown in Table 3.8.

Target	teff	grav	kzz	mh	co	Reduced X^2
0415	850	3160	4	-0.5	2.5	147.516
0535	550	3160	2	0.5	1.5	1722.780
0146	600	3160	4	-0.5	2.5	20.791
2220	500	3160	7	-0.5	2.5	87.454
0825	475	562	2	1	0.5	3074.180
1405	525	3160	2	0.5	1.5	1455.721
1541	525	3160	4	1	1.5	3093.527

Table 3.8 This table compiles the best fit Elf Owl models for each target. These are the best fits using both the NIRSPEC and MIRI data, weighting the MIRI data more to account for weaker resolution. The reduced X^2 is given for each best fit for reference.

3.2.1 Carbon to Oxygen Ratio

The carbon to oxygen ratio significantly affects the shape of the spectral curve and is perhaps the most significant parameter in this study. This parameter could also be a major stumbling block in forward fitting the Elf Owl models. It governs prominent absorption features associated with molecules such as CO and CO2. While carbon-to-oxygen ratio is crucial for understanding atmospheric composition, the detailed molecular interactions are not adequately captured by the model. The models frequently underpredict the observed flux, particularly in the 4.4 μm region and beyond 7 μm. This suggests that the models overestimate absorption strength in regions where carbon-oxygen chemistry is most important.

By nature of how stars form, stars including the Sun as well as M dwarfs such as Trappist-1 have low carbon to oxygen ratios generally between 0.4 and 0.6. Gas giants, such as Jupiter, have much higher carbon to oxygen ratios. Jupiter has a carbon to oxygen ratio of 2.9. It is typically assumed that while brown dwarfs are not massive enough to qualify for the Jeans mass, they still form from a gas collapse process. However, this study suggests that these Y dwarfs may have formed more

similarly to planets with ice capture. This could also explain the higher metallicity which will be discussed later.

This theory of brown dwarf formation does not fully explain my data. For example, 0415 is a T type brown dwarf which is much better studied and considered to have a lower carbon to oxygen ratio that what I have found [citation needed]. It also comes out to be metal poor which would be difficult to explain if it formed like a planet. 0825 has the opposite problem. While it appears to be metal rich, it is comparatively carbon poor.

The dwarfs 0535, 1405, and 1541 are fairly similar and it makes sense to assume that they had similar formation stories. If they formed recently by the process that forms planets, then this could explain their temperatures, metallicities, and carbon to oxygen ratios. If 0415 has a high carbon to oxygen ratio and a low metallicity, then this could be explained by it being a much older brown dwarf but one that formed similarly to planets. 0825 is probably the hardest to explain as it is very star-like in its carbon to oxygen ratio but it is very cool and its metallicity suggests that it is much younger which are contradictory attributes. Perhaps 0825 does turn out to be a binary system.

CO ratio	0415	0535	0146	2220	0825	1405	1541
0.5	1.354	1.256	2.141	1.562	0.318*	1.304	1.265
1.0	1.185	1.140	1.572	1.241	1.046	1.014	1.085
1.5	1.092	0.169*	1.250	1.097	1.090	0.343*	0.578*
2.5	5.336*	0.962	0.038*	0.109*	1.075	1.108	0.920

Table 3.9 This table shows the change in residuals of each of the target objects relative to the Carbon to Oxygen ratio with all other parameters fixed based on the best fit as shown in Table 3.8. The top row shows the object. The far left column shows the changing Carbon to Oxygen parameter value. The values with the "$*$" next to them are the sum total residual difference between the flux of the target and the scaled flux of the model at the designated best fit Carbon to Oxygen parameter value. The remaining values in each column show the factor change based on the varying parameter compared to the best fit value.

3.2.2 Effective Temperature

With the exception of 0415, all objects in this study fall firmly within effective temperature ranges consistent with Y-dwarf classifications. Spectroscopically, effective temperature controls the overall shape of the spectrum by determining the relative magnitude of the blue versus red portions. Hotter objects exhibit more flux in the 3.5–5 μm region, while cooler objects show enhanced flux beyond 7 μm. This behavior is expected in both the models and the observations. However, effective surface temperature is poorly constrained in these models making it difficult to use to spectroscopically classify each object. More sophisticated spectroscopic classification techniques should be used to constrain temperature which will also help constrain surface gravity as it has an inversely proportional relationship to effective surface temperature. For brown dwarfs, temperature is a function of age and initial mass, both are difficult to determine. Improvement on the Elf Owl models could benefit by including age and mass, but the constraint here is that we do not yet understand the relationship completely.

3.2.3 Surface Gravity

Surface gravity alters spectral shape, but it does not appear to be a defining parameter. Variation in the surface gravity does not significantly affect the reduced X^2 in any of the model fits. This means the models are likely inconclusive in determining the true surface gravities for these objects. Notably, nearly all objects yield a best fit gravity of 3160 m/s^2—the max value the models allow—with the exception being 0825. Again, this value is poorly constrained and may require more information about the objects mass in order to become usefull. High surface gravities are physically plausible for Y dwarfs, as their lower temperatures reduce convective pressure support, leading to higher densities and stronger gravity. The effect on the spectra of increasing surface gravity should decrease absorption of heavier molecules as they sink below the atmosphere.

Teff	0415	0535	0146	2220	0825	1405	1541
450				1.031	1.129		
475				1.014	0.318*	0.903	0.962
500		0.999		0.109*	1.129	1.006	0.997
525		0.976	1.062	1.033	1.069	0.343*	0.578*
550		0.169*	0.988	1.075	1.111	1.049	1.020
575		1.001	0.980			1.060	1.070
600		1.100	0.038*				
650			1.072				
750	1.133						
800	1.024						
850	5.336*						
900	1.056						
950	1.175						

Table 3.10 This table shows the change in residuals of each of the target objects relative to the Surface Temperature with all other parameters fixed based on the best fit as shown in Table 3.8. The top row shows the object. The far left column shows the changing Surface Temperature parameter value. The values with the "$*$" next to them are the sum total residual difference between the flux of the target and the scaled flux of the model at the designated best fit Surface Temperature parameter value. The remaining values in each column show the factor change based on the varying parameter compared to the best fit value.

grav	0415	0535	0146	2220	0825	1405	1541
178					0.994		
316	1.402	1.129	1.612	1.503	0.910	1.410	1.039
562	1.373	0.985	1.269	1.347	0.318*	1.294	0.999
1000	0.939	1.034	1.116	1.174	1.090	1.180	1.010
1780	0.957	0.967	1.009	1.060	1.139	1.048	0.972
3160	5.336*	0.169*	0.038*	0.109*		0.343*	0.578*

Table 3.11 This table shows the change in residuals of each of the target objects relative to the Surface Gravity with all other parameters fixed based on the best fit as shown in Table 3.8. The top row shows the object. The far left column shows the changing Surface Gravity parameter value. The values with the "$*$" next to them are the sum total residual difference between the flux of the target and the scaled flux of the model at the designated best fit Surface Gravity parameter value. The remaining values in each column show the factor change based on the varying parameter compared to the best fit value.

3.2.4 Vertical Mixing

Vertical mixing, or eddy diffusion, plays an important role in shaping the spectra by accounting for processes such as dredging. The should be one of the most important values as it would be the mechanism that circulates certain molecules that would have fallen below the photosphere allowing them to produce an absorption spectra. Carbon monoxide and carbon dioxide ought to have condensed below the photosphere making weak absorption, however, we see strong absorption of both of these molecules in these targets. Consequently, most of these objects have high vertical mixing when weighting to the NIRSPEC region as that is where the CO and CO2 features are. However, this value goes down for the MIRI region. More suprisingly it drops further for the best fit over the whole curve. This shows that vertical mixing modifies how prominent the features due to metallicity and carbon to oxygen ratio are in the spectra.

Kzz	0415	0535	0146	2220	0825	1405	1541
2	1.030	0.169*	1.045	1.263	0.318*	0.343*	0.956
4	5.336*	1.244	0.038*	1.180	1.237	1.355	0.578*
7	1.048	1.500	1.728	0.109*	1.597	1.619	1.248
8	1.091	1.532	1.944	1.108	1.833	1.712	1.314
9	1.137	1.601	2.300	1.220	1.960	1.835	1.399

Table 3.12 This table shows the change in residuals of each of the target objects relative to the Vertical Mixing with all other parameters fixed based on the best fit as shown in Table 3.8. The top row shows the object. The far left column shows the changing Vertical Mixing parameter value. The values with the "$*$" next to them are the sum total residual difference between the flux of the target and the scaled flux of the model at the designated best fit Vertical Mixing parameter value. The remaining values in each column show the factor change based on the varying parameter compared to the best fit value.

3.2.5 Metallicity

Previous work by another student in our group found that metallicity does not significantly affect the spectra for late-type T dwarfs. However, metallicity seems to be much more impactful to the fits with early-type Y dwarfs. Metallicity is far more constrained than effective surface temperature and surface gravity. It affects the strength of the flux in the MIRI region and the carbon dioxide and cabron monoxide absorption region. Higher metallicity increases the spectral flux between 8-12 μm and decreases it between 4.2-5 μm. This is likely due to reemission.

Based on the elemental evolution model of the universe, we should expect higher metallicity to correlate with later forming brown dwarfs but this is an assumption that may not always be true. Getting the proper motion of these objects may help in determining if they formed alongside population I or population II stars which would give more insight into their initial mass function. However, as discussed, there may be different ways in which these objects form which would also

affect their metallicity. If they form more planet-like then they will have greater metallicities and if they form more star-like then they will have lower metallicities.

In the subsection on the carbon to oxygen ratio I mentioned that 0825 looks different from the other objects in that it has a star-like carbon to oxygen ratio but is also quite metal rich. This could suggest a unique process where the object started forming as a low mass star but the process was interrupted leaving it as a cool brown dwarf. It would have formed recently based on its high metal content.

I mostly ignore that 0146 and 2220 are metal poor because of the limited data I have on them. Nearly all the objects have a best fit that places them as metal poor if I only consider the NIRSPEC data. Therefore, I can assume that I have insufficient data allowing for the best fit for these objects, given more spectra, would result in higher metallicities.

mh	0415	0535	0146	2220	0825	1405	1541
-1.0	1.469	1.400	1.408	1.261	1.554	1.594	1.420
-0.5	5.336	1.565	0.038*	0.109*	1.680	1.712	1.526
0.0	0.990	1.309	1.696	1.527	1.619	1.348	1.304
0.5	1.557	0.169*	2.741	2.068	1.235	0.343*	1.101
0.7	1.898	1.102	3.027	2.305	1.020	1.193	1.052
1.0	2.160	1.273	3.794	2.808	0.318*	1.531	0.578*

Table 3.13 This table shows the change in residuals of each of the target objects relative to the Metallicity with all other parameters fixed based on the best fit as shown in Table 3.8. The top row shows the object. The far left column shows the changing Metallicity parameter value. The values with the "$*$" next to them are the sum total residual difference between the flux of the target and the scaled flux of the model at the designated best fit Metallicity parameter value. The remaining values in each column show the factor change based on the varying parameter compared to the best fit value.

Chapter 4

Conclusion

We are only beginning to probe Y dwarfs with current telescope capabilities. L- and T-type brown dwarfs have been studied extensively for the past 15–20 years, allowing their compositions and atmospheric dynamics to be more thoroughly understood. When applying models developed for L and T dwarfs to Y dwarfs, I find significant limitations in their applicability. This work demonstrates that both near- and mid-infrared data are necessary to constrain the properties of these objects. Reliance on near-infrared spectroscopy alone can lead to misidentification of key physical parameters. While gravity is required to fit the spectra, it is not a precise or well-constrained parameter. Carbon to oxygen ratio, vertical mixing, and metallicity strongly affect spectral features, yet systematic errors in how these parameters are treated lead to persistent discrepancies between models and data. The 4–4.5 μm, carbon monoxide and carbon dioxide, region is alternately over- and underpredicted, and the flux beyond 7 μm along with the ammonia feature is often underpredicted.

Despite discrepencies between the models and observed data, this study into early Y type brown dwarfs reveals an interesting nature about their composition. These brown dwarfs likely do not have solar metallicities nor do they often have star-like carbon to oxygen ratios. This could mean that the initial assumptions that brown dwarfs form from gas collapse similar to the mechanism that drives stellar birth are wrong. It could be that brown dwarfs form more similarly to planets. This

would make them increasingly important for not only exoplanet and atmospheric study but also for understanding the initial mass function and galactic archaeology. How these objects form can inform us on their abundance and of molecular evolution in our galaxy.

Future progress in this field will depend on improving the models themselves. A similar challenge once existed in modeling brown dwarfs at the L–T transition, where complex cloud physics and molecular interactions dominated the spectra. Incorporating more detailed cloud modeling and chemical absorption physics proved essential. Future work could involve using tools such as PetitRADTRANS to more precisely model these effects. Also, doing a more complete study including finding information about the proper motion, mass, and spectral classification could better constrain these results. Proper motion would tell us where these objects formed and give us an approximate idea of how recently. The mass can provide incite about the ill-constrained surface gravity and give much needed clarification about what these objects should look like compared to T dwarfs. Spectral classification would allow us to constrain effective surface temperature allowing us to make more assumptions about metallicity and even age when paird with mass.

As we gain a better understanding of the atmospheric dynamics of these ultra-cool worlds, it may become possible to return to forward modeling with a more evolved set of models capable of accurately determining the properties of Y dwarfs.

Appendix A

Model Comparison Graphs

In this appendix section I provide helpful figures to show how each parameter affects the model fit for each spectra. Each figure shows the target spectra and several models plotted on top varying one of the Elf Owls parameters keeping all other parameters constant to the best fit model whether it is coming from the NIRSPEC, MIRI, or full weighted spectrum. This can be helpful as a visual aid to see what the models are doing to the spectra.

A.0.1 0415 NIRSPEC Variable Parameters

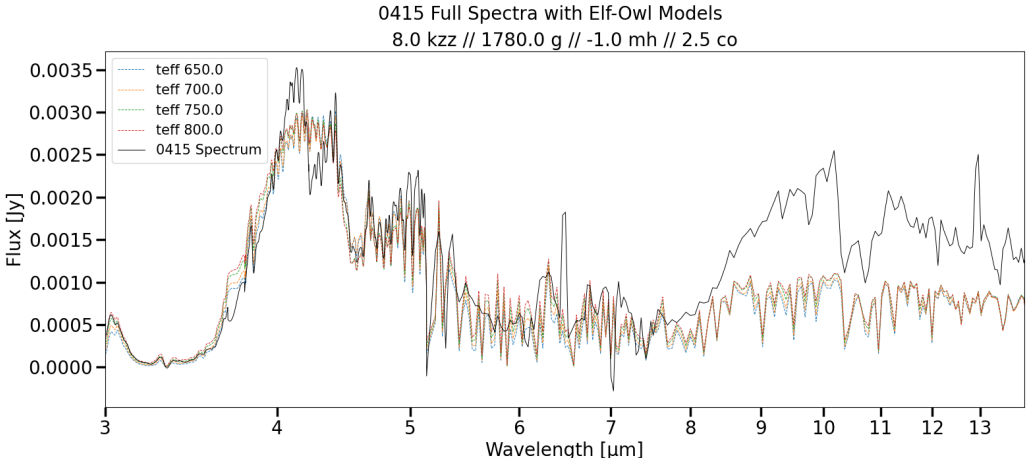

Figure A.1 0415 NIRSPEC Forward Model varying Surface Temperature

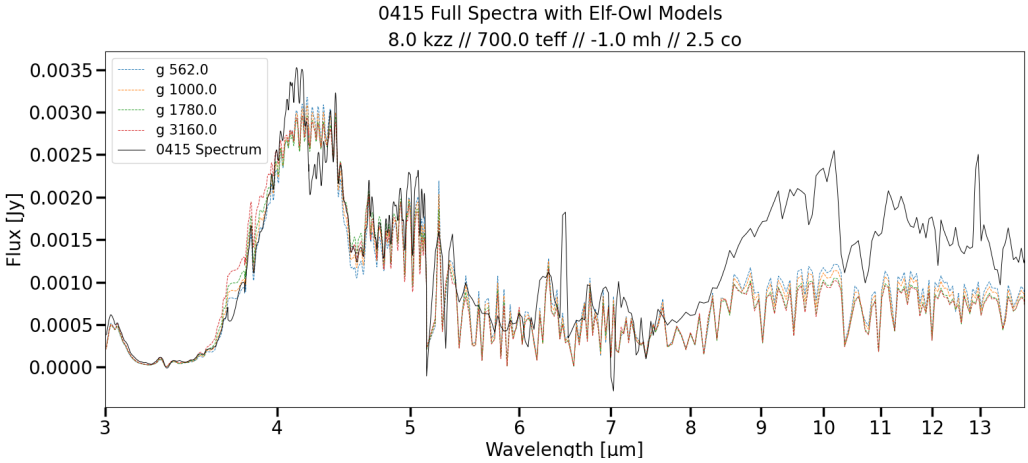

Figure A.2 0415 NIRSPEC Forward Model varying Surface Gravity

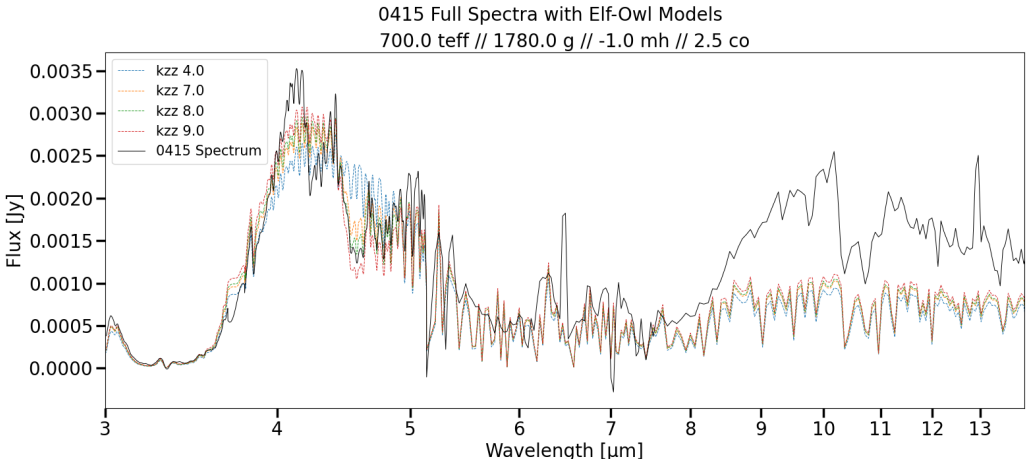

Figure A.3 0415 NIRSPEC Forward Model varying Vertical Mixing

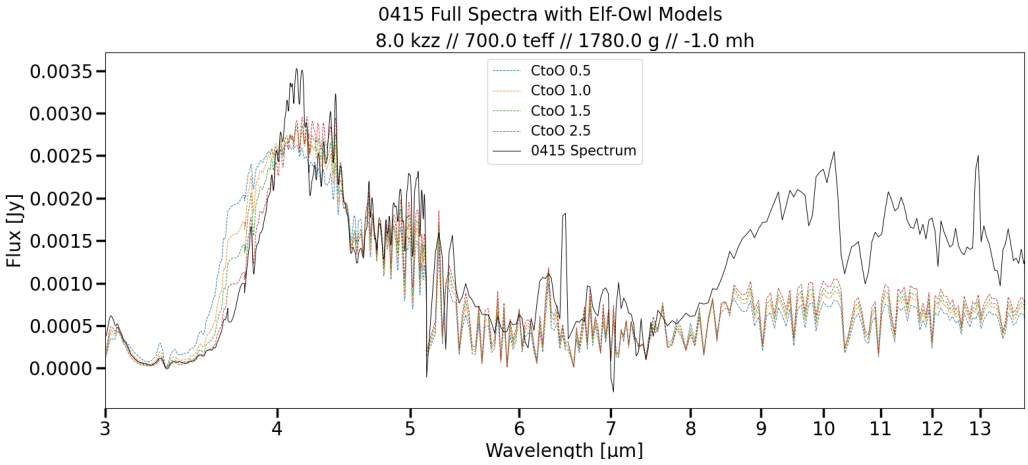

Figure A.4 0415 NIRSPEC Forward Model varying Carbon to Oxygen Ratio

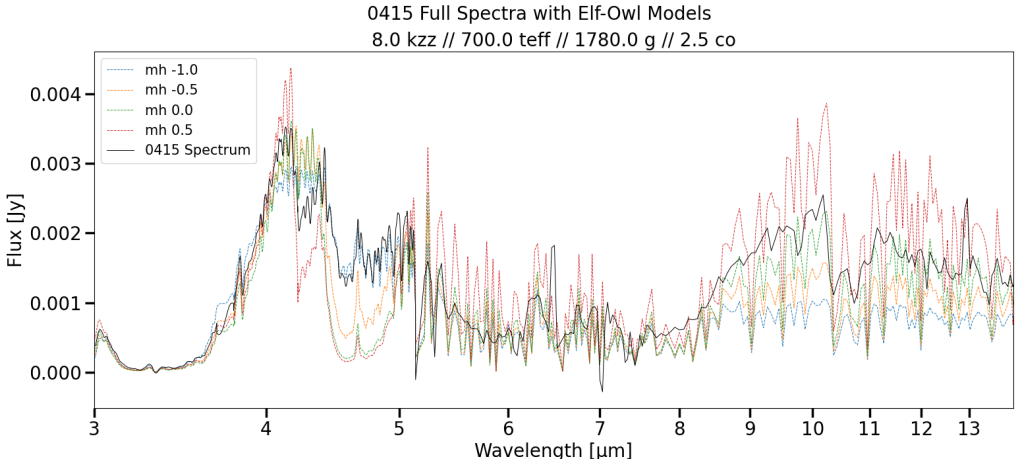

Figure A.5 0415 NIRSPEC Forward Model varying Metallicity

A.0.2 0415 MIRI Variable Parameters

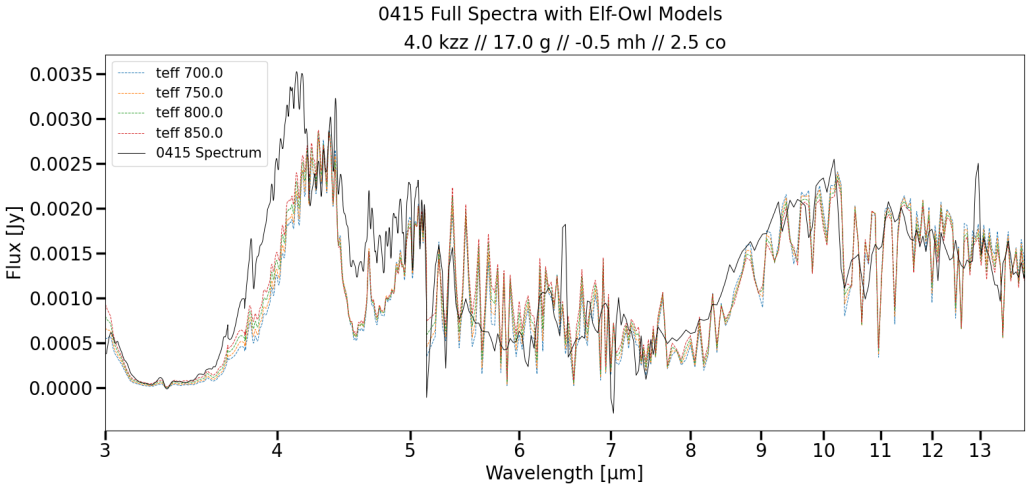

Figure A.6 0415 MIRI Forward Model varying Surface Temperature

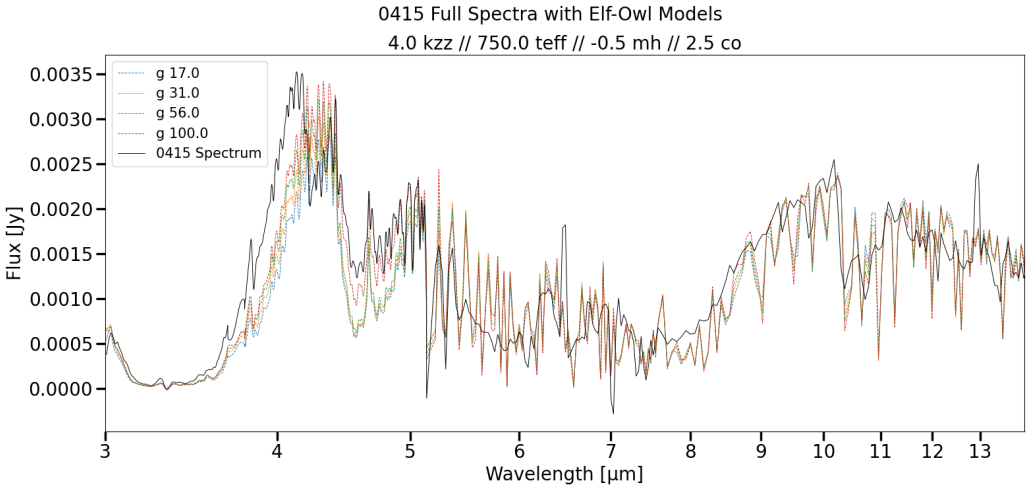

Figure A.7 0415 MIRI Forward Model varying Surface Gravity

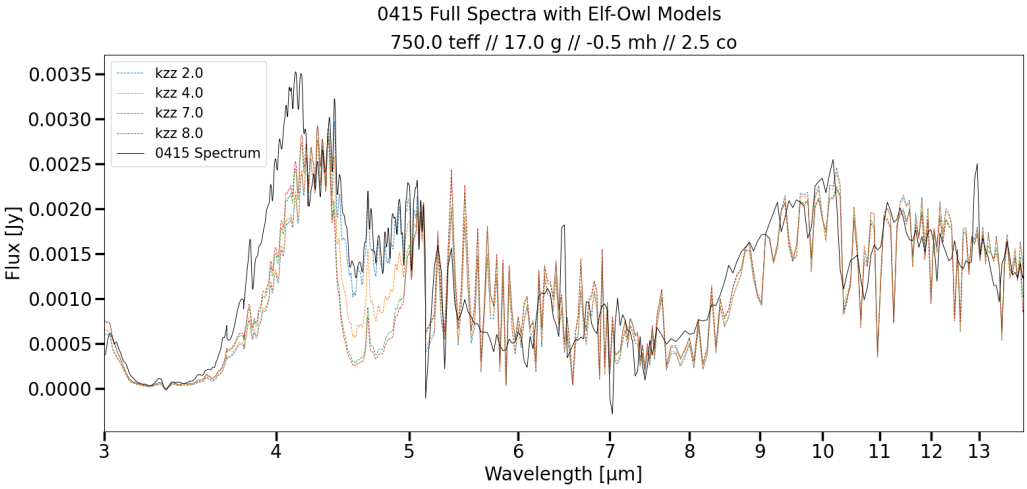

Figure A.8 0415 MIRI Forward Model varying Vertical Mixing

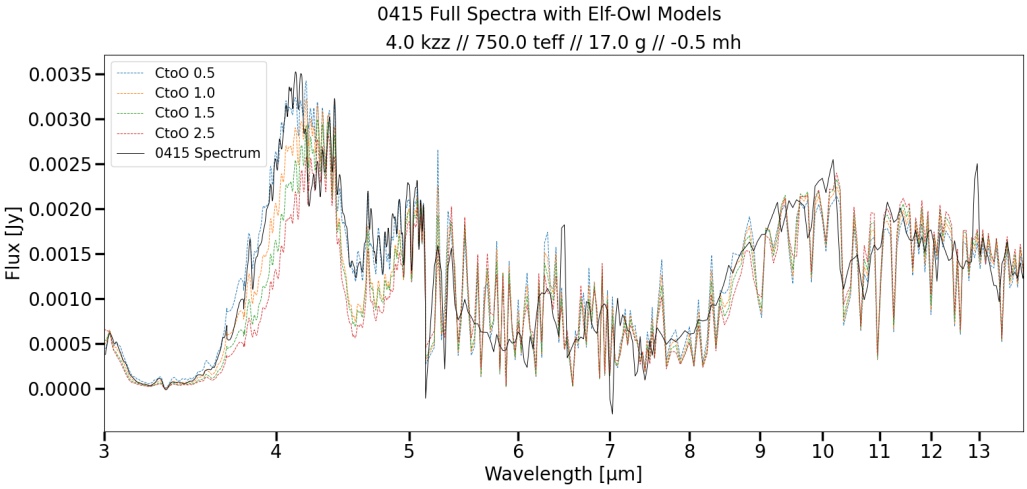

Figure A.9 0415 MIRI Forward Model varying Carbon to Oxygen Ratio

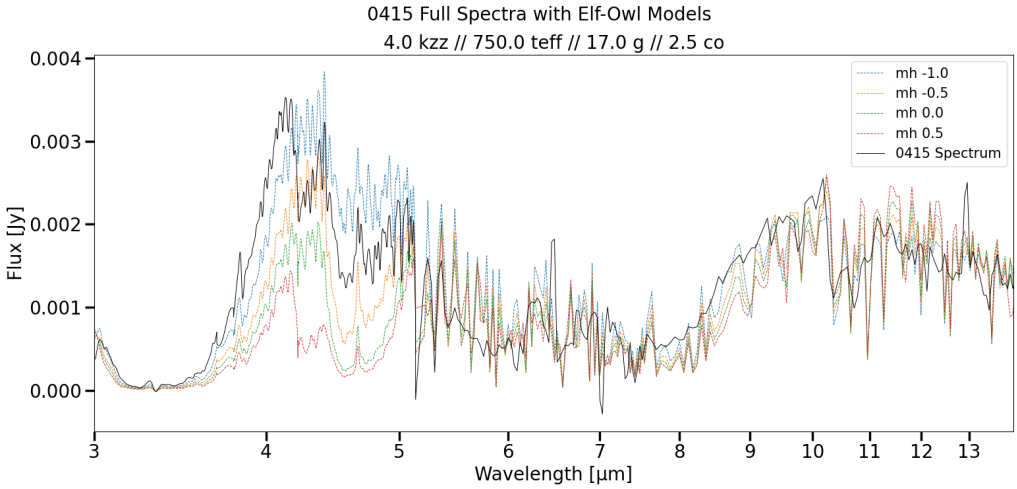

Figure A.10 0415 MIRI Forward Model varying Metallicity

A.0.3 0415 Full Variable Parameters

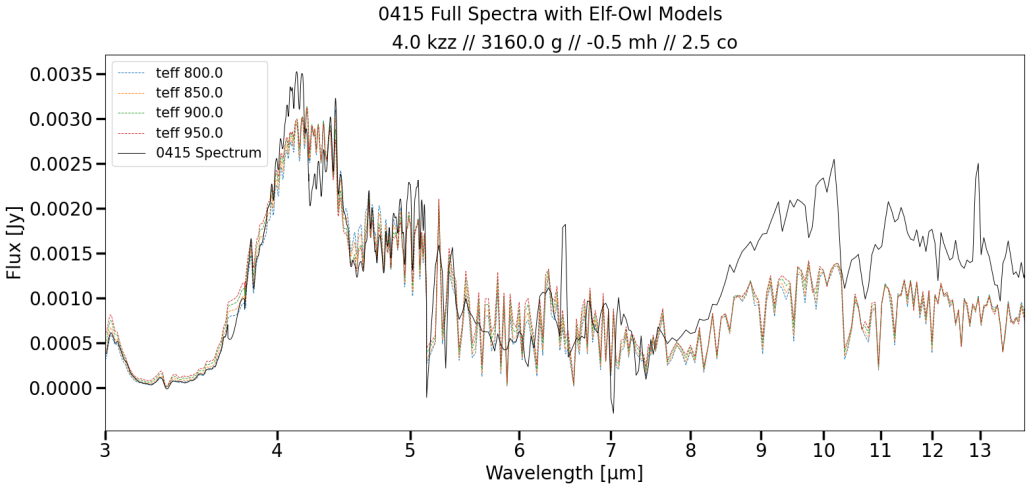

Figure A.11 0415 Full Forward Model varying Surface Temperature

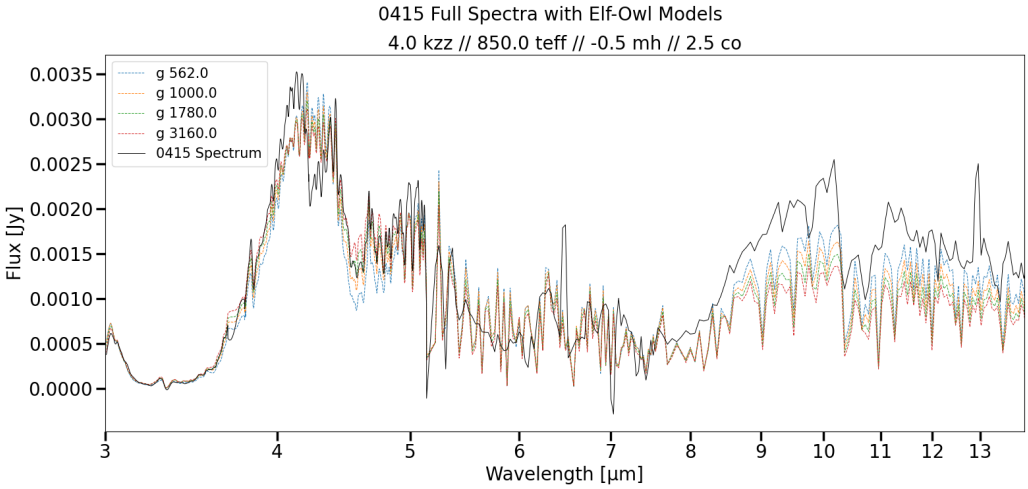

Figure A.12 0415 Full Forward Model varying Surface Gravity

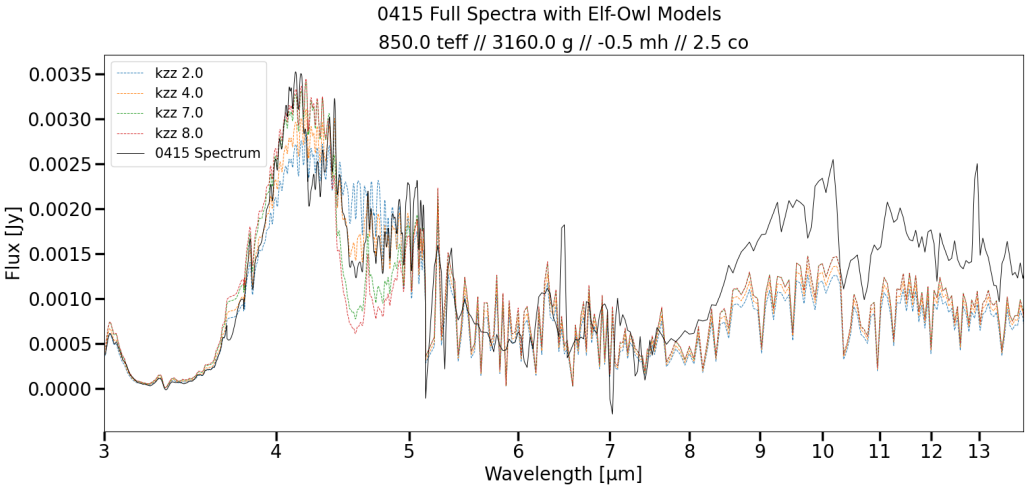

Figure A.13 0415 Full Forward Model varying Vertical Mixing

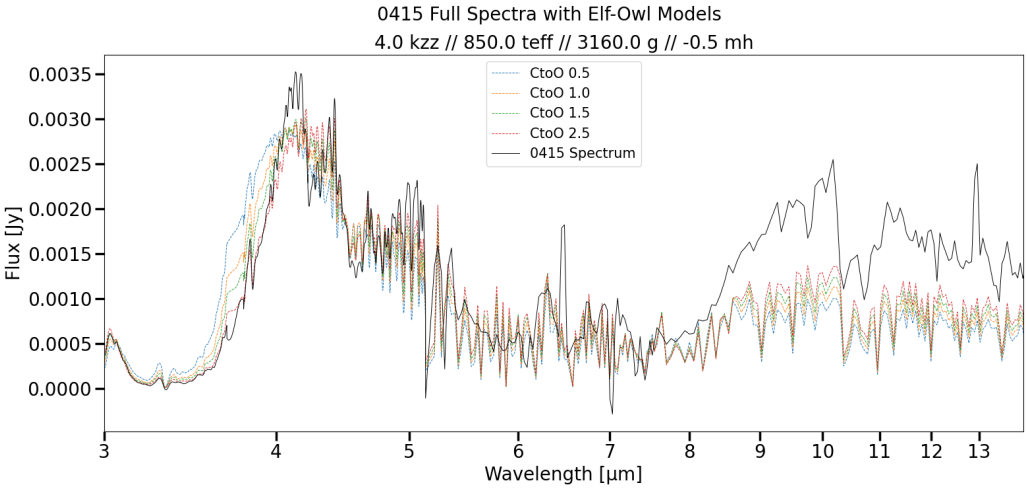

Figure A.14 0415 Full Forward Model varying Carbon to Oxygen Ratio

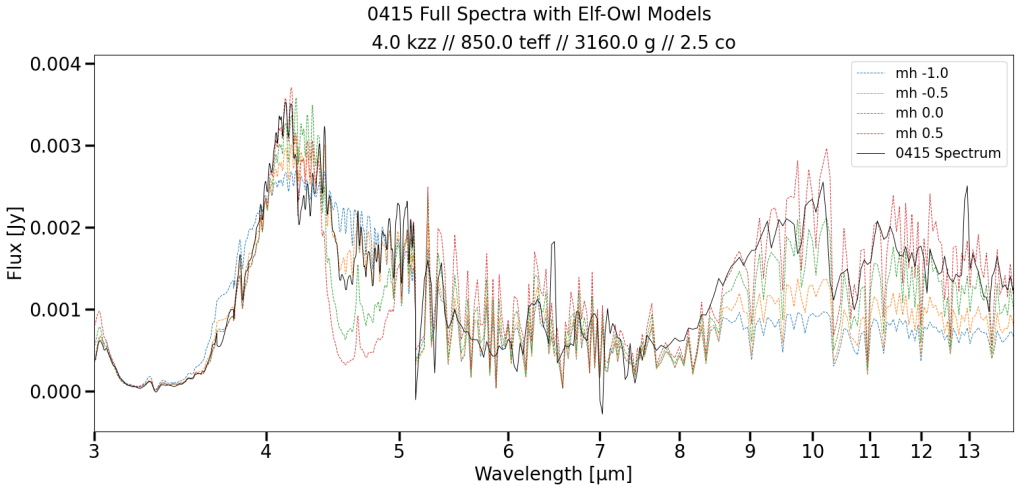

Figure A.15 0415 Full Forward Model varying Metallicity

A.0.4 0535 NIRSPEC Variable Parameters

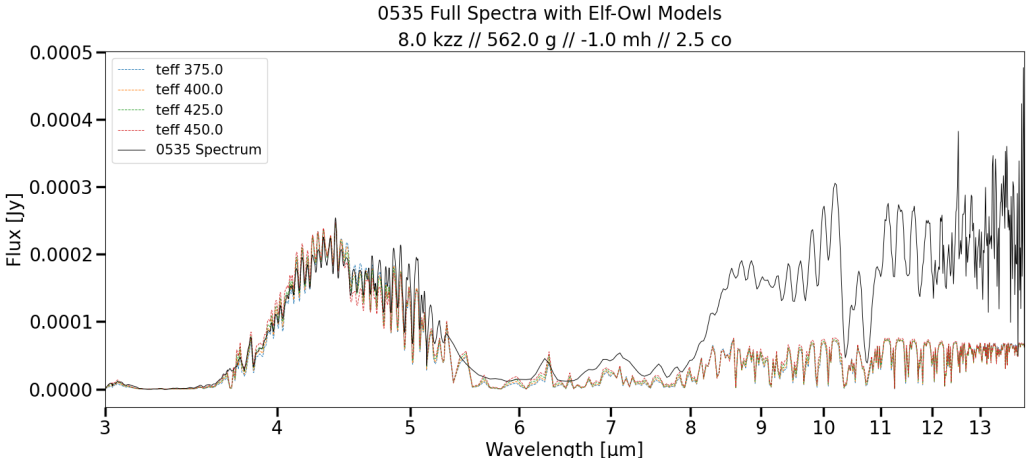

Figure A.16 0535 NIRSPEC Forward Model varying Surface Temperature

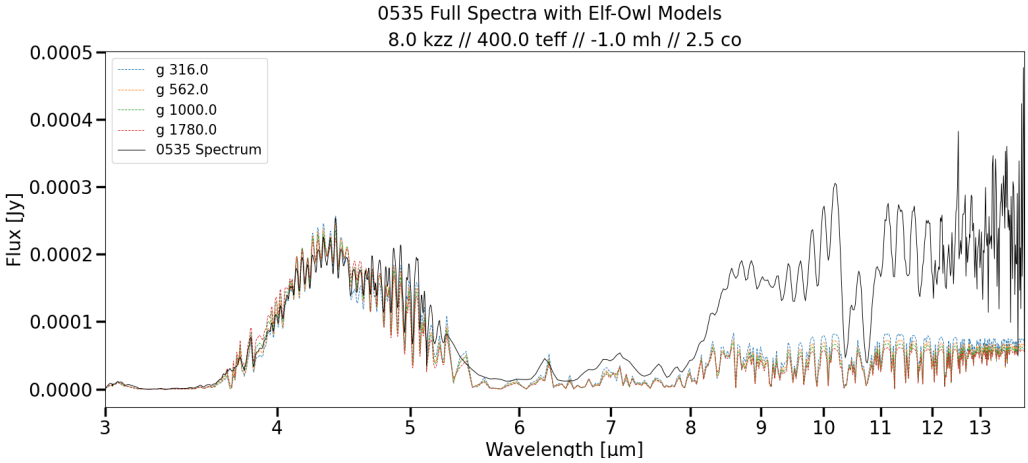

Figure A.17 0535 NIRSPEC Forward Model varying Surface Gravity

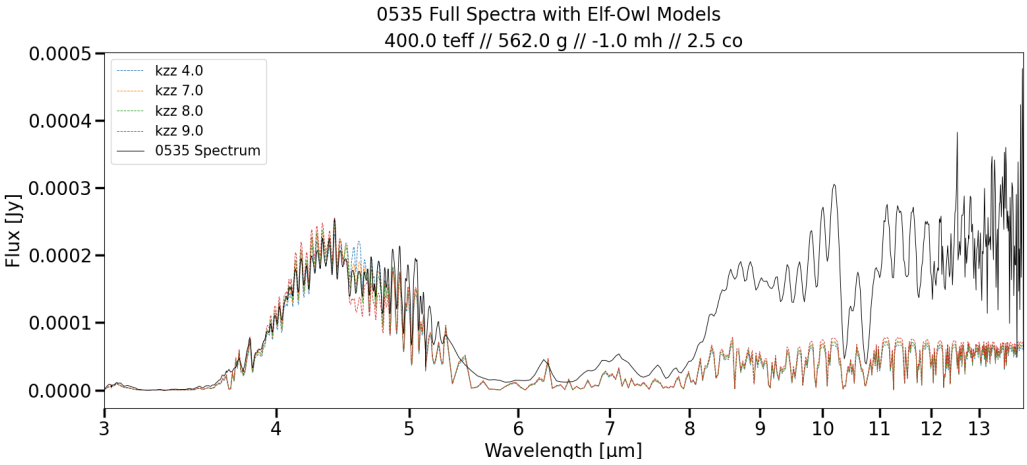

Figure A.18 0535 NIRSPEC Forward Model varying Vertical Mixing

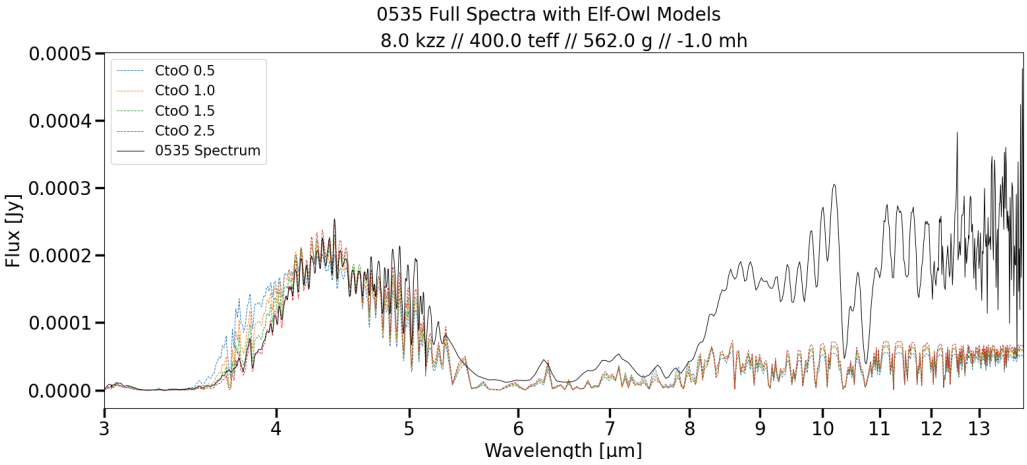

Figure A.19 0535 NIRSPEC Forward Model varying Carbon to Oxygen Ratio

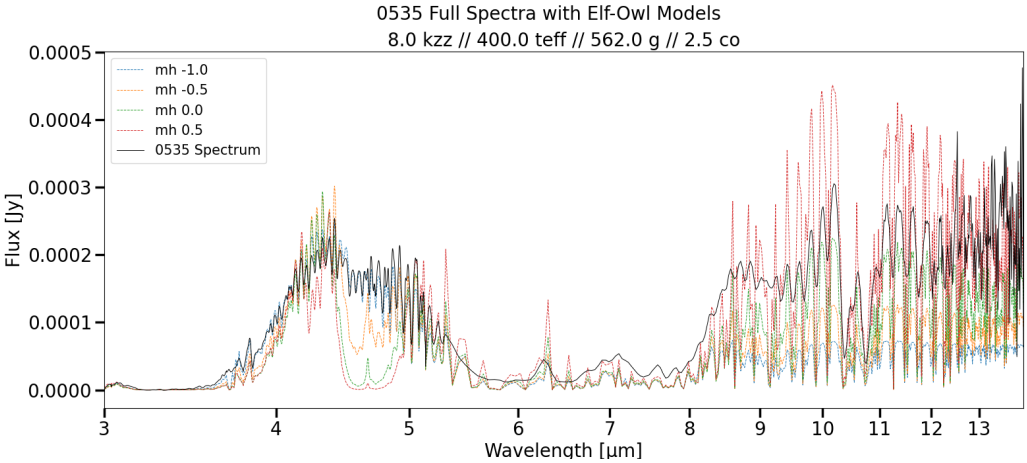

Figure A.20 0535 NIRSPEC Forward Model varying Metallicity

A.0.5 0535 MIRI Variable Parameters

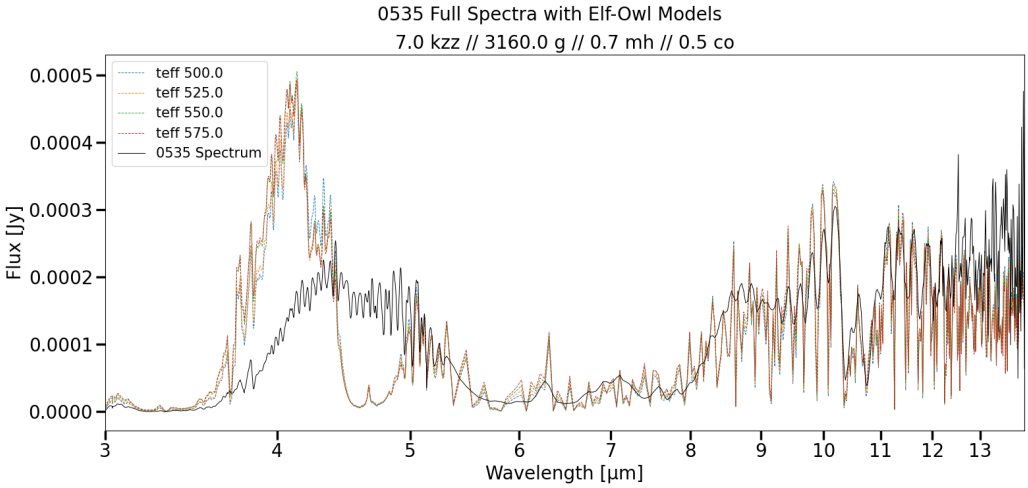

Figure A.21 0535 MIRI Forward Model varying Surface Temperature

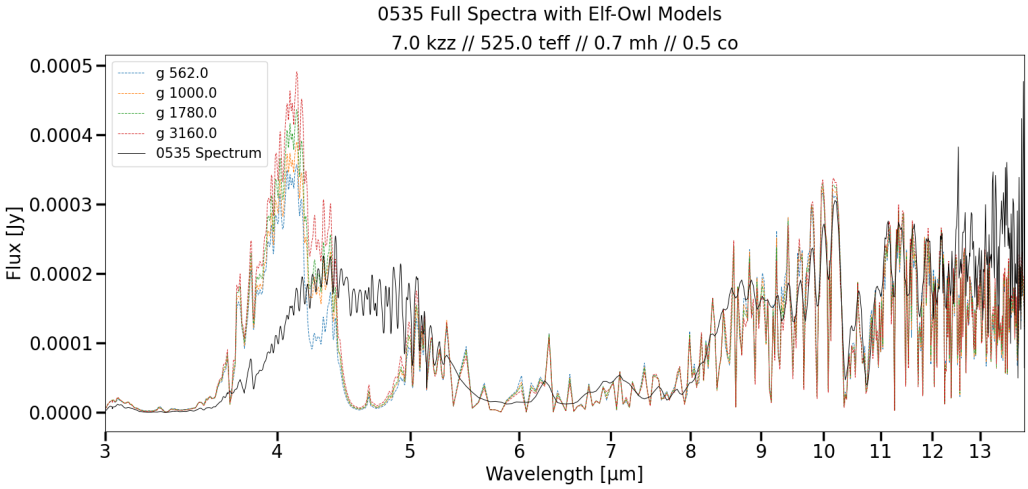

Figure A.22 0535 MIRI Forward Model varying Surface Gravity

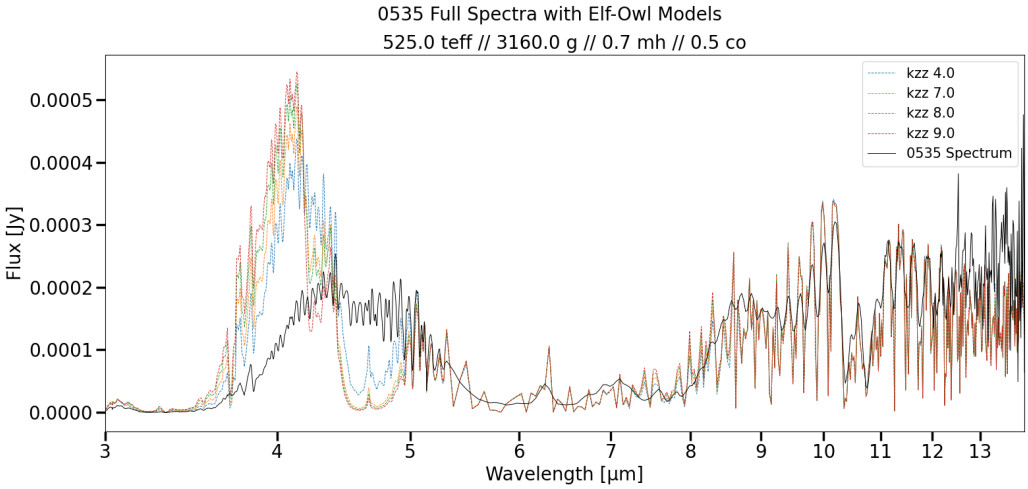

Figure A.23 0535 MIRI Forward Model varying Vertical Mixing

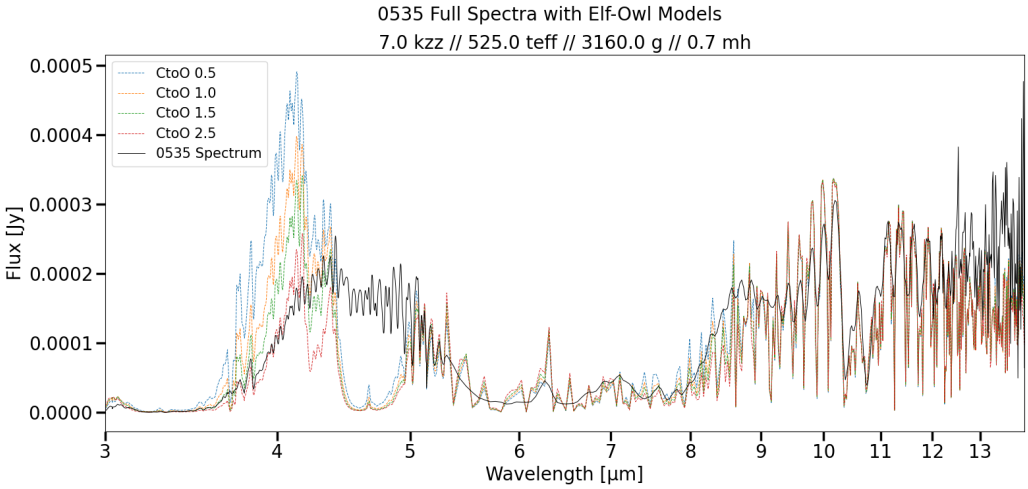

Figure A.24 0535 MIRI Forward Model varying Carbon to Oxygen Ratio

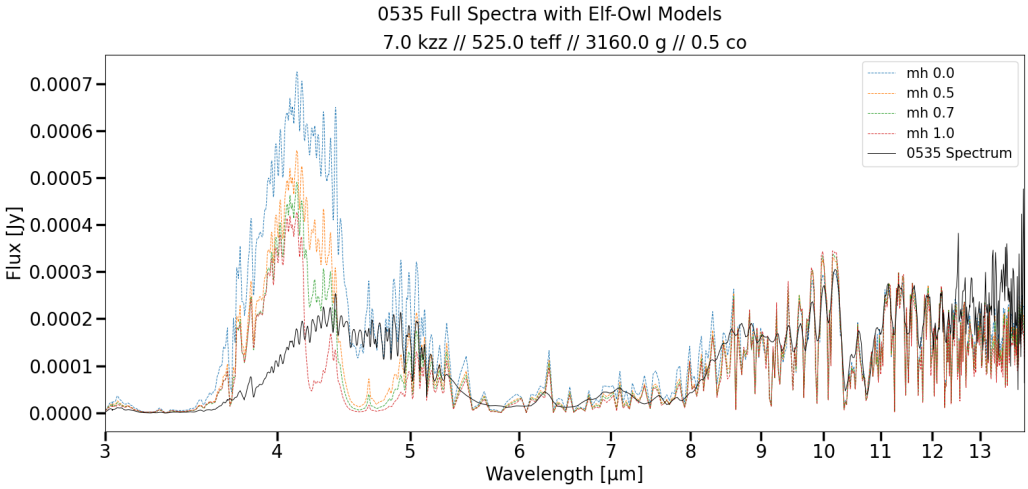

Figure A.25 0535 MIRI Forward Model varying Metallicity

A.0.6 0535 Full Variable Parameters

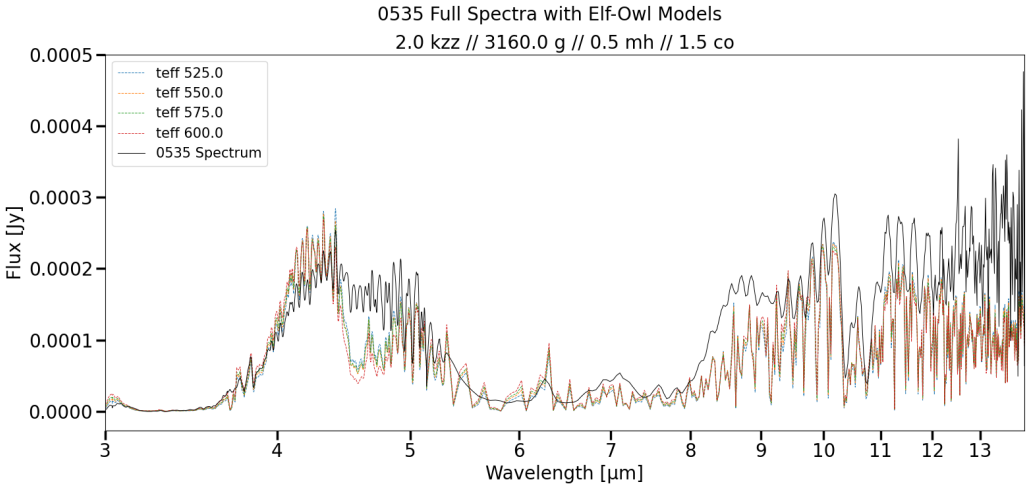

Figure A.26 0535 Full Forward Model varying Surface Temperature

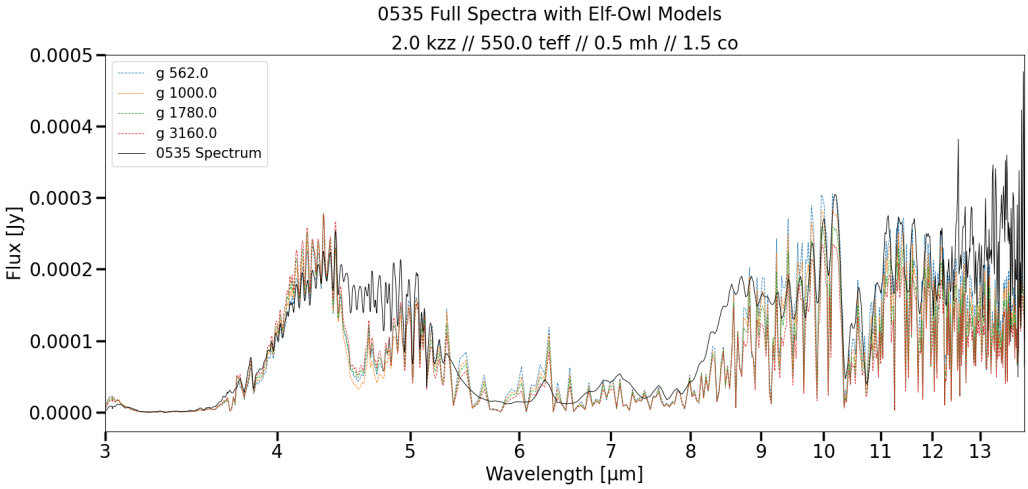

Figure A.27 0535 Full Forward Model varying Surface Gravity

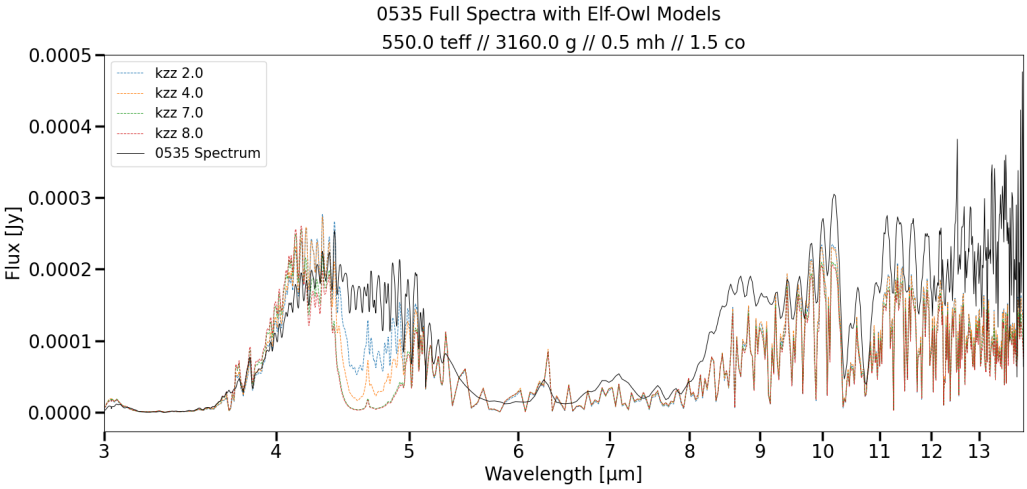

Figure A.28 0535 Full Forward Model varying Vertical Mixing

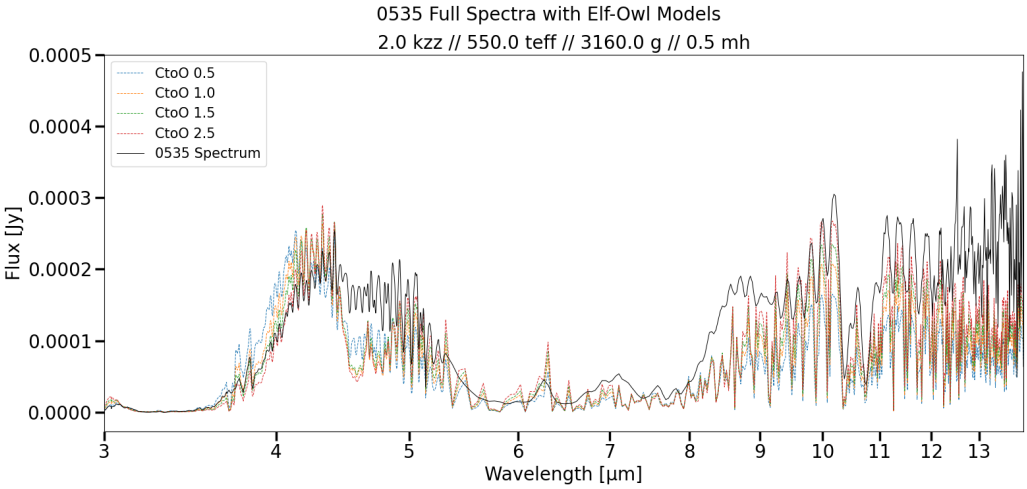

Figure A.29 0535 Full Forward Model varying Carbon to Oxygen Ratio

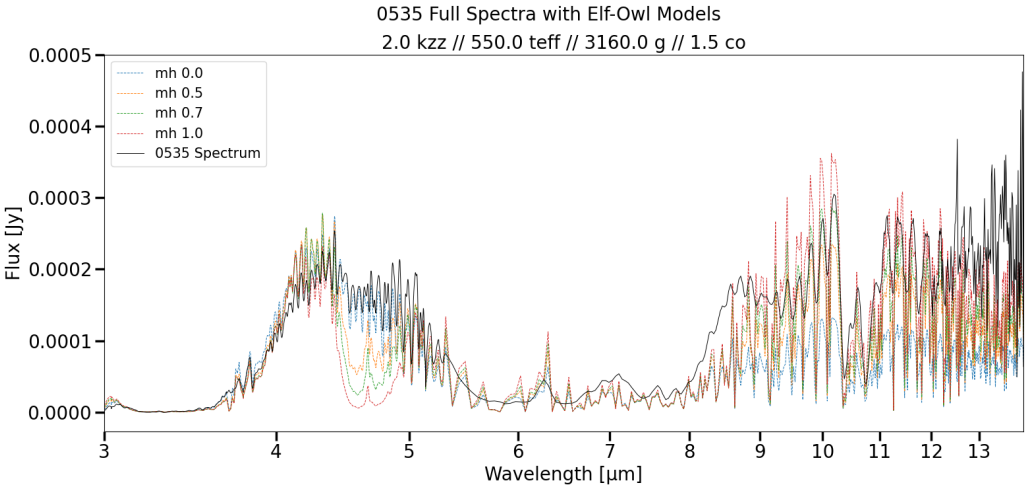

Figure A.30 0535 Full Forward Model varying Metallicity

A.0.7 0146 Best Fit Variable Parameters

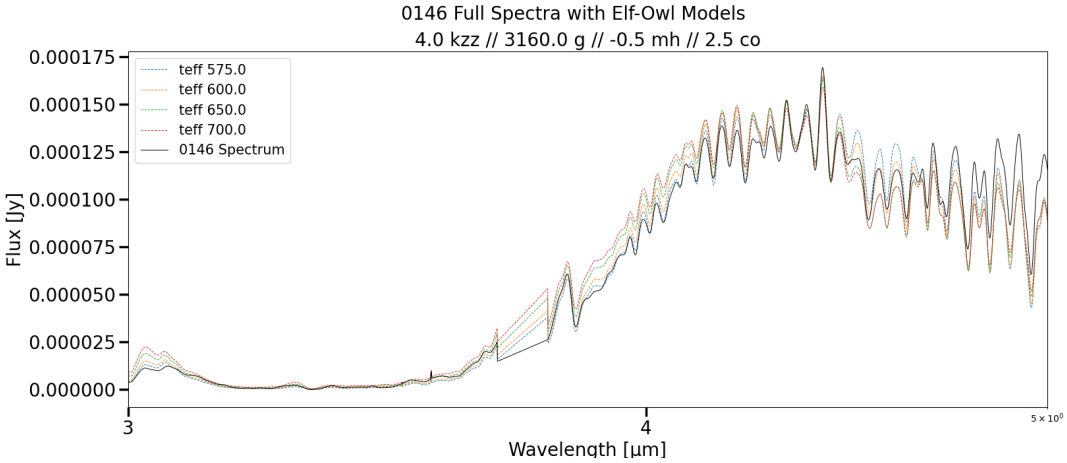

Figure A.31 0146 NIRSPEC Forward Model varying Surface Temperature

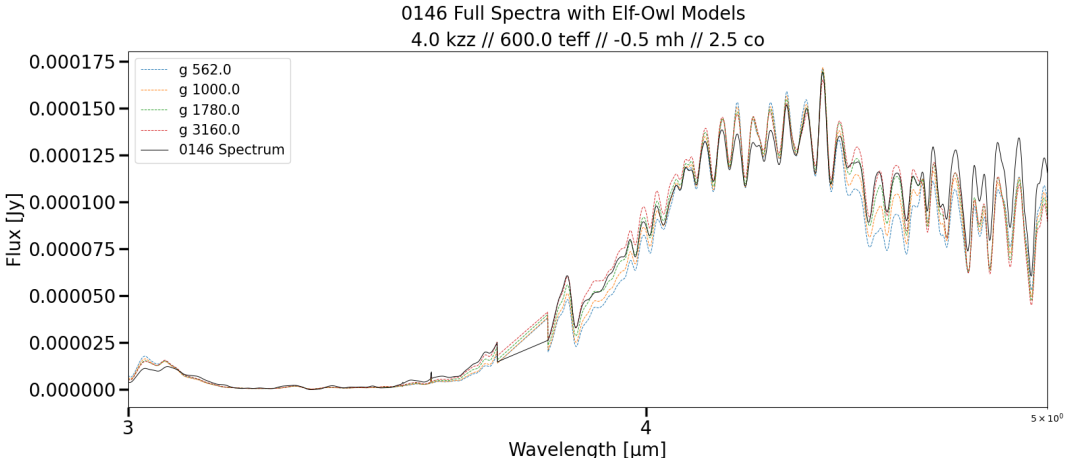

Figure A.32 0146 NIRSPEC Forward Model varying Surface Gravity

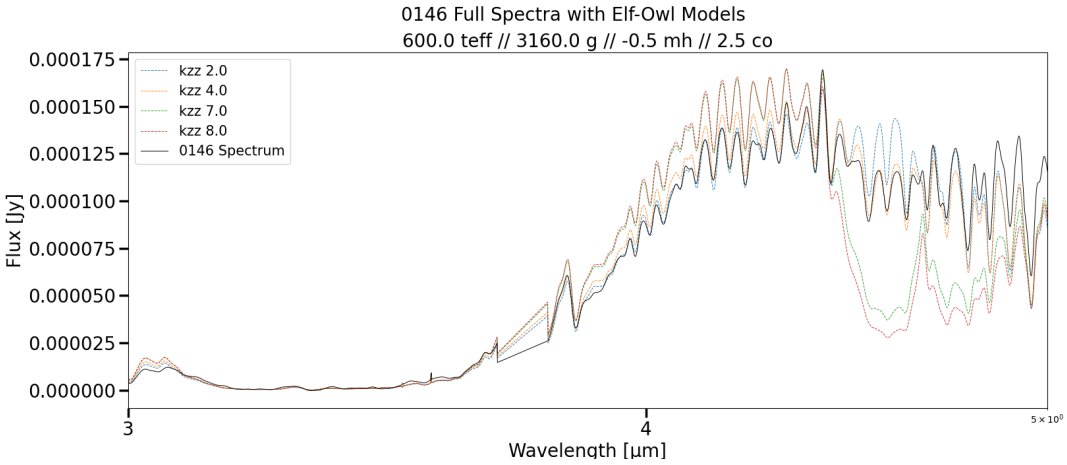

Figure A.33 0146 NIRSPEC Forward Model varying Vertical Mixing

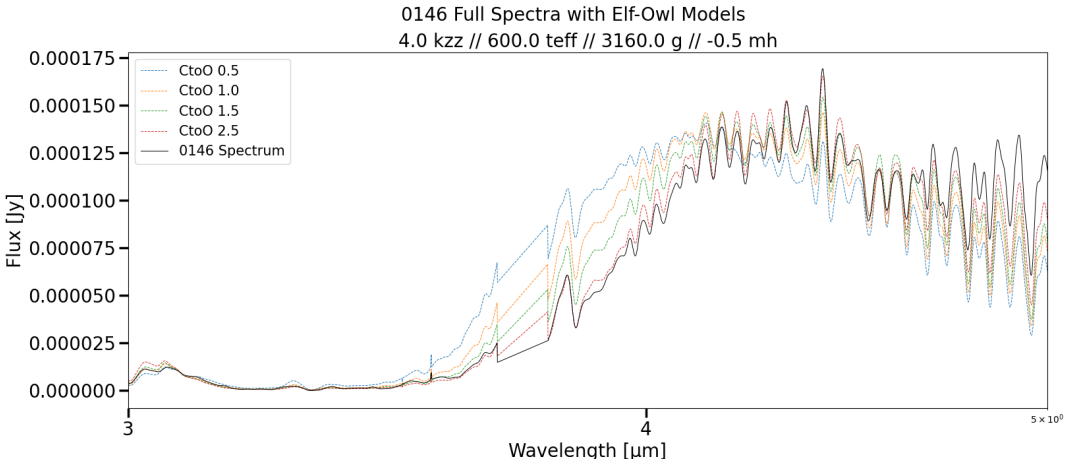

Figure A.34 0146 NIRSPEC Forward Model varying Carbon to Oxygen Ratio

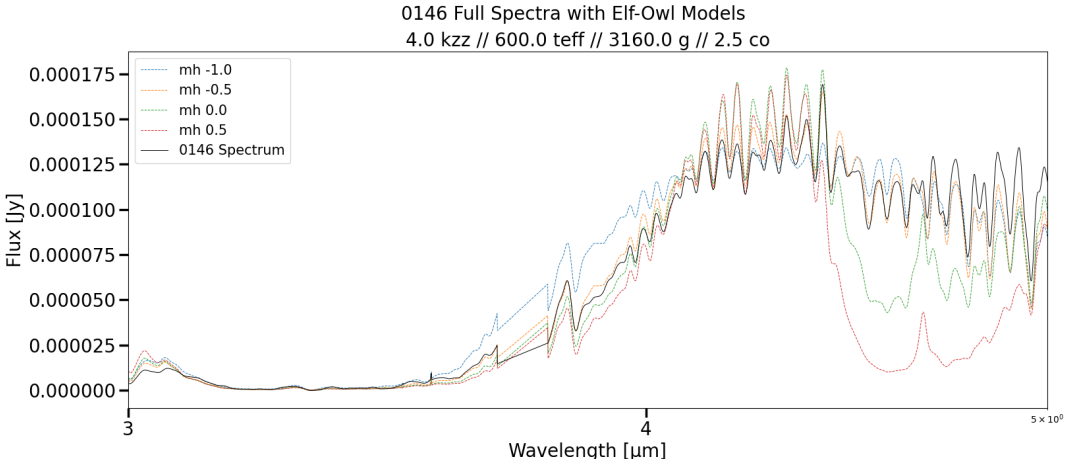

Figure A.35 0146 NIRSPEC Forward Model varying Metallicity

A.0.8 2220 Best Fit Variable Parameters

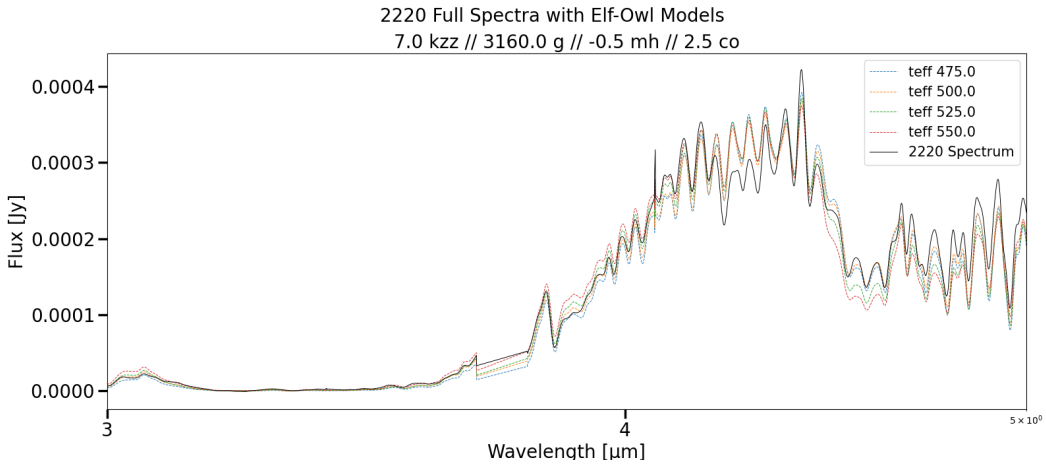

Figure A.36 2220 NIRSPEC Forward Model varying Surface Temperature

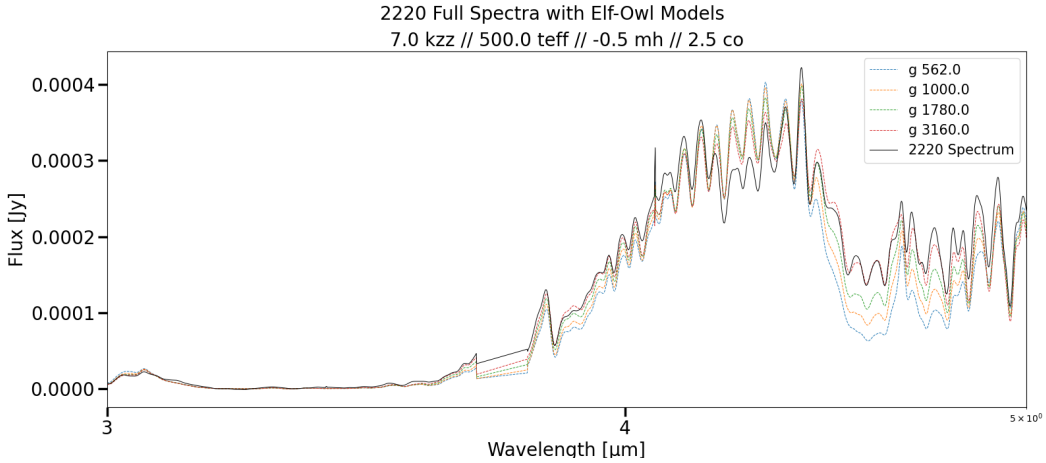

Figure A.37 2220 NIRSPEC Forward Model varying Surface Gravity

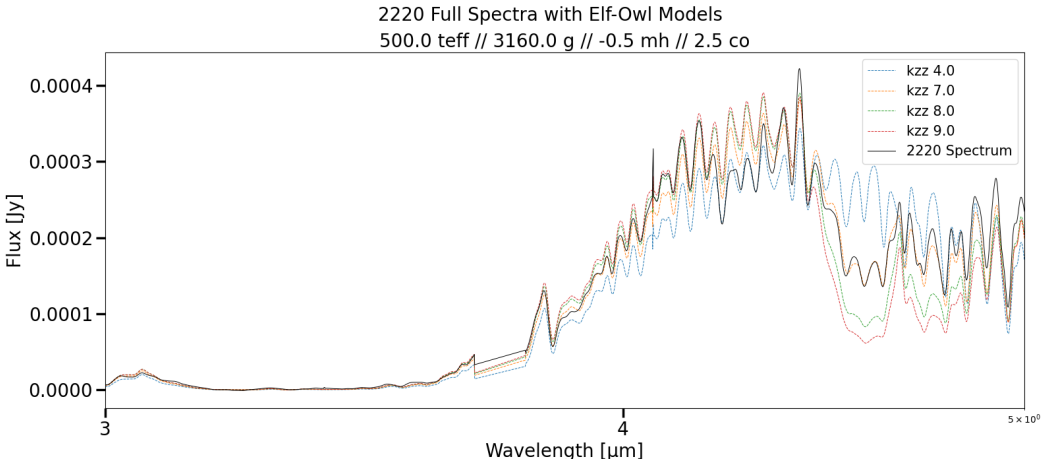

Figure A.38 2220 NIRSPEC Forward Model varying Vertical Mixing

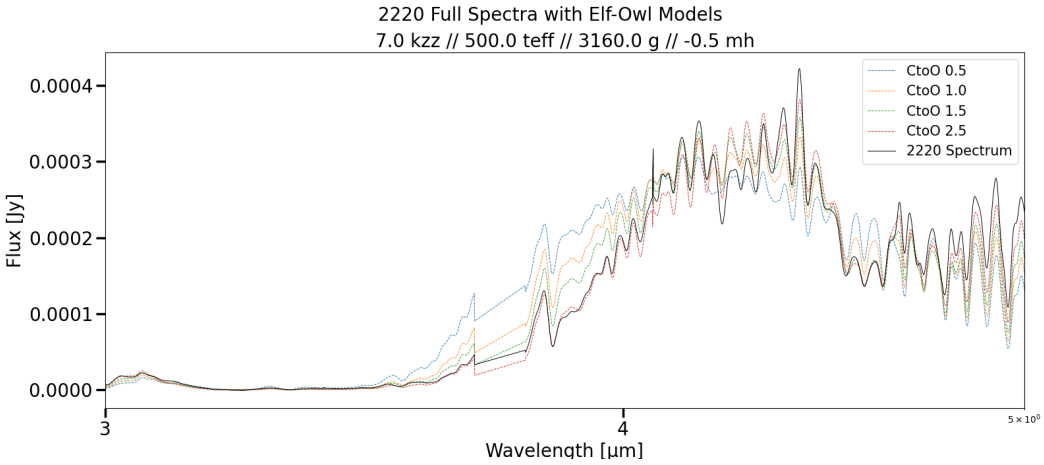

Figure A.39 2220 NIRSPEC Forward Model varying Carbon to Oxygen Ratio

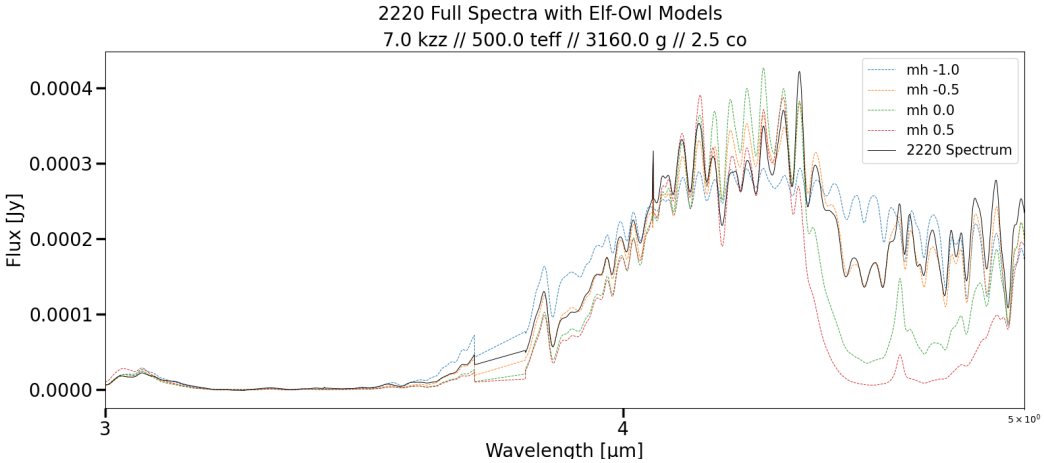

Figure A.40 2220 NIRSPEC Forward Model varying Metallicity

A.0.9 0825 NIRSPEC Variable Parameters

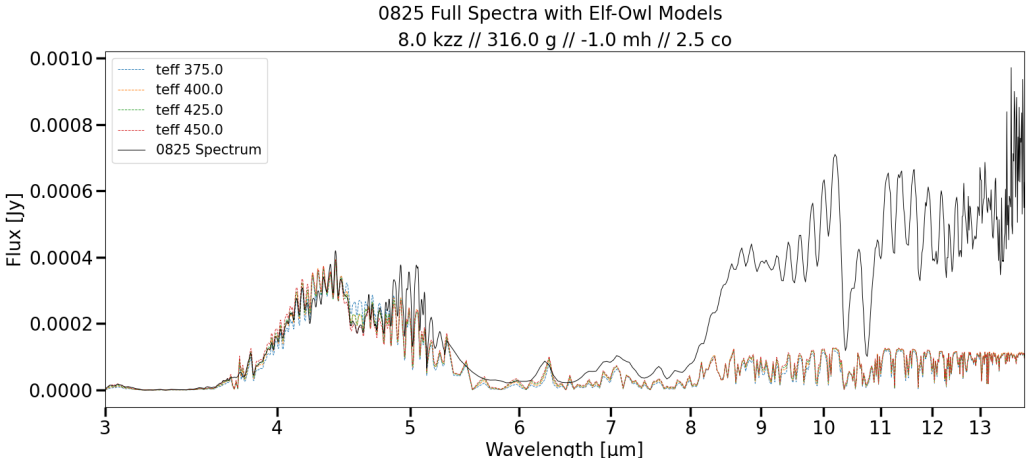

Figure A.41 0825 NIRSPEC Forward Model varying Surface Temperature

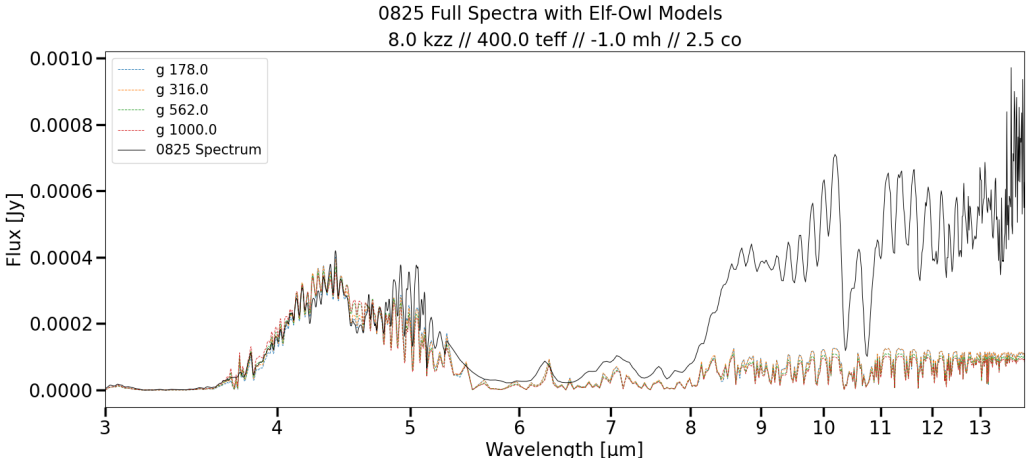

Figure A.42 0825 NIRSPEC Forward Model varying Surface Gravity

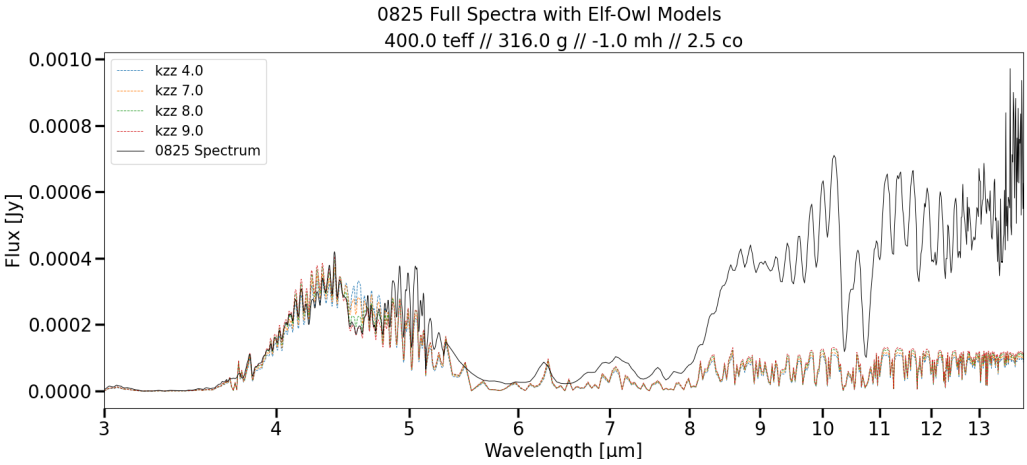

Figure A.43 0825 NIRSPEC Forward Model varying Vertical Mixing

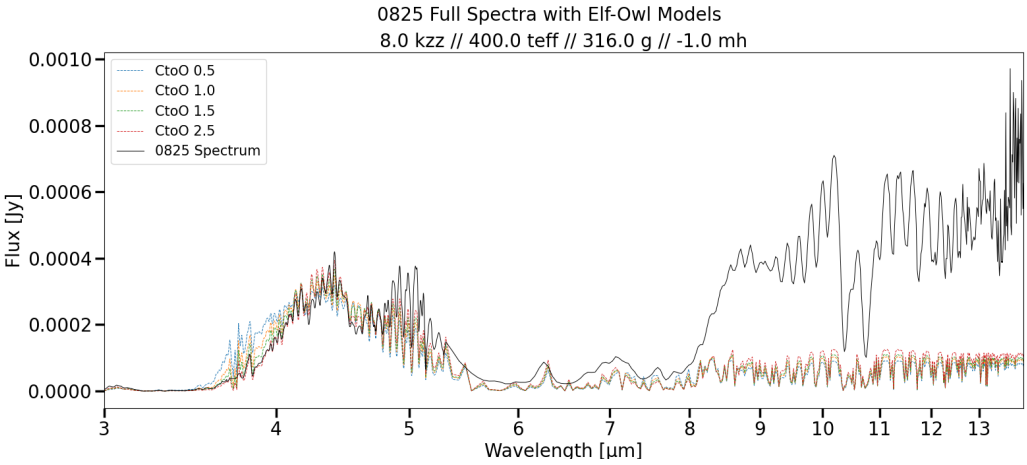

Figure A.44 0825 NIRSPEC Forward Model varying Carbon to Oxygen Ratio

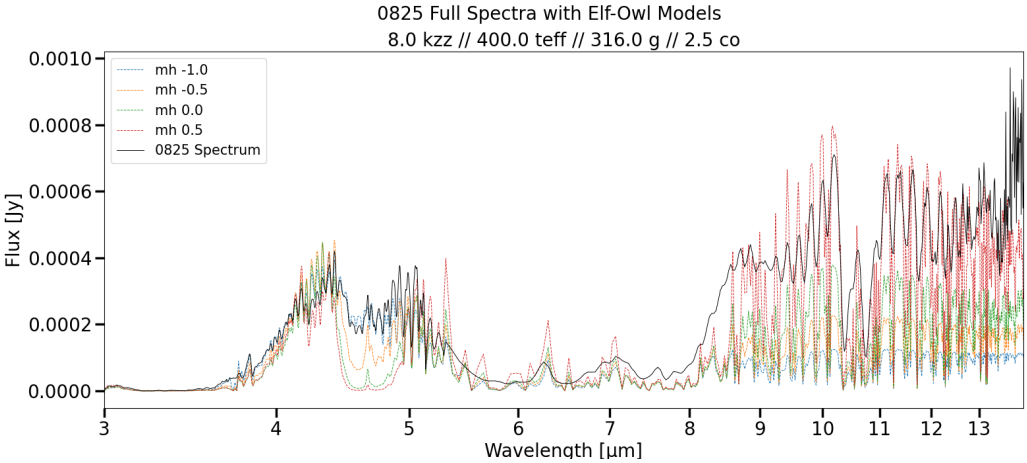

Figure A.45 0825 NIRSPEC Forward Model varying Metallicity

A.0.10 0825 MIRI Variable Parameters

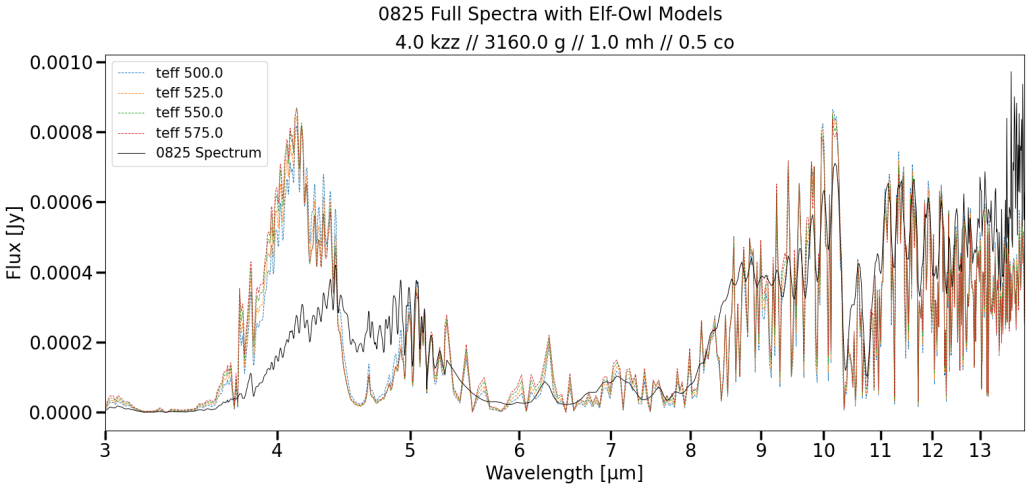

Figure A.46 0825 MIRI Forward Model varying Surface Temperature

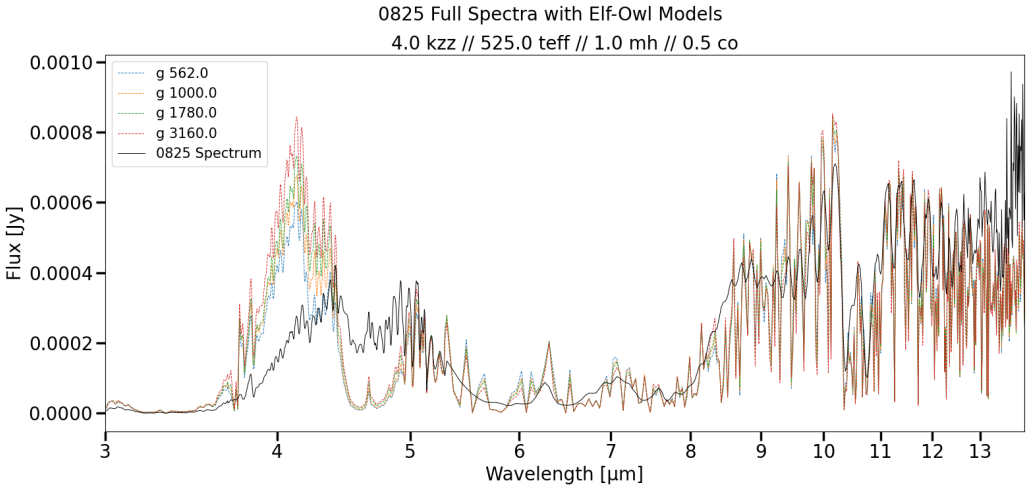

Figure A.47 0825 MIRI Forward Model varying Surface Gravity

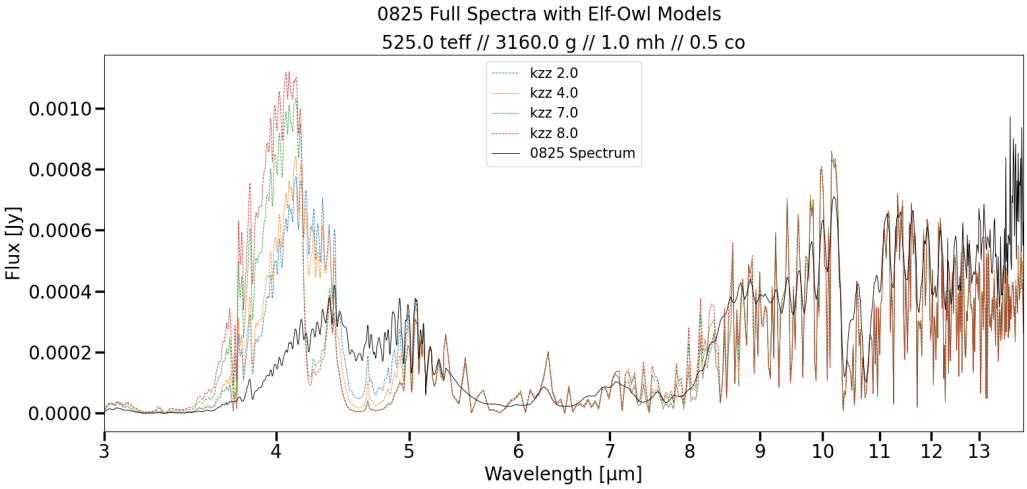

Figure A.48 0825 MIRI Forward Model varying Vertical Mixing

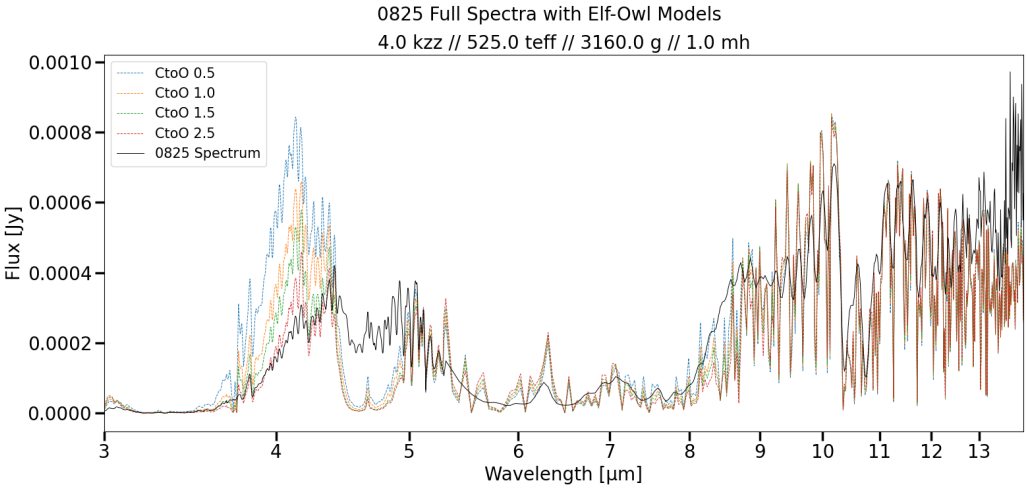

Figure A.49 0825 MIRI Forward Model varying Carbon to Oxygen Ratio

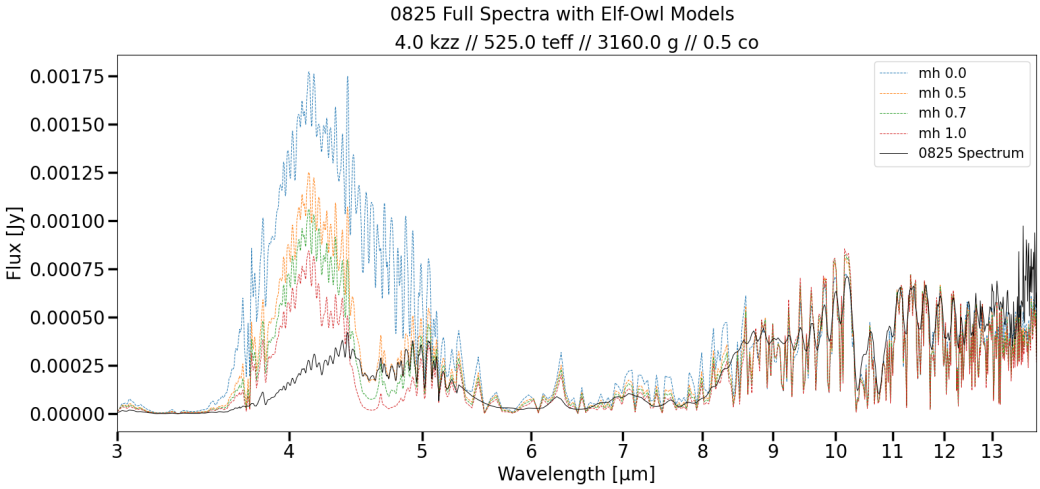

Figure A.50 0825 MIRI Forward Model varying Metallicity

A.0.11 0825 Full Variable Parameters

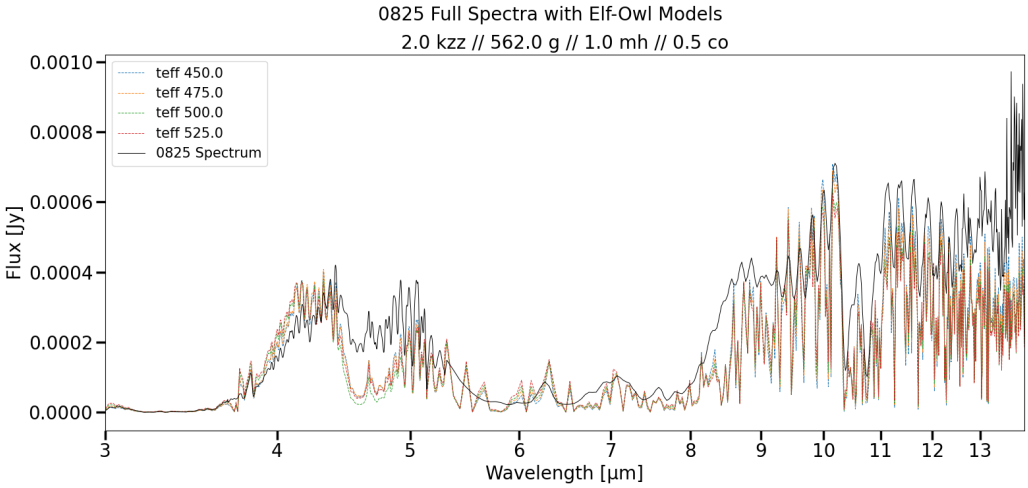

Figure A.51 0825 Full Forward Model varying Surface Temperature

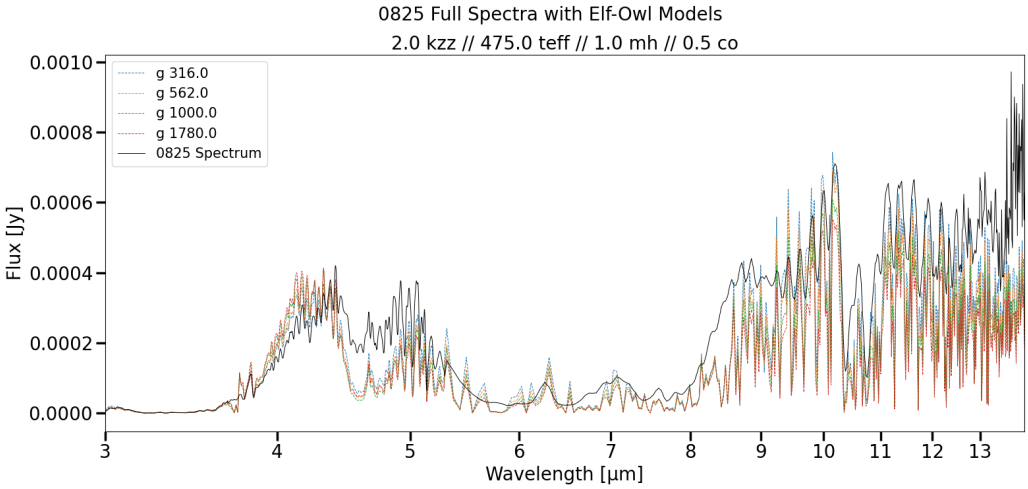

Figure A.52 0825 Full Forward Model varying Surface Gravity

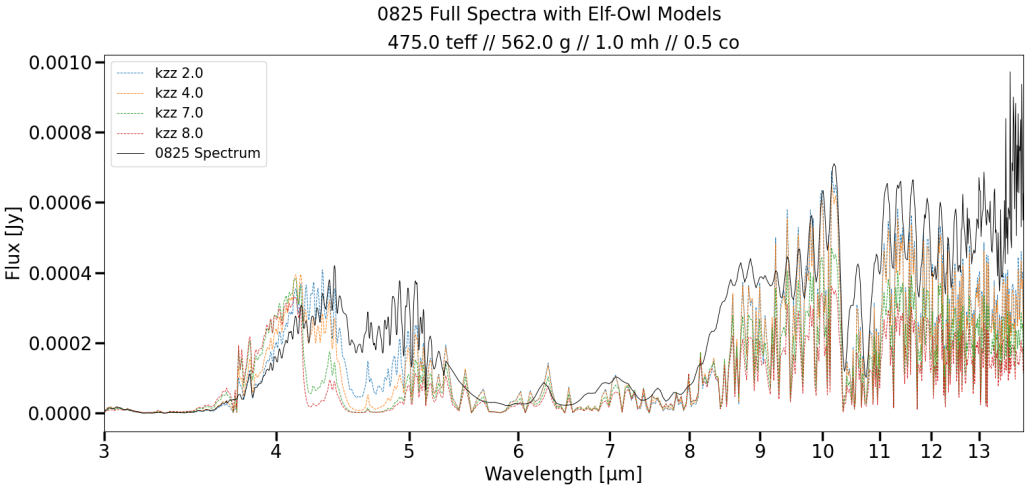

Figure A.53 0825 Full Forward Model varying Vertical Mixing

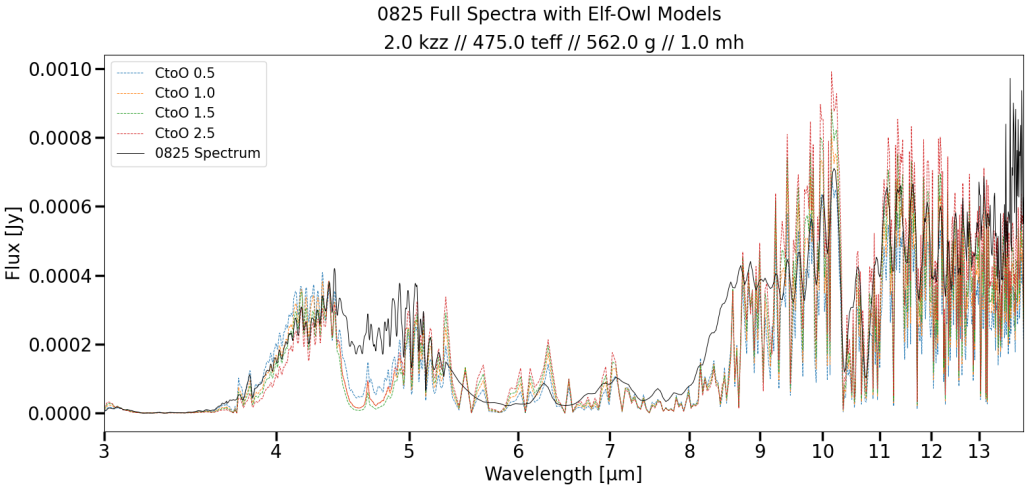

Figure A.54 0825 Full Forward Model varying Carbon to Oxygen Ratio

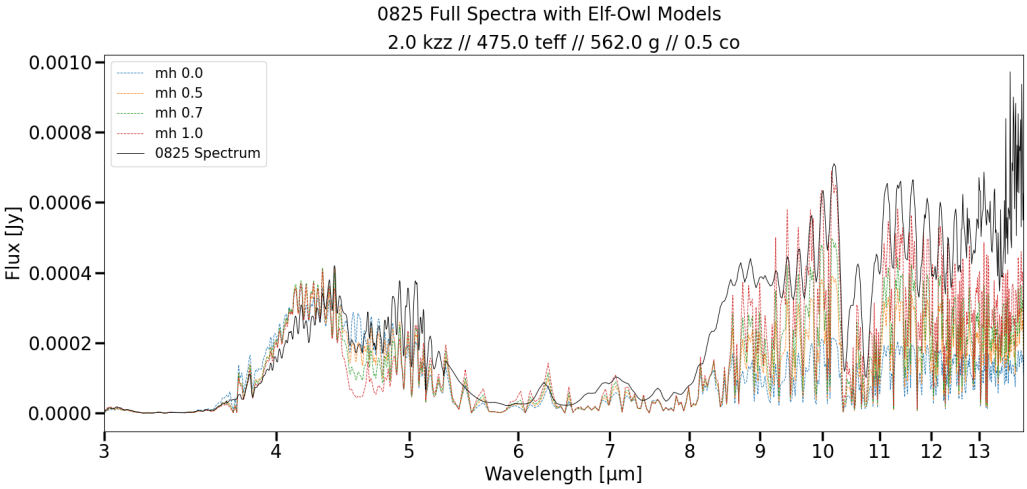

Figure A.55 0825 Full Forward Model varying Metallicity

A.0.12 1405 NIRSPEC Variable Parameters

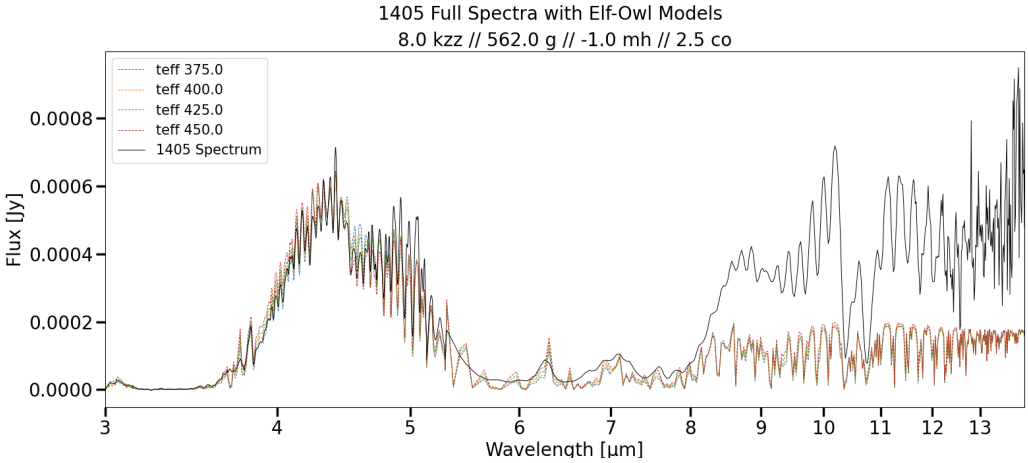

Figure A.56 1405 NIRSPEC Forward Model varying Surface Temperature

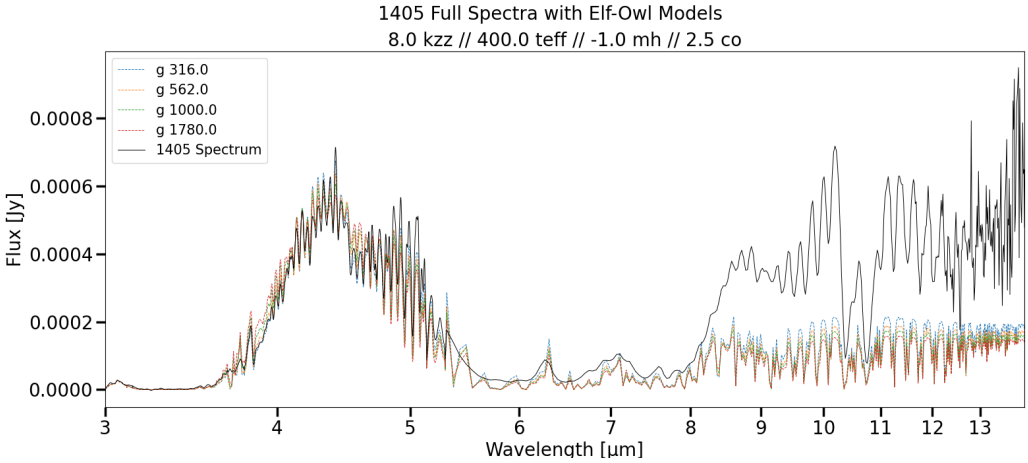

Figure A.57 1405 NIRSPEC Forward Model varying Surface Gravity

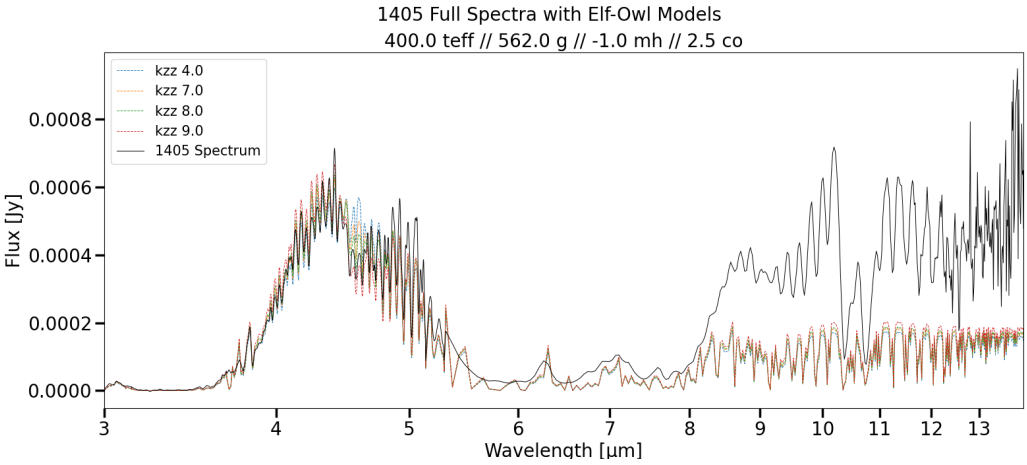

Figure A.58 1405 NIRSPEC Forward Model varying Vertical Mixing

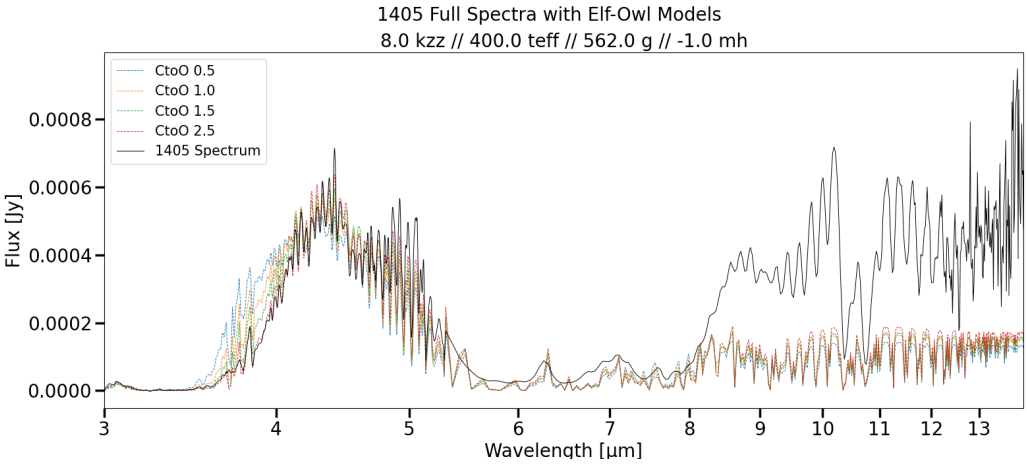

Figure A.59 1405 NIRSPEC Forward Model varying Carbon to Oxygen Ratio

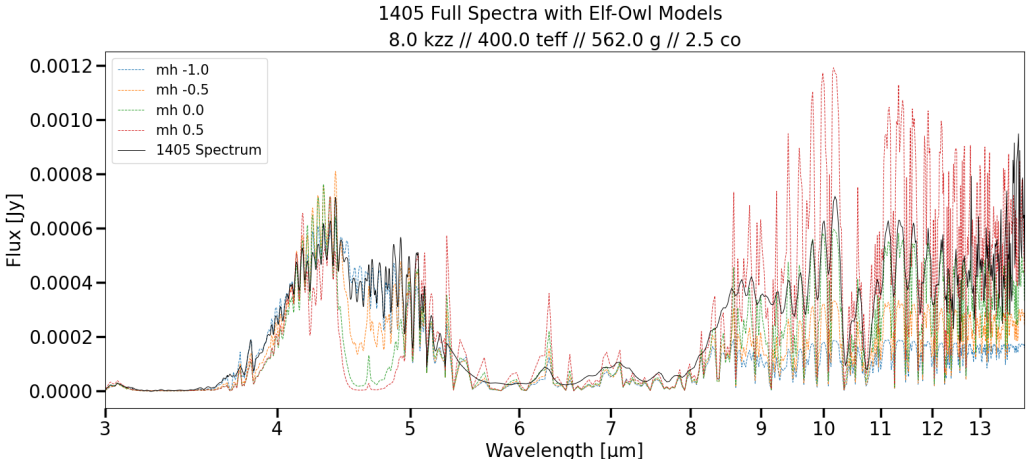

Figure A.60 1405 NIRSPEC Forward Model varying Metallicity

A.0.13 1405 MIRI Variable Parameters

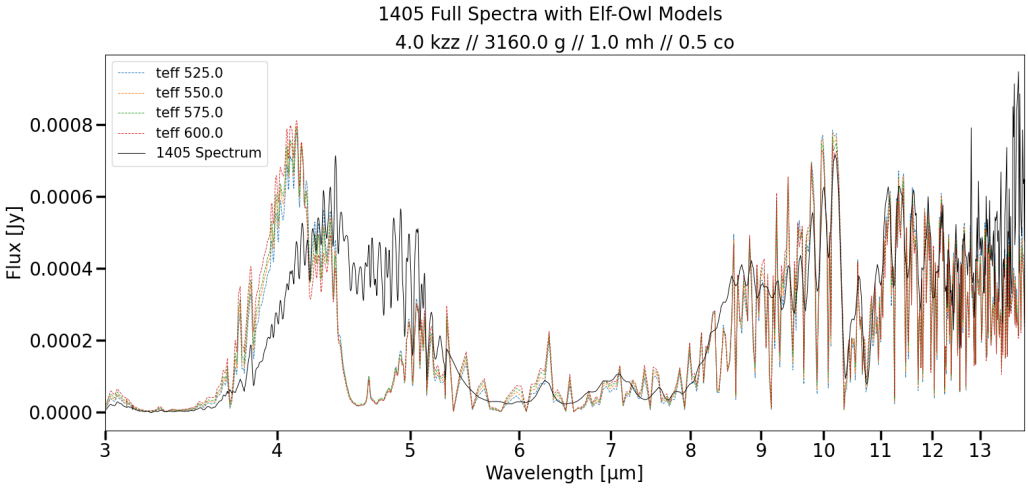

Figure A.61 1405 MIRI Forward Model varying Surface Temperature

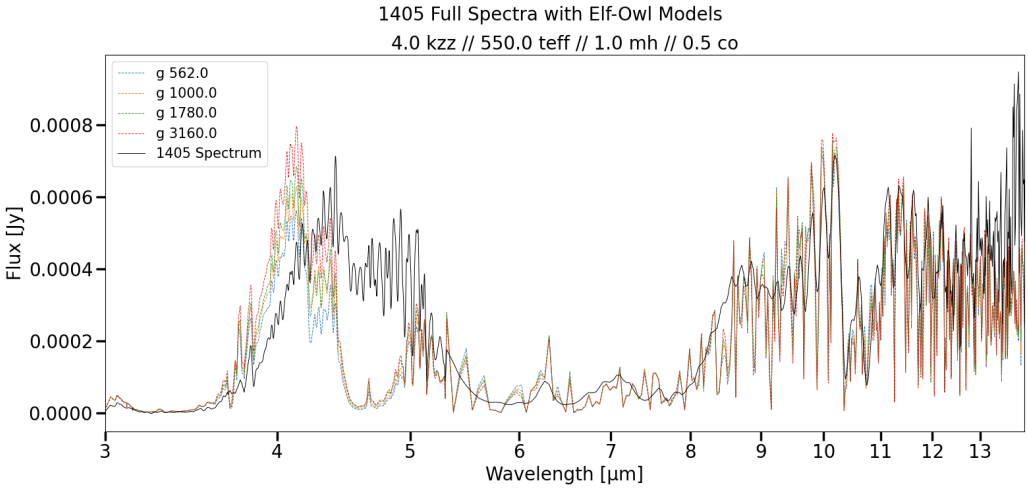

Figure A.62 1405 MIRI Forward Model varying Surface Gravity

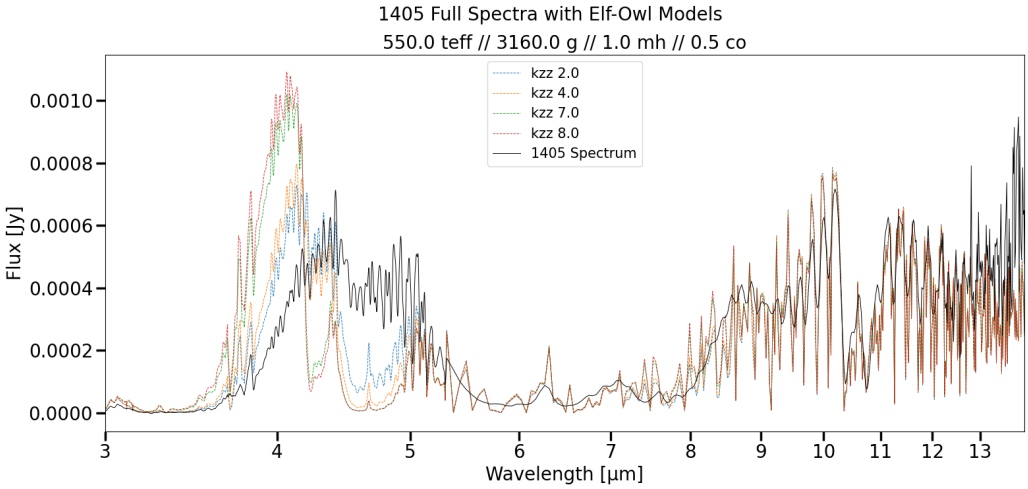

Figure A.63 1405 MIRI Forward Model varying Vertical Mixing

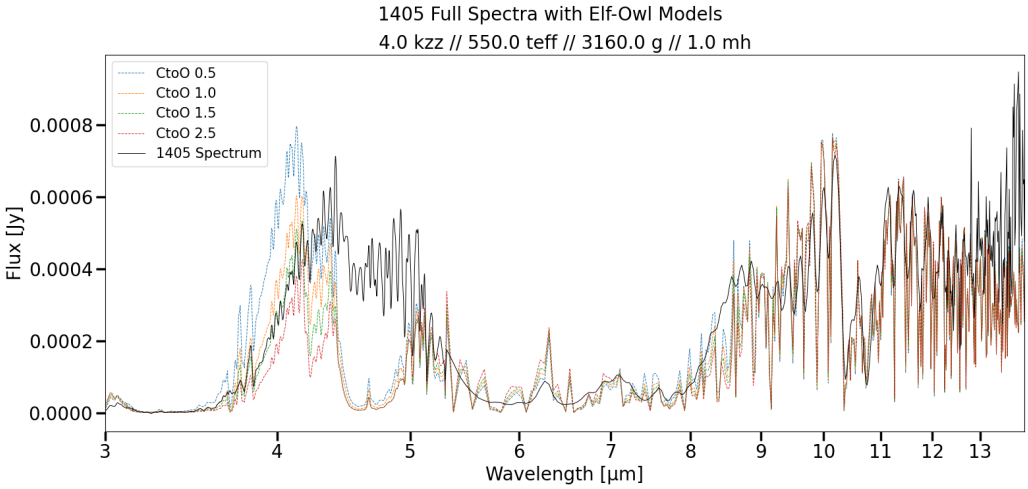

Figure A.64 1405 MIRI Forward Model varying Carbon to Oxygen Ratio

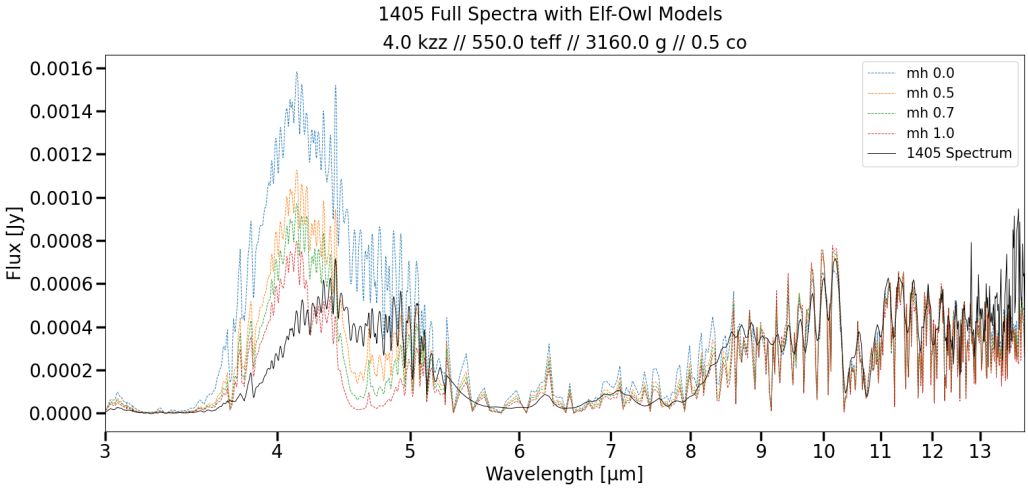

Figure A.65 1405 MIRI Forward Model varying Metallicity

A.0.14 1405 Full Variable Parameters

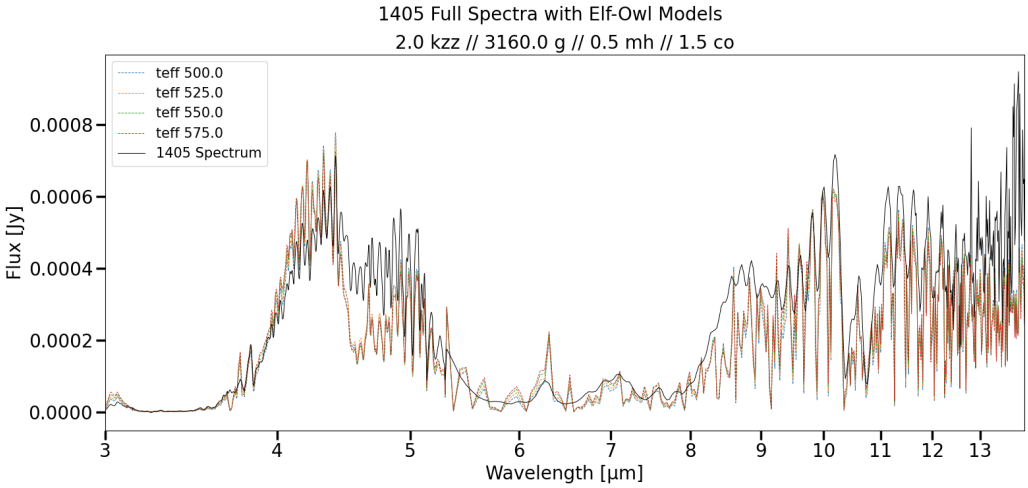

Figure A.66 1405 Full Forward Model varying Surface Temperature

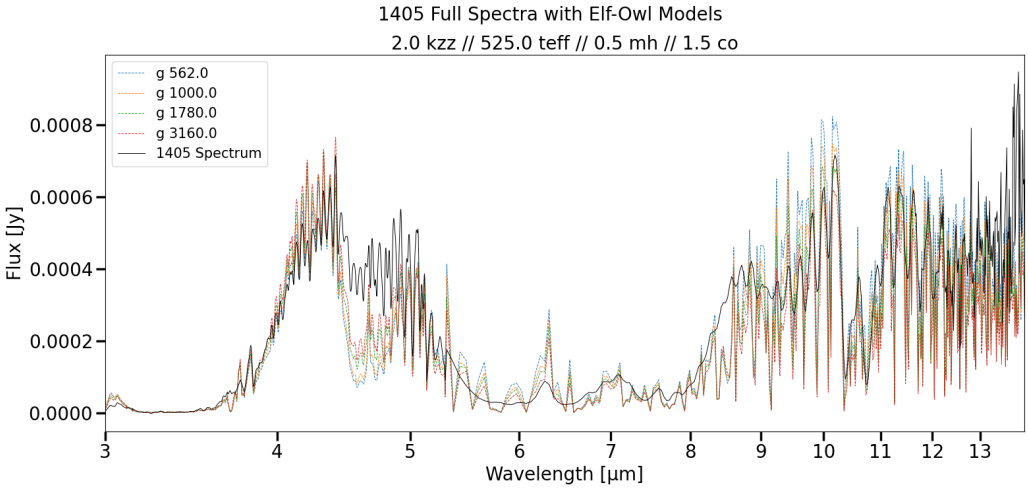

Figure A.67 1405 Full Forward Model varying Surface Gravity

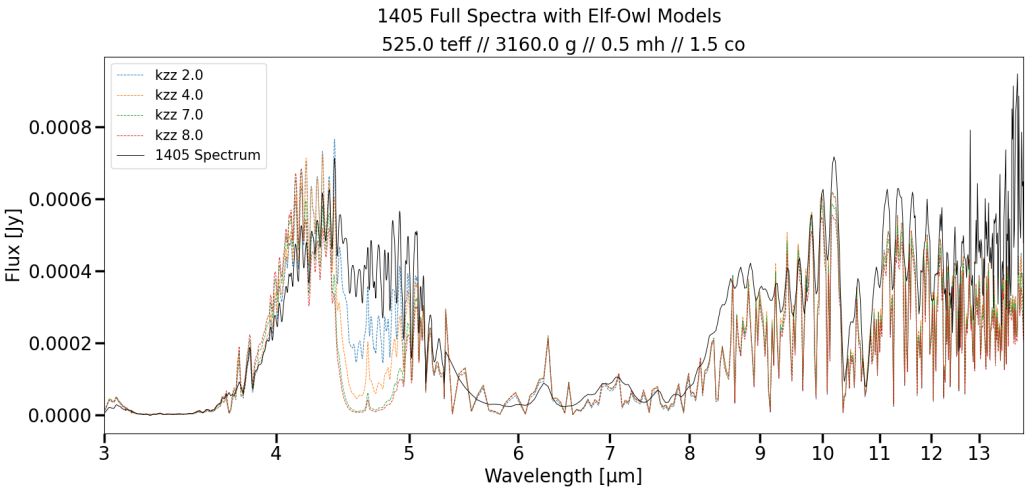

Figure A.68 1405 Full Forward Model varying Vertical Mixing

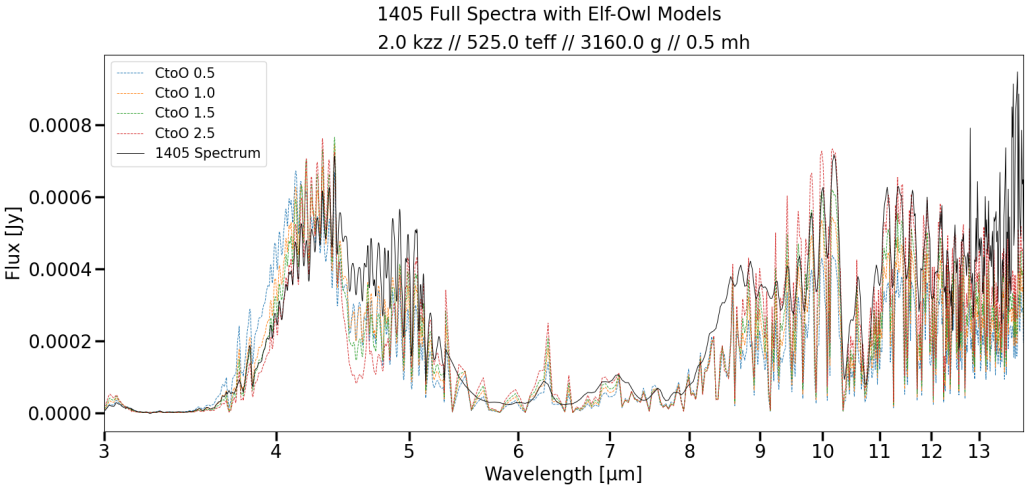

Figure A.69 1405 Full Forward Model varying Carbon to Oxygen Ratio

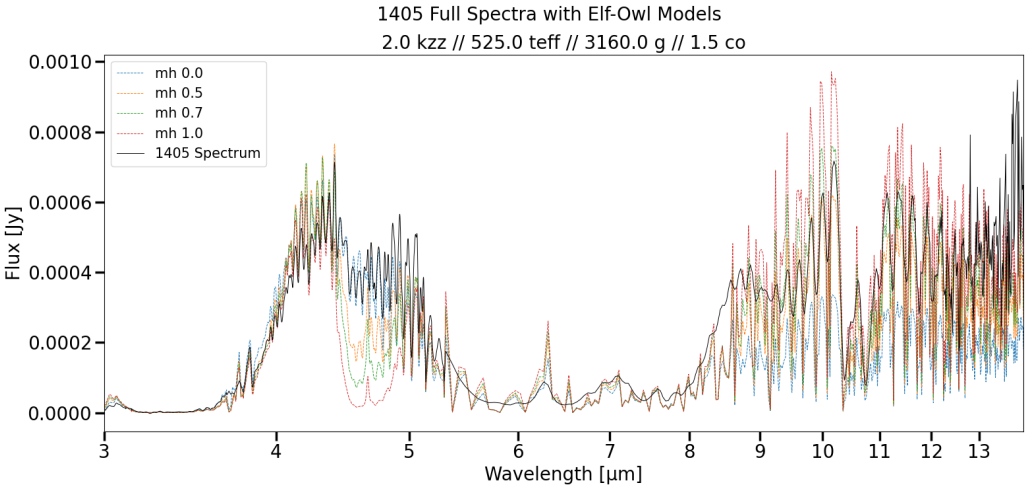

Figure A.70 1405 Full Forward Model varying Metallicity

A.0.15 1541 NIRSPEC Variable Parameters

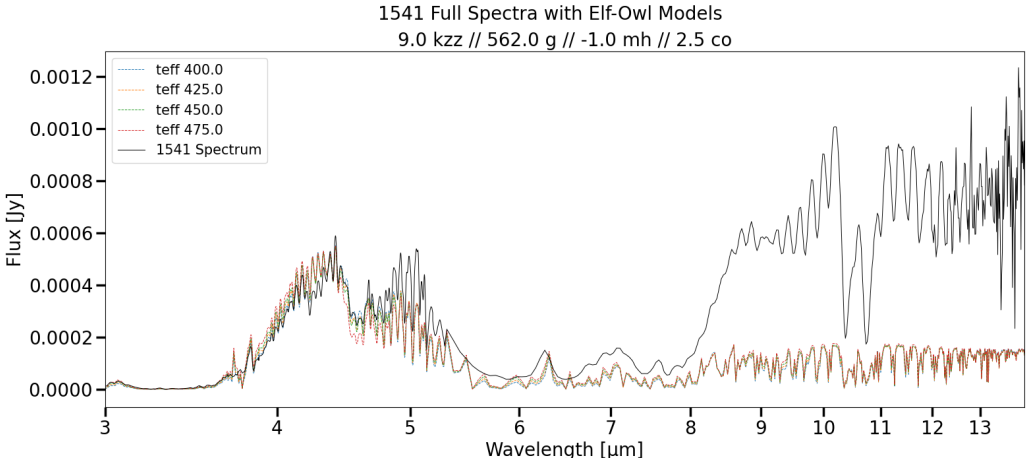

Figure A.71 1541 NIRSPEC Forward Model varying Surface Temperature

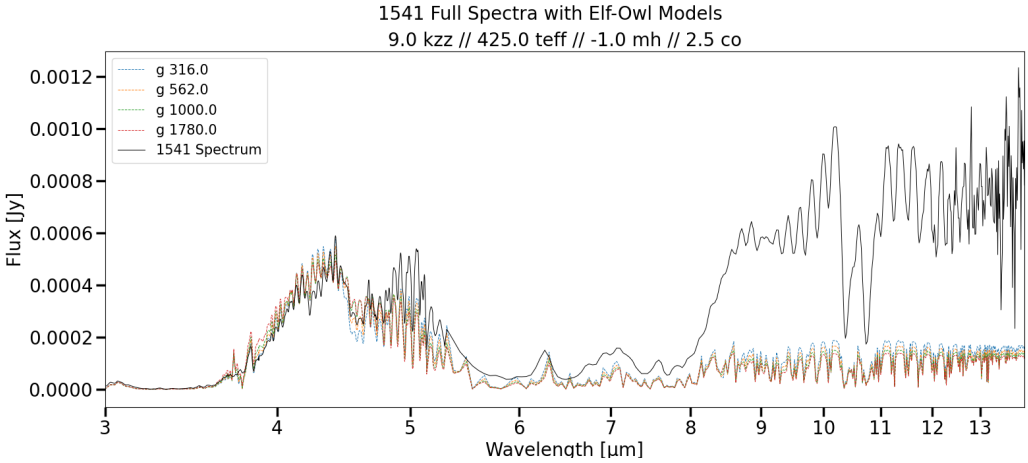

Figure A.72 1541 NIRSPEC Forward Model varying Surface Gravity

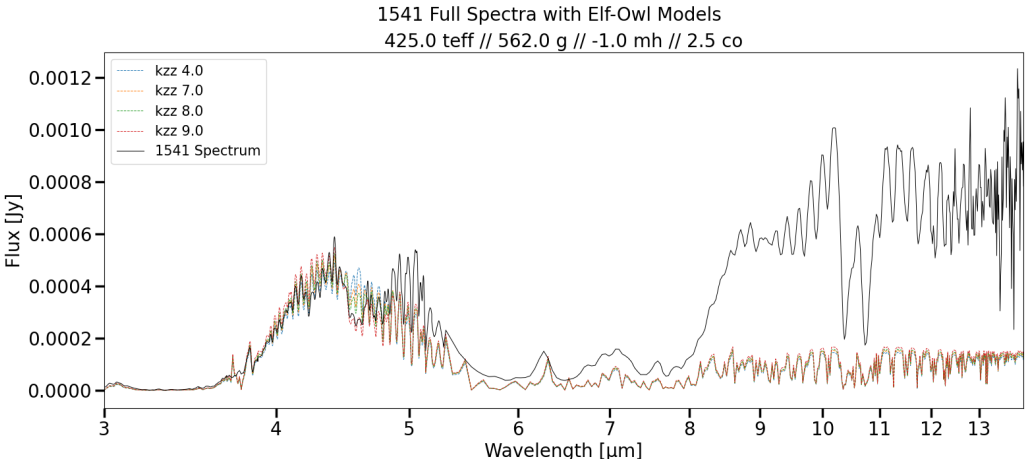

Figure A.73 1541 NIRSPEC Forward Model varying Vertical Mixing

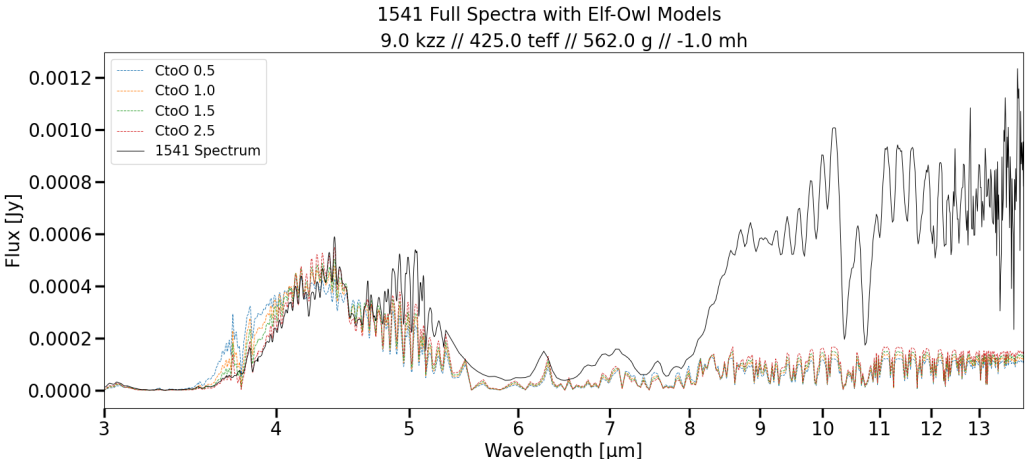

Figure A.74 1541 NIRSPEC Forward Model varying Carbon to Oxygen Ratio

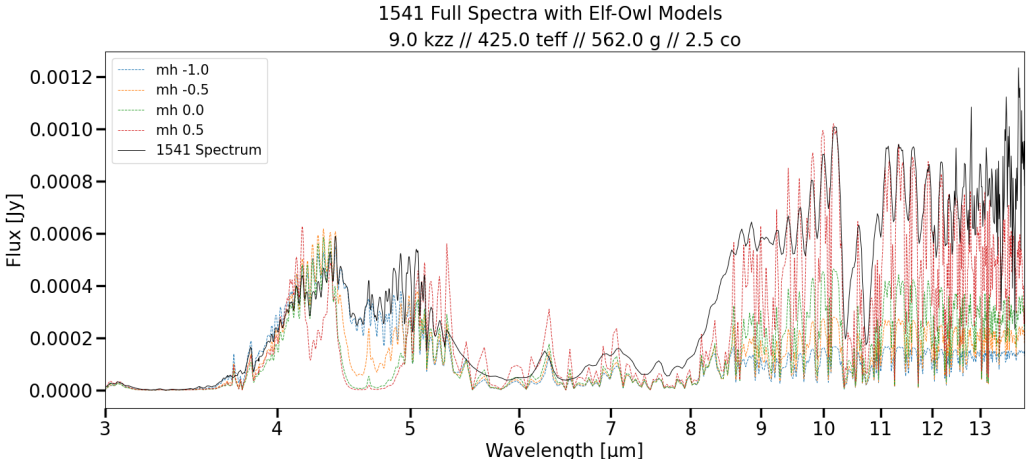

Figure A.75 1541 NIRSPEC Forward Model varying Metallicity

A.0.16 1541 MIRI Variable Parameters

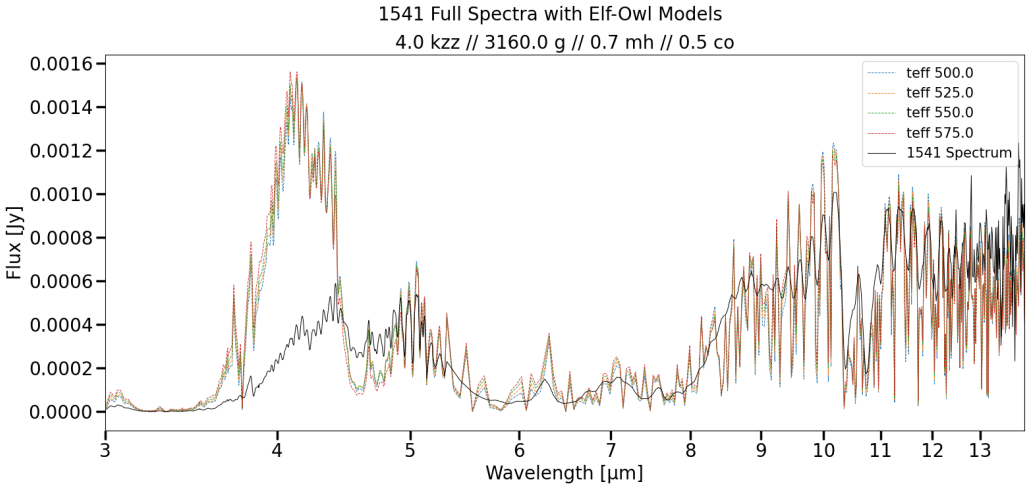

Figure A.76 1541 MIRI Forward Model varying Surface Temperature

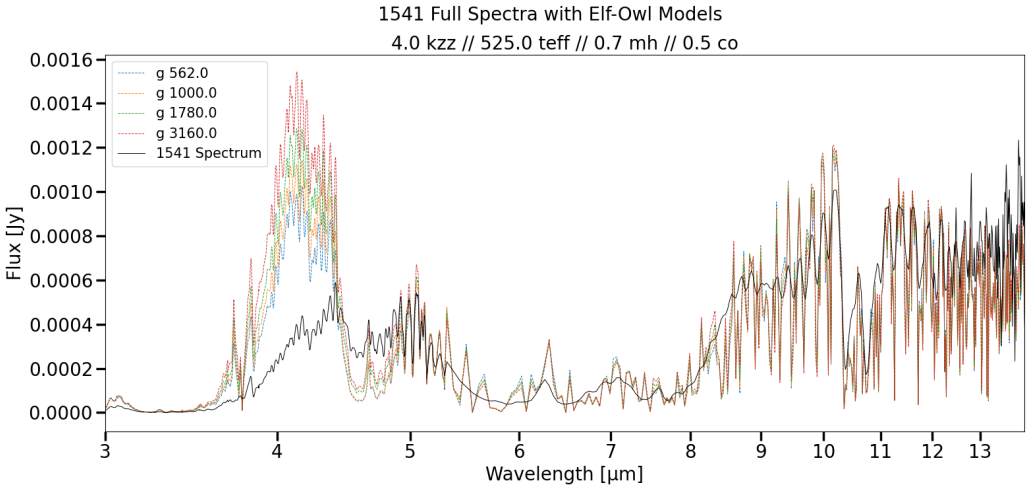

Figure A.77 1541 MIRI Forward Model varying Surface Gravity

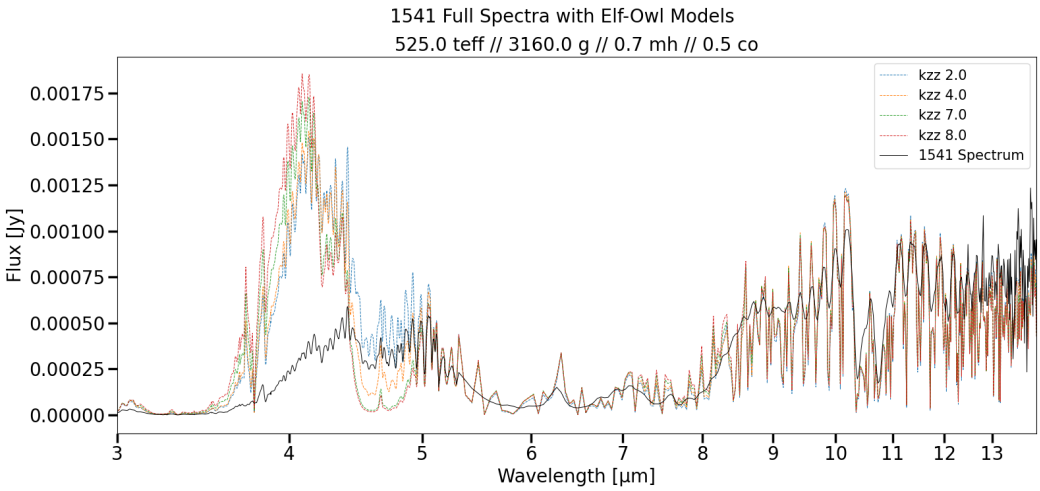

Figure A.78 1541 MIRI Forward Model varying Vertical Mixing

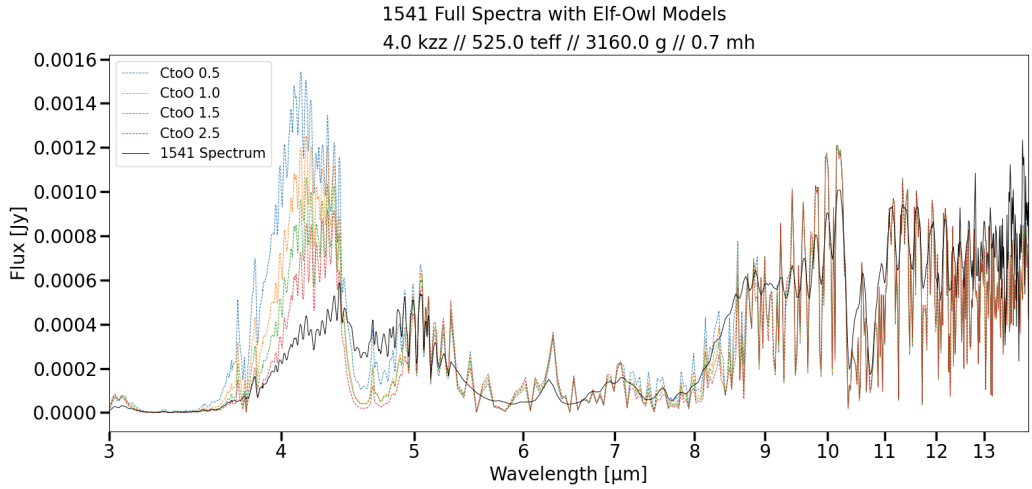

Figure A.79 1541 MIRI Forward Model varying Carbon to Oxygen Ratio

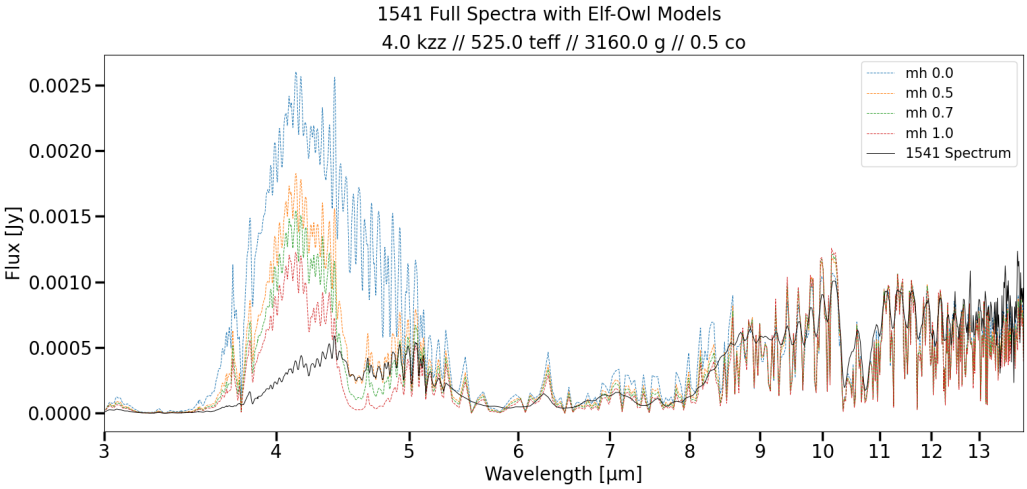

Figure A.80 1541 MIRI Forward Model varying Metallicity

A.0.17 1541 Full Variable Parameters

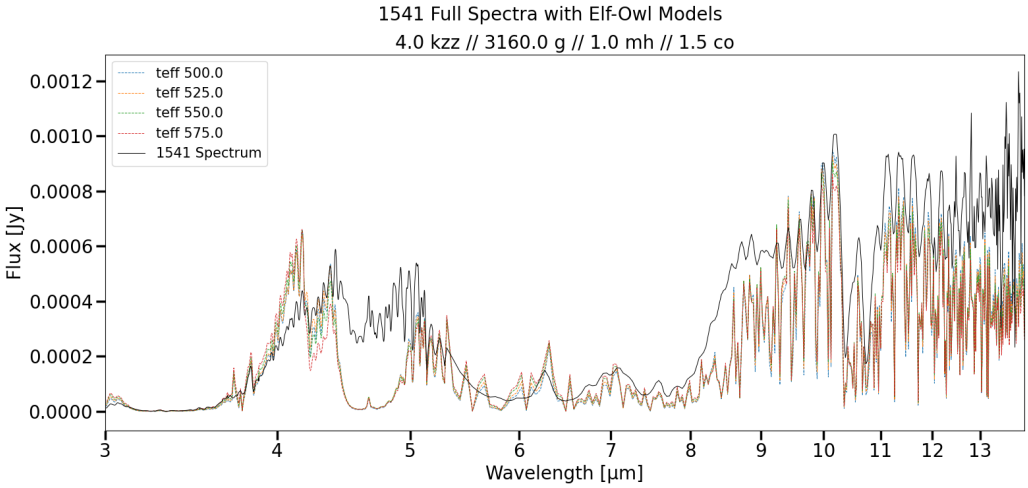

Figure A.81 1541 Full Forward Model varying Surface Temperature

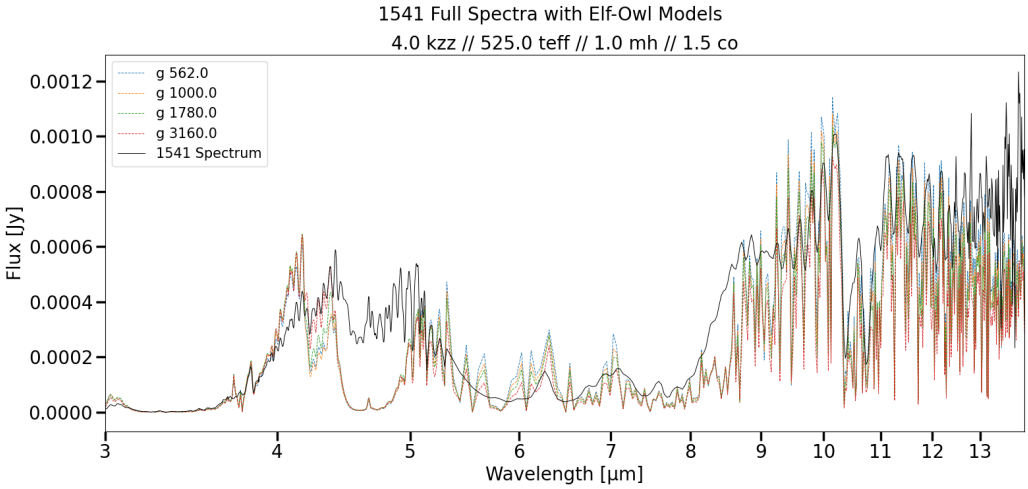

Figure A.82 1541 Full Forward Model varying Surface Gravity

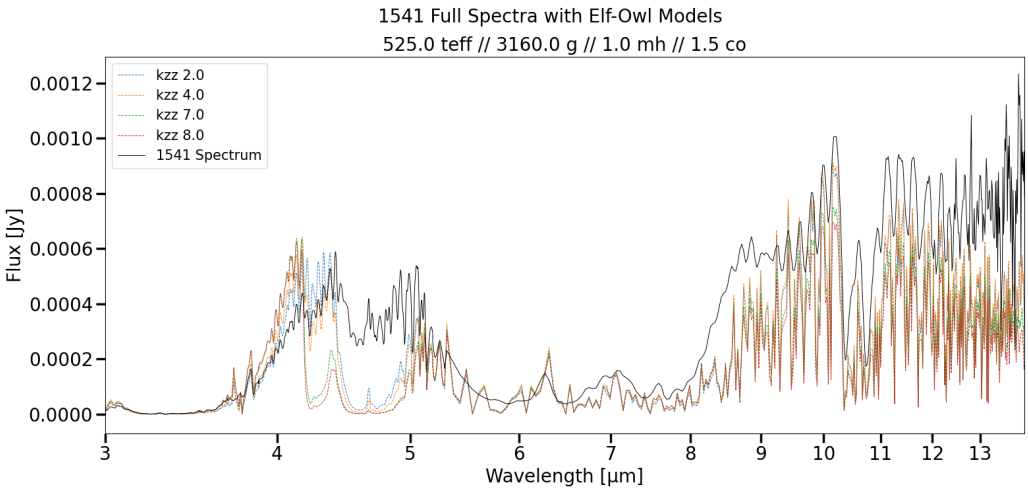

Figure A.83 1541 Full Forward Model varying Vertical Mixing

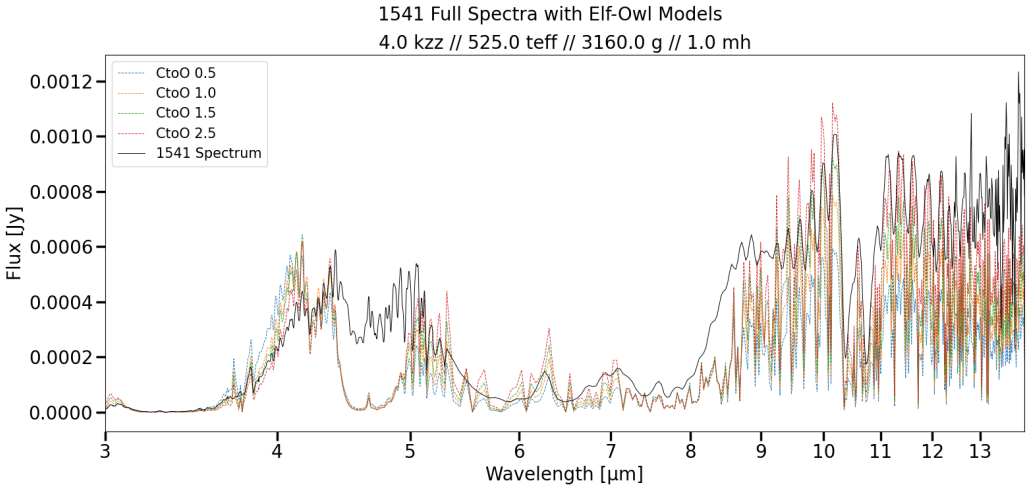

Figure A.84 1541 Full Forward Model varying Carbon to Oxygen Ratio

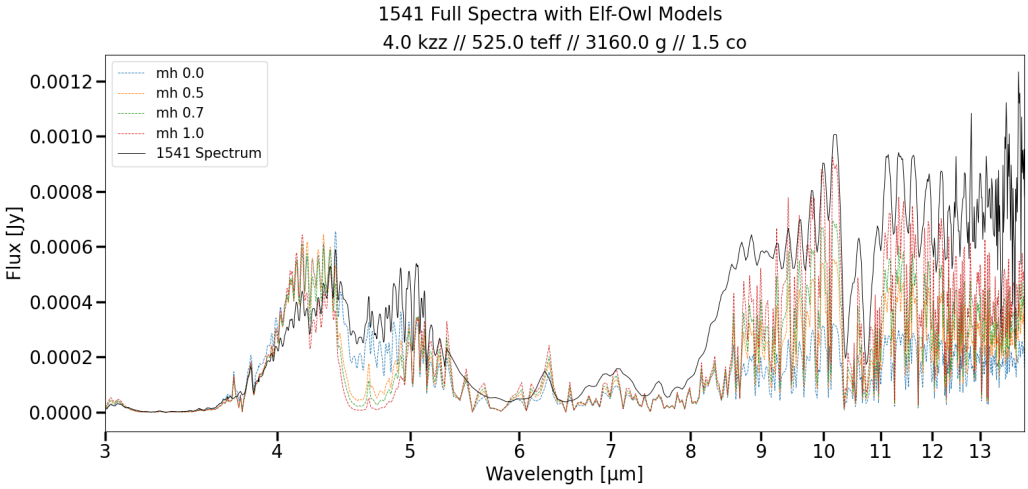

Figure A.85 1541 Full Forward Model varying Metallicity

Appendix B

Forward Modeling Code

B.1 Running the Code

B.1.1 Spectra Formatting

Nearly everything you need to run the foward modeling code is in the JWST_Forward modeling folder accessible under my account, jam469, on the BYU Physics and Astronomy lab machines shared drive. Spectra of objects should be be in .txt files with wavelength, flux (in jy), and error in the first, second, and third columns respectively. If you stitched together spectra from multiple sources you may want to sort the spectra by running the spectra_sort.py program. This can be run within an IDE and by copying the file path of the spectra you want to sort and the name of the file you want to output it to.

B.1.2 Regridding Models

To make the coding run faster you can create pre-regridded models for each of your target objects. To do this, copy the range of Elf-Owl models that you want to be regridded for a specific target and place them into a folder. Then create an ouput folder for the regridded files to go into. Name

it something that relates to the target since you will want to specifically call this folder in later processes. Run the regrid.py within an IDE, inputting the input and output folder paths and the filepath of the spectra you are regridding the models to. This should take between 1-2 hours per spectra.

Alternatively, if you only want to run the entire Forward Modeling script once or twice on an object you could skip the regrid step and run ForwardJWST.py which will regrid the models within the script but not save them anywhere.

B.1.3 Forward Modeling

Finally, we can run the forward models. First create an output folder to organize and keep all your statistics and plots together for a specific target. I would also recommend putting all your target spectra into the folder spectra/ for organization. Open a terminal from inside JWST_Forward/ and you should be able to run the forward modeling program as a python script. If you want to change the weighting you will need to open up the code and adjust the code there. For my purposes, this was easiest to hard code in and adjust when needed. You can run the code from terminal by typing:

python ForwardJWST_noregrid.py spectra/[spectra file].txt [regridded models folder]/ [output folder]/[statistics and plot output filename]

Example: python ForwardJWST_noregrid.py spectra/0146_Full.txt 0146_models_regrid/ 0146_forwardmodels/00_09_01

B.1.4 Output

The python script will output two files named by the last path you input into the terminal command. It will ouput a .txt file which dumps the path of model files and their coresponding chi_square values and scale factors in order from smallest chi_square to greatest. The second file will be a .png

of two plots. The first will be a plot of the whole spectra of the target in grey and the best fit (lowest chi square) model in blue dash. The other plot will show a specific region, hard coded to be 3-5um.

B.2 Forward Modeling Code

```
import os
import numpy as np
from scipy.interpolate import interp1d
from scipy.optimize import leastsq
from scipy.optimize import minimize
from scipy.ndimage import gaussian_filter1d
from tqdm import tqdm
import argparse
import matplotlib.pyplot as plt
import matplotlib.ticker as tk
import seaborn
import pandas as pd
import csv
import re

def load_spectrum_with_uncertainty(file_path):
    """Load spectrum with uncertainties: wavelength, flux, uncertainty."""
    data = np.loadtxt(file_path)
    return data[:, 0], data[:, 1], data[:, 2]

def load_spectrum_wo_uncertainty(file_path):
    """Load spectrum with uncertainties: wavelength, flux """
    data = np.loadtxt(file_path)
    return data[:, 0], data[:, 1]

def region_weight(wavelengths):
    """
    Define region-based weights. Modify this function for your specific regions.
    """
    weights = np.ones_like(wavelengths)

    weights[(wavelengths > 2.8) & (wavelengths < 5.2)] = 0
    weights[(wavelengths > 5) & (wavelengths < 12)] = 1
    #weights[(wavelengths > 5) & (wavelengths < 12)] = 1
    weights[(wavelengths < 2.8)] = 0

    return weights

def compute_weighted_scale_factor(target_flux, model_flux, target_unc, wave):
    """Compute regionally and statistically weighted scale factor."""
    region_wt = region_weight(wave)
    weights = region_wt / (target_unc ** 2)
    numerator = np.sum(weights * target_flux * model_flux)
    denominator = np.sum(weights * model_flux ** 2)
    return numerator / denominator

def compute_weighted_chi_square(target_flux, model_flux_scaled, target_unc, wave):
    """Compute regionally and statistically weighted chi-square."""
    region_wt = region_weight(wave)
    weights = region_wt / (target_unc ** 2)
```

```
    chi2 = np.sum(weights * (target_flux - model_flux_scaled) ** 2)
    return chi2

def adaptive_smooth(wavelength, flux, resolution_thresholds=(0.001, 0.01),
smoothing_sigmas=(5, 2, 0)):
    # Calculate local wavelength spacing
    spacing = np.gradient(wavelength)

    # Create an array for sigma values per point
    sigma_per_point = np.zeros_like(flux)

    # Assign smoothing based on resolution
    high_thresh, low_thresh = resolution_thresholds
    sigma_high, sigma_med, sigma_low = smoothing_sigmas

    for i in range(len(spacing)):
        if spacing[i] <= high_thresh:
            sigma_per_point[i] = sigma_high
        elif spacing[i] <= low_thresh:
            sigma_per_point[i] = sigma_med
        else:
            sigma_per_point[i] = sigma_low

    # Interpolate between varying smoothing levels using gaussian_filter1d multiple
times
    # We'll run 3 filters and blend based on the sigma choice
    flux_high = gaussian_filter1d(flux, sigma_high)
    flux_med = gaussian_filter1d(flux, sigma_med)
    flux_low = flux.copy()

    # Interpolate between filtered fluxes
    smoothed_flux = np.zeros_like(flux)
    for i in range(len(flux)):
        if sigma_per_point[i] == sigma_high:
            smoothed_flux[i] = flux_high[i]
        elif sigma_per_point[i] == sigma_med:
            smoothed_flux[i] = flux_med[i]
        else:
            smoothed_flux[i] = flux_low[i]

    return smoothed_flux


def process_spectra(target_file, model_folder, output_file):
    # Load target spectrum with uncertainties
    target_wave, target_flux, target_unc =
load_spectrum_with_uncertainty(target_file)

    results = []
```

```
    model_files = [f for f in os.listdir(model_folder) if f.endswith(".txt")]

    for filename in tqdm(model_files, desc="Processing model spectra"):
        model_path = os.path.join(model_folder, filename)
        try:
            model_wave, model_flux = load_spectrum_wo_uncertainty(model_path)

            # Compute weighted scale factor
            scale = compute_weighted_scale_factor(target_flux, model_flux,
target_unc, target_wave)

            # Apply scale
            model_flux_scaled = model_flux * scale

            # Compute chi-square
            chi2 = compute_weighted_chi_square(target_flux, model_flux_scaled,
target_unc, target_wave)

            results.append((model_path, chi2, scale))
        except Exception as e:
            tqdm.write(f"Error processing {model_path}: {e}")

    # Sort results by chi-square
    results.sort(key=lambda x: x[1])

    # Save to output file
    with open(f'{output_file}.txt', 'w') as f:
        f.write("Model_Path\tChi_Square\tScale_Factor\n")
        for path, chi2, scale in results:
            f.write(f"{path}\t{chi2:.6f}\t{scale:.22f}\n") # When dealing with the
ATMO models, in order for the scale not to be calculated to 0, you must increase
this value up to at least 20

    print(f"Results saved to {output_file}.txt")

def plot(target, output_path):
    fig, (ax1, ax2) = plt.subplots(2, 1, figsize=(18,12))
    target_wav, target_flux = load_spectrum_wo_uncertainty(target)
    output_file = np.loadtxt(f'{output_path}.txt', dtype=str)
    model_path = output_file[1][0]
    scale_factor = float(output_file[1][2])
    model_data = np.loadtxt(model_path)
    model_wav = model_data[:,0]
    model_flux = model_data[:,1]*scale_factor

    smodel_flux = adaptive_smooth(model_wav, model_flux)
    starget_flux = adaptive_smooth(target_wav, target_flux)

    ax1.plot(model_wav, smodel_flux, linestyle='--', label='Model')
    ax1.plot(target_wav, starget_flux, color='grey', label='Object')
```

```
    maxwav = max(target_wav)
    ax1.semilogx()
    formatter = tk.FuncFormatter(lambda x, pos: f'{x:g}')
    ax1.xaxis.set_major_formatter(formatter)
    ax1.xaxis.set_major_locator(tk.MaxNLocator(maxwav))

    ax1.set_title('Full Spectra')
    ax1.set_xlabel('Wavelength [μm]')
    ax1.set_ylabel('Flux [Jy]')

    ax2.plot(model_wav, smodel_flux, linestyle='--', label='Model')
    ax2.plot(target_wav, starget_flux, color='grey', label='Object')
    ax2.set_xlim(3.5, 5)
    ax2.set_title('JWST NIRSPEC')
    ax1.set_xlabel('Wavelength [μm]')
    ax1.set_ylabel('Flux [Jy]')

    plt.suptitle(f'{model_path}')
    plt.legend()

    plt.savefig(f'{output_path}.png')
    #plt.show()
    plt.close()

def txt_to_csv(txt_file, csv_file):
    # Regular expressions to extract parameters
    patterns = {
        "logzz": re.compile(r"logzz_([0-9eE.+-]+)"),
        "temp": re.compile(r"teff_([0-9eE.+-]+)"),
        "gravity": re.compile(r"grav_([0-9eE.+-]+)"),
        "co": re.compile(r"co_([0-9eE.+-]+)")
    }

    with open(txt_file, "r") as infile, open(csv_file, "w", newline="") as outfile:
        writer = csv.writer(outfile)

        # Write CSV header
        writer.writerow([
            "path",
            "chi",
            "scale_factor",
            "logzz",
            "temp",
            "gravity",
            "co"
        ])

        # Skip the first row
        next(infile)
```

```
        for line in infile:
            if not line.strip():
                continue

            parts = line.split()
            path = parts[0]
            chi_sq = parts[1]
            scale_factor = parts[2]

            # Extract values from path
            extracted = {}
            for key, pattern in patterns.items():
                match = pattern.search(path)
                extracted[key] = match.group(1) if match else ""

            writer.writerow([
                path,
                chi_sq,
                scale_factor,
                extracted["logzz"],
                extracted["temp"],
                extracted["gravity"],
                extracted["co"]
            ])

def createHeatMap(inFile,mapName):
    df = pd.read_csv(inFile,usecols=('temp','gravity','chi'))
    noDuplicates = df.drop_duplicates(subset=['temp', 'gravity'])
    data = noDuplicates.pivot(index='temp', columns=['gravity'], values='chi')
    plt.figure(figsize=(10, 10))
    plt.title(f'{inFile} Heat Map')
    seaborn.heatmap(data)
    plt.savefig(f'{mapName}_heat.png')
    plt.close()

if __name__ == "__main__":
    parser = argparse.ArgumentParser(description="Compare spectra via chi-square
statistics.")
    parser.add_argument("target", help="Path to the target spectrum .txt file")
    parser.add_argument("model_folder", help="Folder containing model spectra .txt
files")
    parser.add_argument("output", help="Output file to save results")

    args = parser.parse_args()
    process_spectra(args.target, args.model_folder, args.output)
    plot(args.target, args.output)
    txt_to_csv(f'{args.output}.txt', f'{args.output}.csv')
    createHeatMap(f'{args.output}.csv', args.output)
```

B.3 Binary Modeling Code

```
import os
import numpy as np
from scipy.interpolate import interp1d
from scipy.optimize import leastsq
from scipy.optimize import minimize
from scipy.ndimage import gaussian_filter1d
from tqdm import tqdm
import argparse
import matplotlib.pyplot as plt
import matplotlib.ticker as tk

def load_spectrum_with_uncertainty(file_path):
    """Load spectrum with uncertainties: wavelength, flux, uncertainty."""
    data = np.loadtxt(file_path)
    return data[:, 0], data[:, 1], data[:, 2]

def load_spectrum_wo_uncertainty(file_path):
    """Load spectrum with uncertainties: wavelength, flux """
    data = np.loadtxt(file_path)
    return data[:, 0], data[:, 1]

def region_weight(wavelengths):
    """
    Define region-based weights. Modify this function for your specific regions.
    """
    weights = np.ones_like(wavelengths)

    weights[(wavelengths > 2.8) & (wavelengths < 5.2)] = 0
    weights[(wavelengths > 5) & (wavelengths < 12)] = 1
    weights[(wavelengths < 2.8)] = 0

    return weights

def compute_weighted_scale_factor(target_flux, model_flux, target_unc, wave):
    """Compute regionally and statistically weighted scale factor."""
    region_wt = region_weight(wave)
    weights = region_wt / (target_unc ** 2)
    numerator = np.sum(weights * target_flux * model_flux)
    denominator = np.sum(weights * model_flux ** 2)
    return numerator / denominator

def compute_weighted_chi_square(target_flux, model_flux_scaled, target_unc, wave):
    """Compute regionally and statistically weighted chi-square."""
    region_wt = region_weight(wave)
    weights = region_wt / (target_unc ** 2)
    chi2 = np.sum(weights * (target_flux - model_flux_scaled) ** 2)
    return chi2

def adaptive_smooth(wavelength, flux, resolution_thresholds=(0.001, 0.01),
smoothing_sigmas=(5, 2, 0)):
```

```
    # Calculate local wavelength spacing
    spacing = np.gradient(wavelength)

    # Create an array for sigma values per point
    sigma_per_point = np.zeros_like(flux)

    # Assign smoothing based on resolution
    high_thresh, low_thresh = resolution_thresholds
    sigma_high, sigma_med, sigma_low = smoothing_sigmas

    for i in range(len(spacing)):
        if spacing[i] <= high_thresh:
            sigma_per_point[i] = sigma_high
        elif spacing[i] <= low_thresh:
            sigma_per_point[i] = sigma_med
        else:
            sigma_per_point[i] = sigma_low

    # Interpolate between varying smoothing levels using gaussian_filter1d multiple
times
    # We'll run 3 filters and blend based on the sigma choice
    flux_high = gaussian_filter1d(flux, sigma_high)
    flux_med = gaussian_filter1d(flux, sigma_med)
    flux_low = flux.copy()

    # Interpolate between filtered fluxes
    smoothed_flux = np.zeros_like(flux)
    for i in range(len(flux)):
        if sigma_per_point[i] == sigma_high:
            smoothed_flux[i] = flux_high[i]
        elif sigma_per_point[i] == sigma_med:
            smoothed_flux[i] = flux_med[i]
        else:
            smoothed_flux[i] = flux_low[i]

    return smoothed_flux


def process_spectra(target_file, model_folder, output_file):
    # Load target spectrum with uncertainties
    target_wave, target_flux, target_unc =
load_spectrum_with_uncertainty(target_file)

    results = []

    model_files = [f for f in os.listdir(model_folder) if f.endswith(".txt")]

    for filename in tqdm(model_files, desc="Processing model spectra"):
        model_path = os.path.join(model_folder, filename)
        try:
```

```
            model_wave, model_flux = load_spectrum_wo_uncertainty(model_path)

            # Compute weighted scale factor
            scale = compute_weighted_scale_factor(target_flux, model_flux,
target_unc, target_wave)

            # Apply scale
            model_flux_scaled = model_flux * scale

            # Compute chi-square
            chi2 = compute_weighted_chi_square(target_flux, model_flux_scaled,
target_unc, target_wave)

            results.append((model_path, chi2, scale))
        except Exception as e:
            tqdm.write(f"Error processing {model_path}: {e}")

    # Sort results by chi-square
    results.sort(key=lambda x: x[1])

    # Save to output file
    with open(f'{output_file}.txt', 'w') as f:
        f.write("Model_Path\tChi_Square\tScale_Factor\n")
        for path, chi2, scale in results:
            f.write(f"{path}\t{chi2:.6f}\t{scale:.6f}\n")

    print(f"Results saved to {output_file}.txt")

def plot(target, output_path):
    fig, (ax1, ax2) = plt.subplots(2, 1, figsize=(18,12))
    target_wav, target_flux = load_spectrum_wo_uncertainty(target)
    output_file = np.loadtxt(f'{output_path}.txt', dtype=str)
    model_path = output_file[1][0]
    scale_factor = float(output_file[1][2])
    model_data = np.loadtxt(model_path)
    model_wav = model_data[:,0]
    model_flux = model_data[:,1]*scale_factor

    smodel_flux = adaptive_smooth(model_wav, model_flux)
    starget_flux = adaptive_smooth(target_wav, target_flux)

    ax1.plot(model_wav, smodel_flux, linestyle='--', label='Model')
    ax1.plot(target_wav, starget_flux, color='grey', label='Object')

    maxwav = max(target_wav)
    ax1.semilogx()
    formatter = tk.FuncFormatter(lambda x, pos: f'{x:g}')
    ax1.xaxis.set_major_formatter(formatter)
    ax1.xaxis.set_major_locator(tk.MaxNLocator(maxwav))
```

```
    ax1.set_title('Full Spectra')
    ax1.set_xlabel('Wavelength [μm]')
    ax1.set_ylabel('Flux [Jy]')

    ax2.plot(model_wav, smodel_flux, linestyle='--', label='Model')
    ax2.plot(target_wav, starget_flux, color='grey', label='Object')
    ax2.set_xlim(5, 12)
    ax2.set_title('JWST NIRSPEC')
    ax1.set_xlabel('Wavelength [μm]')
    ax1.set_ylabel('Flux [Jy]')

    plt.suptitle(f'{model_path}')
    plt.legend()

    plt.savefig(f'{output_path}.png')
    #plt.show()

if __name__ == "__main__":
    parser = argparse.ArgumentParser(description="Compare spectra via chi-square
statistics.")
    parser.add_argument("target", help="Path to the target spectrum .txt file")
    parser.add_argument("model_folder", help="Folder containing model spectra .txt
files")
    parser.add_argument("output", help="Output file to save results")

    args = parser.parse_args()
    process_spectra(args.target, args.model_folder, args.output)
    plot(args.target, args.output)
```

B.4 Convert Elf Owl Models to text file

```
import xarray as xr
import numpy as np
import os

# Path to the folder containing model files
model_folder = 'C:/Users/jamap/Desktop/Research/elfowl/output_700.0_800'
output_folder = 'C:/Users/jamap/Desktop/Research/elfowl/elfowl_models'

# Ensure the output folder exists
os.makedirs(output_folder, exist_ok=True)

# Conversion factor from erg/s/cm²/cm to Janskys (using microns)
conversion_factor = 3.33564095e-15

# Loop through all files in the model folder
for model_file in os.listdir(model_folder):
    if model_file.endswith('.nc'):  # Only process .nc files
        model_path = os.path.join(model_folder, model_file)

        # Load the xarray dataset
        ds = xr.load_dataset(model_path)

        # Extract wavelength and flux from the dataset
        wavelength = ds['wavelength'].values  # Replace with actual variable name
for wavelength
        flux = ds['flux'].values  # Replace with actual variable name for flux

        # Convert flux from erg/s/cm²/cm to Janskys using microns
        flux_jy = (flux * conversion_factor) * (wavelength**2)

        # Combine wavelength and flux into a single array
        data = np.column_stack((wavelength, flux_jy))

        # Generate the output filename by changing the extension from .nc to .txt
        output_filename = os.path.splitext(model_file)[0] + '.txt'
        output_file_path = os.path.join(output_folder, output_filename)

        # Save to a text file
        np.savetxt(output_file_path, data, fmt='%.6e', comments='') # I took at the
header: header='Wavelength Flux',

        print(f"Saved: {output_file_path}")
```

B.4.1 Unit Conversion

```
import numpy as np

def convert_to_jansky(input_file, output_file):
    try:
        data = np.loadtxt(input_file)
    except Exception as e:
        print(f"Error loading file: {e}")
        return

    if data.shape[1] != 3:
        print("Error: Input file must have three columns: wavelength, flux,
uncertainty.")
        return

    wavelength = data[:, 0]  # in microns
    flux_lambda = data[:, 1]  # in erg/s/cm^2/Å
    uncertainty_lambda = data[:, 2]

    # Convert flux and uncertainty to Jansky
    factor = (wavelength*1e4)**2 * (3.33564*1e4)
    flux_nu = flux_lambda * factor
    uncertainty_nu = uncertainty_lambda * factor

    # Stack the data and save
    converted_data = np.column_stack((data[:,0], flux_nu, uncertainty_nu))
    np.savetxt(output_file, converted_data)

    print(f"Converted spectrum saved to '{output_file}'.")

# Example usage:
convert_to_jansky("C:/Users/jamap/Desktop/Research/Data/text_files/0415/data_w_error
s/0415_keck.txt",
"C:/Users/jamap/Desktop/Research/Data/text_files/0415/data_w_errors/jy_0415_keck.txt
")
```

```
import numpy as np
import os

# Speed of light in m/s
C = 2.99792458e8  # [m/s]

def convert_wm2um_to_jy(input_file, output_file):
    # try:
    data = np.loadtxt(input_file, comments='#')
    # except Exception as e:
    #     print(f"Error loading file: {e}")
    #     return
    #
    # if data.shape[1] != 3:
    #     print("Error: Input file must have three columns: wavelength (μm), flux
(W/m^2/μm), uncertainty.")
    #     return

    wavelength_um = data[:, 0]
    flux_lambda = data[:, 1]
    #uncertainty_lambda = data[:, 2]

    # Conversion factor to Jy
    factor = (wavelength_um)**2 * 1e26 / (C*1e6)

    flux_jy = flux_lambda * factor
    # uncertainty_jy = uncertainty_lambda * factor

    converted_data = np.column_stack((wavelength_um, flux_jy))#, uncertainty_jy))
    np.savetxt(output_file, converted_data, fmt="%.6e")

    print(f"Converted spectrum saved to '{output_file}'.")

# Example usage:
in_path =
'/home/byu.local/jam469/Downloads/ATMO_2020_models/atmosphere_models/NEQ_weak_spectr
a'
out_path = '/data/jam469/ATMONEQW'
model_files = [f for f in os.listdir(in_path) if f.endswith(".txt")]
for filename in model_files:
    model_path = os.path.join(in_path, filename)
    out_model_path = os.path.join(out_path, filename)
    convert_wm2um_to_jy(model_path, out_model_path)

#
convert_wm2um_to_jy("/home/byu.local/jam469/Downloads/ATMO_2020_models/atmosphere_mo
dels/CEQ_spectra/spec_T200_lg2.5_CEQ.txt",
"/data/jam469/ATMOCEQ/spec_T200_lg2.5_CEQ.txt")
```

B.4.2 Regridding

```
import os
import numpy as np
from scipy.interpolate import interp1d
from tqdm import tqdm

def load_spectrum_with_uncertainty(file_path):
    """Load spectrum with uncertainties: wavelength, flux, uncertainty."""
    data = np.loadtxt(file_path)
    return data[:, 0], data[:, 1], data[:, 2]

def load_spectrum_wo_uncertainty(file_path):
    """Load spectrum with uncertainties: wavelength, flux """
    data = np.loadtxt(file_path)
    return data[:, 0], data[:, 1]

def process_spectra(target_file, model_folder, output_folder):
    # Load target spectrum with uncertainties
    target_wave, target_flux, target_unc =
load_spectrum_with_uncertainty(target_file)

    model_files = [f for f in os.listdir(model_folder) if f.endswith(".txt")]

    for filename in tqdm(model_files, desc="Processing model spectra"):
        model_path = os.path.join(model_folder, filename)
        model_wave, model_flux = load_spectrum_wo_uncertainty(model_path)

        # Determine valid wavelength range
        model_wave_min = np.min(model_wave)
        model_wave_max = np.max(model_wave)

        # Mask target spectrum to model wavelength coverage
        valid_mask = (target_wave >= model_wave_min) & (target_wave <=
model_wave_max)
        twave = target_wave[valid_mask]
        tflux = target_flux[valid_mask]
        tunc = target_unc[valid_mask]

        # Interpolate model flux and uncertainty to masked target wavelengths
        flux_interp_func = interp1d(model_wave, model_flux, kind='linear',
bounds_error=False, fill_value=0.0)
        model_flux_interp = flux_interp_func(twave)
        model_data = np.column_stack((target_wave, model_flux_interp))
        np.savetxt(f"{output_folder}{filename}", model_data)

process_spectra("spectra/1541_Full.txt", "/data/jam469/ATMONEQS",
"/data/jam469/JWST_Forward/atmo_regrid_1541/")
```

Bibliography

Ackerman, A. S., & Marley, M. S. 2001, ApJ, 556, 872

Beiler, S. A., Cushing, M. C., Kirkpatrick, J. D., Schneider, A. C., Mukherjee, S., & Marley, M. S. 2023, ApJ, 951, L48

Burgasser, A. J., Geballe, T. R., Golimowski, D. A., Leggett, S. K., Kirkpatrick, J. D., Knapp, G. R., & Fan, X. 2003, in IAU Symposium, Vol. 211, Brown Dwarfs, ed. E. Martín, 377

Cushing, M. C., Kirkpatrick, J. D., Schneider, A., Beiler, S. A., & Cayago, A. 2021, Bolometric Luminosities of Cool Brown Dwarfs: The Key to Their Effective Temperatures and the Mass Function, JWST Proposal. Cycle 1, ID. #2302

Dupuy, T. J., Liu, M. C., & Leggett, S. K. 2015, ApJ, 803, 102

Faherty, J. K., et al. 2021, Explaining the Diversity of Cold Worlds, JWST Proposal. Cycle 1, ID. #2124

Kirkpatrick, J. D., et al. 1999, ApJ, 519, 802

—. 2008, ApJ, 689, 1295

—. 2012, ApJ, 753, 156

Knapp, G. R., et al. 2004, AJ, 127, 3553

Leggett, S. K., Morley, C. V., Marley, M. S., & Saumon, D. 2015, ApJ, 799, 37

Leggett, S. K., Morley, C. V., Marley, M. S., Saumon, D., Fortney, J. J., & Visscher, C. 2013, ApJ, 763, 130

Marley, M. S., & Robinson, T. D. 2015, ARA&A, 53, 279

Morley, C. V., et al. 2024, ApJ, 975, 59

Mukherjee, S., et al. 2024, ApJ, 963, 73

Sanghi, A., et al. 2023, ApJ, 959, 63

Schneider, A. C., et al. 2015, ApJ, 804, 92

Suárez, G., & Metchev, S. 2022, MNRAS, 513, 5701

Turner, S. K., Stephens, D. C., Scoresby, C. B., & Miller, J. A. 2025, A Survey Of Model Fits to Brown Dwarf Spectra Through the L-T Sequence